Investigations of Time Domain Optical Memory Applications in Rare Earth Crystals

Timothy Russell Dyke
August 2002

A thesis submitted for the degree of Doctor of Philosophy of The Australian National University

Statement of Authorship

The Content of this thesis, except where due reference is made, is entirely my own work.

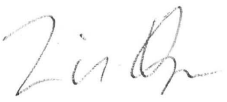

Timothy Russell Dyke

August 2002

Acknowledgements

Firstly I would like to express my appreciation and thanks to my supervisors, Professor Neil Manson and Dr Matt Sellars. In particular I am grateful for their patience, humour, and enthusiasm, and particularly for being there when things were tough. Without their willingness to share their knowledge and time this thesis would not have been possible.

Thank you to the technical staff of the Laser Physics Centre for always being prepared with an emergency rescue, and to my colleagues for valuable discussion, in particularly Dr John Martin.

I have appreciated the friendship and support of my friends, both within physics and elsewhere.

I am very grateful to my family, particularly my parents, for their patience and their unwavering confidence throughout this work.

Finally I want to say thank you to Jot and Ess for providing much needed "Fuzz Therapy" and to Kylie for her love and tolerance and for going through it all with me. Hopefully now I can share with you a very well earned holiday.

Abstract

This thesis explores the advantages in both performance and in the variety of usable techniques for time domain optical memories when a phase and frequency stable optical system is used.

Time domain memory is based on coherent transient and three pulse echo techniques in particular. The origin of these techniques and the background theory is discussed in the initial Chapter. Chapter 2 provides a description of the experimental system used with special emphasis placed on the frequency stabilised tunable dye laser system developed in the Laser Physics Centre, and the phase sensitive detection system used with it. This composite system was capable of a frequency stability of 100 Hz over periods of the order of milliseconds.

The optical computer memory component was achieved through using the persistent hole burning effect in crystals and this is explored in Chapter 3. The narrow spectral lines and long hole lifetimes found in rare earth centres in crystals make these crystals interesting candidates for optical memory applications samples of these materials were used exclusively throughout the work. The hole burning mechanism in all the cases studied is due to optically induced redistribution of population in the hyperfine levels. This is first discussed in general terms and then explored in specific relation to crystals of $CaF_2:Pr^{3+}$ and $EuCl_3.6H_2O$ – materials studied largely for general interest. A third material $Y_2SiO_5:Eu^{3+}$ was considered to have potential as an optical memory hole burning material. The essential parameters of this material associated with time domain memory capability were measured and the value of the material for memory uses fully assessed. Subsequently the material is used in various demonstrations of time domain memory techniques.

The main thrust of the thesis is contained in chapters 4 and 5. There are two aspects. Using a phase stable laser, time domain memory has capability not available other wise. One of these capabilities is the ability to reinforce, erase or modify stored information. This is demonstrated in Chapter 4. In addition, the signals are detected using phase sensitive techniques that also increases the range of time domain

techniques. These newly available techniques include the opportunity to measure and then reset laser frequency drifts , to store information in orthogonal channels or to store and recall any arbitrary optical waveform. These techniques are demonstrated in Chapter 5, which is then followed by a "Concluding Remarks" Chapter emphasising the value in the phase sensitive techniques developed in this thesis. There is also an exploration (included as an appendix) of the transient waveforms that can be obtained when larger area pulses are used as input, including a type of photon echo not previously noted in the literature.

Contents

Chapter 1 Introduction

1.1 Overview

Currently available data storage systems all function by separating data into individual bits and then storing each bit in a spatially distinct location. The natural consequence of this is that the minimum spatial volume into which a single bit can be reduced limits the maximum density of data that can be stored. In the case of optical memory systems such as compact discs this volume is determined by the diffraction of the light used and thus by the frequency of the light. This limitation is a serious technological issue, and considerable work is being done to try to push the practical limits.

With the discovery of persistent spectral holeburning in some inhomogeneously broadened optical transitions, it was realized that wavelength could be used as another dimension in which to store data (Szabo 1975, Castro 1978). Considerable work has since been done on this concept as a way of simultaneously storing multiple bits of data at a single diffraction limited spatial location. This method has the potential to dramatically increase memory storage volumes, present materials offer increases of up to 10^7 times in storage capacity (Equall 94).

The concept behind spectral holeburning is that when a sufficiently high resolution laser is used to excite an inhomogeneously broadened optical transition, the laser will only excite those centers which are actually resonant with the laser. This leaves the majority of the centres in the ground state, and so if a second laser is subsequently scanned in frequency across the inhomogeneous line it will be absorbed normally, except at frequencies of the first laser, where the absorption will be reduced. The band of reduced absorption is a spectral hole, and in most materials it lasts for the lifetime of the electronic excited state. However in some materials the centers excited by the first laser can relax to a different state than the initial ground state, leading to a population depletion

at that transition frequency, and thus a longer lived spectral hole. Possible examples of this different state might be another hyperfine state within the electronic ground state, or a state resulting from a photochemical or photophysical change induced in the material. The common theme however is that the lifetime of the relaxed state is significantly longer than the lifetime of the electronic excited state. The consequent reduction in the population of ground state centers at the frequency of the fixed laser means that experimentally the frequency scanned laser will detect a dip in the inhomogeneous absorption profile after the first laser has been removed and the electronic excited state has fully decayed. This is a persistent spectral hole, and the process of creating it is known as spectral holeburning (Moerner 1988).

The technique of using a persistent spectral holeburning material as a memory thus involves using laser light to burn a hole at a particular frequency, then moving the laser to a new frequency and burning another hole. In this way binary data would be stored bit by bit, with the presence of a hole indicating a "1" and the absence of a hole indicating a "0". The number of distinct persistent spectral holes that can be burnt into an absorption line is determined by the ratio between the inhomogeneous linewidth of the transition and the spectral hole linewidth, which in turn is dependant on the homogeneous linewidth of the individual centers and the laser linewidth. For a very stable high resolution laser the dominant contribution to the holewidth will be the inhomogeneous linewidth of the centers and it is the ratio based on this scenario that was used to generate the value of 10^7 listed above. Once data has been encoded across the whole inhomogeneous line at one spatial location, the laser could then be moved to another spatial location and the process repeated, allowing all of the advantages of the spatial dimensions to be retained. There has in fact been some considerable work done on storing spectral hole data at a large number of spatial locations simultaneously using techniques drawn from spatial holography (Wild 1991).

Concentrating on the single location storage of data, it is clear that there are advantages to using a spectral holeburning memory, but it was realized that such a system would be inherently slow(Mossberg 82). This is both because each bit needs to be burnt

individually and also because the resolution of the laser pulse used to burn the hole will be limited by its Fourier width, and so to burn a hole with resolution limited by the homogeneous width of the centers the pulse duration needs to be longer than the coherence lifetime (T_2) of the optical transition. Similarly the scanning laser will need to be scanned on a timescale that is slow compared to T_2 to avoid artificially broadening the detected holes (Mossberg 82).

This situation changed in 1982 when Mossberg (Mossberg 1982) suggested the use of time rather than frequency as the additional dimension into which data could be stored. The technique suggested by Mossberg used the stimulated photon echo phenomenon, in which the data is encoded as the delay between two short pulses. Provided that these pulses occur within T_2 of each other, the two pulses interact through their transfer of coherence to the centres and this interaction produces a spectral holeburning pattern in the frequency domain that extends for the Fourier width of the pulses and is modulated at a frequency determined by the delay between the two pulses. When a third pulse is later used to stimulate these modulated centers a coherent light pulse is emitted by the system, delayed from the third pulse by the same delay as occurred between the first two pulses; this is the photon echo. This modulation storage occurs whenever two pulses are overlapping in spectral frequency and within the T_2 timescale, and accordingly stimulated echoes can be used to store multiple pulse delays in the same spectral frequency range as part of a single pulse sequence. Because the data is accessed in parallel, rather than in series as with direct holeburning, both the writing and reading speeds of the memory can be enhanced. Because the response bandwidth of the system is determined by the frequency range of the emitting centers, the actual speeds attainable are also limited by the total inhomogeneous linewidth, and in theory the same volume of data as a frequency domain memory can be stored, except that the writing and retrieval times are potentially the same as for one bit of frequency domain memory. It is this time domain optical memory (TDOM) technique that is the basis of the work described in this volume.

There have been many variations proposed to this scheme, such as hybrid memories which use the TDOM technique with longer pulses which then step through the

inhomogeneous linewidth at intervals determined by the Fourier width of the pulses. All TDOM systems have been faced the constraints of the available persistent holeburning materials and the technical limitations of the hardware, such as lasers. Many of the ingenious variations of the TDOM technique, such as the use of impulse equivalent pulses (Shen 96a) have been proposed as compromises to allow the functional effects of these constraints to be reduced.

In addition to being able to support persistent spectral holeburning, the ideal materials for TDOM applications have a number of other requirements. (i) To store a large volume of data it is necessary for the sample to have a large ratio between the inhomogeneous linewidth and the homogeneous linewidth. (ii) To store data for long time periods it is necessary for the lifetime of the holes to be long. (iii) The separation of different states within the electronic ground state should be sufficiently large so that single pulses do not simultaneously excite more than one transition. Exciting more than one transition produces a modulation known as quantum beats (Kroll 1991) within the amplitude envelope of retrieved echoes, which in turn reduces the reliability of the signal. (iv) The holeburning efficiency or branching ratio should be high to allow the strongest possible signal for a modest level of input power. (v) A high signal efficiency also requires that the electronic transition have both a high oscillator strength, and that a minimum of input energy is lost though non-radiative pathways. (vi) The material should have a homogeneous linewidth which is independent of external factors which in turn implies that the T_2 of the transition should be approaching the population lifetime limit of $2T_1$. At present the materials that best match this description are trivalent rare earth crystals cooled to cryogenic temperatures, however a more detailed discussion of all of these points is included in chapter 3 dealing with materials.

The choice of trivalent rare earth centers creates a technical difficulty because those rare earth centers which best match the above description have very narrow homogeneous linewidths, hundreds of Hz in some cases, and correspondingly long T_2 lifetimes, of the order of milliseconds. These narrow lines and long lifetimes have been inconvenient as the tunable dye lasers that produce light of suitable wavelengths to access the rare earth

transitions have been only commercially available with resolutions of the order of MHz. Thus the phase and frequency stability of these laser systems could only be relied upon on timescales of microseconds, three orders of magnitude less than the timescales available within the material. Because of this timescale mismatch, most of the techniques used for TDOM occur in only a small fraction of the available storage window, or alternately utilize methods that are largely insensitive to variations in the phase and frequency of the laser source, and in fact have rarely considered how techniques utilizing phase information may be of value.

Akmediev (Akmediev 1990) was the first to suggest that consideration of phase might be useful for TDOM. He suggested that a relative phase reversal of 180° in two otherwise identical data storage sequences could be used to selectively erase the stored data. Subsequent experimental tests of this proposal were successful only when the timescales involved were restricted to a few microseconds, leaving the technique of little practical value (Elman 1996). This restriction has similarly restricted other phase sensitive concepts such as using TDOM techniques for all optical data processing, and perhaps as importantly, it has stifled consideration of new phase or frequency sensitive techniques that would only be valuable with sufficient system stability. The present work is qualitatively different. By utilizing a suitably stabilized laser system along with phase sensitive detection of optical transients, the current study demonstrates that previously described techniques such as erasure can be applied effectively at practical timescales, and also demonstrates some new and potentially useful techniques that are only possible with good phase and frequency stability.

1.2 Background and Theory:

Coherent transients, in the form of the spin echo, were first described by Erwin Hahn in 1950 (Hahn 1950). Hahn discussed applying RF pulses to glycerine, which were in resonance with the proton NMR spin flip transition, and subsequently observing spontaneous RF emission from the material. This emission showed a simple exponential decay after one pulse, but after two pulses displayed as a RF pulse that was delayed from the second pulse. This delay was equal to the time spacing between the two applied pulses. He described these phenomena as a free induction decay and a spin echo respectively. As an aside, it is interesting to note that a proposal for using echoes as a memory technique was described in 1955 (Anderson 1955), using the same glycerine NMR transition. The authors demonstrated the storage of 450 data echoes. However as the memory involved only the single transition the storage lifetime was limited by the T_1 of 70 ms.

Photon echoes, the coherent transient equivalent of spin echoes in the optical region, were described in 1964 by Kurnit et al. (Kurnit 1964). They described similar observations to Hahn's except that they were using a pulsed ruby laser to excite the 693.5 nm electronic transition in ruby.

The Bloch model was developed by Felix Bloch (Bloch 1946), to provide a theoretical framework for the behaviour of spin ½ NMR transitions and is a semi-classical description of a two level system interacting with a single driving field. This model was subsequently adopted into the optical regime by Feynman et al. (Feynman 1957), who made the connection that the model could be applied to any two level atom ensemble, rather than only an ensemble based on spin flip transitions.

In the Bloch model, the state of a two level ensemble driven by an external field, E, can be described by three variables, namely; the population inversion, w, and two orthogonal components of the transition dipole, u and v. These variables can be written as a vector, which is known as the Bloch vector (Levenson 1988),

$$R = u\hat{1} + v\hat{2} + w\hat{3} \qquad (1.2.1)$$

The optical Bloch equations then give the time evolution of these variables as (Levenson 1988),

$$\begin{aligned} &\dot{u} + \Delta v + \chi w \sin\phi + u/T_2 = 0 \\ &\dot{v} - \Delta u - \chi w \cos\phi + v/T_2 = 0 \\ &\dot{w} - \chi(v\cos\phi + u\sin\phi) + (w - w^o)/T_1 = 0 \end{aligned} \qquad (1.2.2)$$

where Δ is the detuning of the driving field from resonance with the transition and χ is the Rabi frequency. The Rabi frequency is given by the scalar product of the dipole moment and the amplitude of the driving field as shown,

$$\chi = \mu \bullet E_o / \hbar \qquad (1.2.3)$$

where μ is the dipole moment vector. ϕ represents the phase difference between the driving field and the u component of the dipole moment. T_1 and T_2 are decay constants that are specific to the system being studied. T_1 represents the decay of the population inversion, w, back to –1, and T_2 represents the dephasing of the u and v components of the dipole moment back to w^o (thermal equilibrium).

The observable quantity in this system is given by the polarisation (P) (Levenson 1988) as shown

$$P = \frac{N\mu}{2}(u - iv)e^{-i\omega t} + cc \qquad (1.2.4)$$

where N is the number of centers and the real and complex components of the polarisation give the observed phases of the output emission.

For a material with inhomogeneous broadening, the detuning frequency described above varies as a range of values, and consequently the polarisation is found by integrating over the whole inhomogeneous line.

$$\langle P \rangle = \int_{-\infty}^{\infty} G(\omega_o) P(\omega_o) d\omega_o \qquad (1.2.5)$$

Where $G(\omega_o)$ describes the spectral density of the centres. This is particularly necessary for the materials studied in this work as the inhomogeneous linewidth is always much greater than the available pulse Fourier width, and consequently the detuning frequency can be much greater than the Rabi frequency for some centres.

To aid in conceptualisation the Bloch equations can be given a geometric interpretation through the definition of a pseudo field vector β, as shown

$$\beta = \chi u(\cos\phi)\hat{1} + \chi v(\sin\phi)\hat{2} + \Delta w\hat{3} \qquad (1.2.6)$$

In this case the Bloch vector R precesses around the pseudo field as shown,

$$dR/dt = \beta \times R + [relaxation\ \ terms] \qquad (1.2.7)$$

With the relaxation occurring on a timescale of T_2.

Based on this it is apparent that if a short resonant pulse is applied to a system where R is orthogonal to β, a common situation with coherent transients, then R will rotate around β through an angle θ as given by,

$$\theta = \int_{t_{start}}^{t_{end}} \chi(t) dt$$

(1.2.8)

This angle (θ) is known as the pulse area.

Free Induction Decays

The Bloch equations are impossible to solve analytically except under certain specific conditions. One if these soluble conditions is the steady state solution where a constant filed is applied for a time >>T_2. The analytic solution fo this condition is reproduced below as it is illustrative for describing the formation of a free induction decay. In this work solutions for the Bloch equations in more complex situations have been obtained through the use of a numerical evaluation using a 4th order Runge-Kutta integration (Kreyszig 1988).

The simplest Bloch equation situation for free induction decay is where a constant driving field has reached a steady state before being switched off, the derivation for which can be found in the reference (Levenson 1988). The steady state solution of the Bloch equations is,

$$u(\infty) = \frac{-\Delta\chi}{\Delta^2 + T_2^{-2} + \chi^2 T_1 / T_2}$$

$$v(\infty) = \frac{-\chi}{\Delta^2 + T_2^{-2} + \chi^2 T_1 / T_2}$$

$$w(\infty) = \frac{-\chi^2 T_1 / T_2}{\Delta^2 + T_2^{-2} + \chi^2 T_1 / T_2} \qquad (1.2.9)$$

The free induction decay signal is then obtained by using 1.2.9 as the initial conditions of the free evolution solution of the Bloch equations (1.2.10) where for example u(∞) from 1.2.9 is used as the value for u_0 in 1.2.10,

$$\begin{aligned} u(t) &= [u_o \cos(\Delta t) - v_o \sin(\Delta t)]e^{-t/T_2} \\ v(t) &= [v_o \cos(\Delta t) + u_o \sin(\Delta t)]e^{-t/T_2} \\ w(t) &= [1-(w_o+1)]e^{-t/T_1} \end{aligned} \qquad (1.2.10)$$

These values are used to calculate the polarisation, which is integrated over the inhomogeneous line to give 1.2.11,

$$\begin{aligned} \langle P \rangle = \mu\chi e^{-t/T_2} \int_{\infty}^{\infty} \frac{-G(\omega_o)(\Delta + i/T_2)}{(\Delta^2 + T_2^{-2})} e^{-i\omega_o t} d\omega_o - \\ \mu\chi^3 e^{-t/T_2} \int_{\infty}^{\infty} \frac{-G(\omega_o)(\Delta + i/T_2)T_1/T_2}{(\Delta^2 + T_2^{-2})(\Delta^2 + T_2^{-2} + \chi^2 T_1/T_2)} e^{-i\omega_o t} d\omega_o \end{aligned} \qquad (1.2.11)$$

The polarisation has two distinct terms, the first one ($\alpha\chi$) represents the linear free induction decay. This signal is due to excitation of the entire inhomogeneous line and decays with a lifetime on the order of T_2* (the coherence time of the inhomogeneous line). The second term ($\alpha\chi^3$) represents the third order free induction decay. This signal is due to the saturation of those centres whose resonant frequencies lie close to the frequency of the applied field, in other words the spectral hole. The phase of the third order decay is inverted with respect to the phase of the first order decay, this is due to the differing source of the two emissions. The first order decay results from centres initially in the ground state being excited up into a coherent superposition and thus emitting coherently, the third order decay results from atoms that (as a result of the long preparatory pulse) are already in the excited state and begin emitting coherently when

excited down into the coherent superposition. If it is assumed the inhomogeneous line profile, $G(\omega_o)$, is essentially constant, which is reliably the case with the very broad linewidths found in the solid materials studied in this work, then the third order polarisation is given by,

$$\langle P \rangle^3 = \frac{\pi i G(\omega)\mu\chi^3 T_1 \exp[-(t/T_2)(1+\sqrt{\chi^2 T_1 T_2 - 1})]}{T_2^{-1} + \chi^2 T_1 + \sqrt{(T_2^{-1} + \chi^2 T_1 / T_2)}} \exp^{-i\omega t} \qquad (1.2.12)$$

From 1.2.12 it can be determined (Levenson 1988) that the decay rate of the third order FID amplitude is given by,

$$T_{obs}^{-1} = (1/T_2)(1+\sqrt{\chi^2 T_1 T_2} + 1) \qquad (1.2.13)$$

which in the limit of a weak driving field simplifies to $2/T_2$. One half of this decay rate is due to the inhomogeneous broadening of the spectral hole during burning, while the other half is due to the intrinsic relaxation rate of the ensemble of centres at the driving field frequency.

Delayed free induction decay

If a long pulse has been used to generate a spectral hole then once the pulse stops the presence of the spectral hole will be apparent in the appearance of a third order FID, as described above. The lifetime of this FID will be limited by T_2, however the hole exists in the population distribution and so in a situation where population transfer to other level can be ignored, such as in a two level atom system,the lifetime of the hole will be limited by T_1. If, after the FID has decayed the hole still exists, and the system is again excited with a resonant pulse th response will be affected by this residual. In this case the system will produce an exponential decay FID emission after the second pulse, but the presence

of the existing spectral hole will separately modulate the emission response. In effect the second pulse will produce two distinct FIDs, one with a lifetime determined by the initial pulse parameters and one with a lifetime determined by the parameters of the second pulse. In this case the FID produced due to the pre-existing spectral hole is called a delayed free induction decay (DFID). Because the DFID arises from the presence of a spectral hole in the population distribution of the ensemble, this situation can occur even when the hole is due to persistent spectral holeburning, and the optical state has completely decayed prior to the second pulse. This situation is equivalent to using a single pulse on a spectral line which has a sharply changing $G(\omega_0)$ in the vicinity of the applied field frequency.

The most common experimental use of a DFID involves a long, weak initial pulse, which creates a correspondingly narrow spectral hole, followed by a very short pulse, which produces a wide (and usually shallow) spectral hole. The corresponding FID is thus very short, while the DFID may be very long. This method is thus useful for experiments such as measuring the time resolved linewidth of spectral holes as well as investigating T_1 lifetimes.

Photon Echoes

Photon echoes are perhaps most easily understood if the assumption is made that the applied field is strong, and thus the Rabi frequency is much greater than the largest detuning frequency available within the inhomogeneous line. In this case the effects of detuning can essentially be neglected during the time that the driving field is applied, while the exactly soluble free evolution solution can be applied while the field is off. Such pulses are referred to as being "hard" while a pulse which does not affect the whole inhomogeneous line is called "soft". In this case photon echoes can be well described using the geometric interpretation of the Bloch equations described above.

If a hard pulse of area $\pi/2$ is applied to an ensemble initially at equilibrium, i.e. with all Bloch vectors in the w direction, then after the pulse all of the Bloch vectors will be in

quadrature to the driving field, i.e. parallel to the u axis. Once the pulse has finished the Bloch vectors will each precess around the w axis, at a rate determined by the detuning frequency, and with the direction determined by the sign of the detuning. This will result in a polarisation that will initially be maximum and will then decay as the vectors precess, and is another way of describing the first order FID mechanism. If at a later time the ensemble is subject to another hard pulse, this time of area π then all of the Bloch vectors will effectively be 'reflected' across the v-w plane. Once the second pulse ends the vectors will again precess, however because of the 'reflection' the vectors will now precess in the reverse direction, but at the same rate as before. When the system has evolved for the same duration as initially between the two pulses the vectors will again align along the u axis giving a net polarisation and thus an observable signal. This is the two pulse photon echo, and it will have the signal intensity of the initial FID, reduced by a factor proportional to the incoherent relaxation effects of T_1 and T_2. For this reason two pulse echoes can be used to experimentally measure the relaxation times within an ensemble (Hartmann and Hahn 1962).

Three pulse or stimulated echo can be explained similarly. In this case the first pulse is identical to that used for a two pulse echo, however the area of both the second and third pulses is $\pi/2$ rather than π. The effect of this is that after the second pulse, all of u components of the Bloch vectors have been rotated onto the w axis. These w components neither precess or decay, except via T_1 processes. The third $\pi/2$ pulse rotates these w components onto the u axis, exactly as if the second and third pulses had occurred as a single π pulse. In this case the photon echo occurs after the third pulse, with a delay equal to the delay between the first and second pulses. Both two and three pulse photon echoes can occur if the pulses used are not $\pi/2$ or π, and also if the pulses are soft rather than hard, however the physical interpretation of these situations becomes more difficult

One method of approximating the behaviour of three pulse echoes that has proven valuable, from a TDOM perspective, uses the assumption that all the pulses are weak and of negligibly short duration (Mitsunaga 1992). In this case the pulses can be described simply by their timing (t_1, t_2, and t_3) as well as their amplitudes (E_1, E_2, and E_3). These

assumptions are useful because in this limit the pulse effects on the affected centres is determined purely by the power spectrum (Yariv 1985) of the exciting pulses. Calculating the power spectrum for the first two pulses gives a sinusoidal distribution with a period given by the reciprocal of the delay between the pulses. The frequency (ω) distribution of the w vectors, which is in effect the absorption profile, thus has a sinusoidally modulated component given by,

$$\alpha(\omega) = E_1^* E_2 \exp(i\omega(t_2 - t_1)) \qquad (1.2.14)$$

This is similar to the DFID situation, except that the modification of $G(\omega_o)$ involves a sinusoidal modulation rather than a single hole. Like the DFID however the lifetime of this modulation will be given by the persistent holeburning lifetime.

The response of the system to the third pulse can then be described by the Fourier transform of the population distribution as given above. This gives an output amplitude signal (E_s) of

$$E_s(t) = E_3 \int \alpha(\omega) \exp(i\omega(t - t_3) d\omega \qquad (1.2.15)$$

Combining these two equations produces a delta function occurring at (t_2 - t_1) after the third pulse.

To better reflect the uses of a TDOM system however the above equations can be generalised to the situation where the three input pulses have and arbitrary time profile ($E_1(t)$, $E_2(t)$, $E_3(t)$) . This is the general equation for three pulse photon echoes and can be expressed as

$$E_s(t) = \iiint E_1^*(t_1) E_2(t_2) E_3(t_3) \delta(t_3 + t_2 + t_1 + t) dt_1 dt_2 dt_3 \qquad (1.2.16)$$

This formula can also be expressed as

$$E_s(t) = \int E_1^*(\omega)E_2(\omega)E_3(\omega)\exp(i\omega t)d\omega \qquad (1.2.17)$$

Where E(ω) represent the Fourier transform of E(t). This result is important as it highlights that the output three pulse echo signal is the Fourier transform of the product of the spectra of the three input pulses.

To demonstrate the potential of three pulse echoes for memory and optical data processing applications it is worthwhile to investigate this general equation in situations where one or more of the input pulses approximate delta functions.

In the situation most commonly presented as appropriate for memory applications the first and third pulses are both short, and thus can be replaced by delta functions, while the second pulse is temporally complex, for example as a series of data pulses. In this case the first pulse is called the "write" pulse and occurs at t = 0 while the third pulse is called the "read" pulse, and occurs at t = T. In this case the general equation becomes,

$$E_s(t) = E_2(t - T) \qquad (1.2.18)$$

This describes the replication of the second pulse after time delay T (i.e. after the third pulse. This accurate, but arbitrarily delayed, reproduction of the second pulse is the basis of the simple memory application of the three pulse photon echo.

A second scenario involves replacing both the second and third pulses with a delta function. In this case the second pulse is the write pulse, occurring at t = 0, and the third pulse is again the read pulse at t = T. The general equation then becomes,

$$E_s(t) = E_1^*(T - t) \qquad (1.2.19)$$

The output signal is thus a time reversed replica of the first pulse, occurring after the third pulse.

If only the first pulse is replaced by a delta function, leaving the second and third pulses temporally complex, the general equation gives,

$$E_s(t) = \int E_2(\tau)E_3(t-\tau)d\tau \qquad (1.2.20)$$

This result is the cross convolution of the two temporally complex functions, and indicates that a three pulse echo system can be used to perform single operation cross convolutions between data sets (Babbitt 1987).

Lastly, if the first two pulses are complex, with the third being a delta function the resultant equation is,

$$E_s(t) = \int E_1^*(\tau)E_2(t+\tau)d\tau \qquad (1.2.21)$$

This is the temporal cross correlation of the first two pulses, and again this could be useful for single operation processing of data sets (Babbitt 1987). A specific example of this occurs when both the first and second pulses are identical. In this case the resultant echo output is the autocorrelation function, and consequently could be used for effective pattern recognition. Aspects of this scenario are explored experimentally in chapter 6.

Because the experiments described in this work are sensitive to the phase and frequency stability of the driving fields, it is worthwhile to separate out the applied modulation from the carrier field when writing the expression for the electric field amplitude of the pulses. This is given by,

$$E_p(t) = \varepsilon(t)\exp(i(\omega(t)t + \phi(t))) \qquad (1.2.22)$$

Here the exponential term describes the carrier signal, with a time dependant frequency $\omega(t)$ and phase $\phi(t)$, while $\varepsilon(t)$ represents the applied modulation (i.e. pulse gating) of the beam which may take complex values.

The detected signal $S(t)$ thus depends on the frequency, phase and applied modulation of the carrier as shown,

$$S(t) \propto \varepsilon(t-T)\exp(-i(\phi(t-T)-\phi(t))+(\omega(T)-\omega(0))(t-T)) \qquad (1.2.23)$$

From this it can be seen that if the frequency component [ω(T) - ω(0)] is large then the signal will be dominated the real part of the exponential. Consequently for large frequency changes of the applied field the detected signal will be small. Experimentally this is equivalent to the laser drift reducing the overlap of the bandwidth of the applied pulses. In circumstances where the magnitude of the frequency component is of the order of the phase component, the frequency difference will still produce an attenuation of the detected signal, but it will also produce a phase shift within the detected signal, which with appropriate phase detection, will be indistinguishable from the effect of a phase shift within the applied field. It is thus necessary to use a system that is very stable in both frequency and phase in order to accurately conduct phase sensitive experiments.

From the description of the observable polarisation given earlier, it is clear that the output signal has components that are proportional to u and v. If a local oscillator field E_{lo} is used as part of the detection process, then the signal intensity that will be detected by a photodiode will be,

$$I_{detector} = E_T \bullet E_T^* \qquad (1.2.24)$$

where

$$E_T = E_o + E_s + E_{lo} \qquad (1.2.25)$$

describes the total electric field incident at the detector. E_o represents the field due to the light directly transmitted through the sample without absorption, and E_s is the field due to

the material response. In the detection system used in this work, the signal was detected as a 10MHz heterodyne beat signal, due to a frequency offset of E_{lo}. Since the transmitted beam is blocked during the data acquisition of transients such as echoes and FIDs, E_o can be assumed to be zero. In this case the only 10 MHz terms remaining are given by,

$$I_{detector}(10MHz) = E_s \bullet E_{lo} + cc \qquad (1.2.26)$$

Since the electric field is proportional to the polarisation, the detected signal (S) can be described by,

$$S \propto u\cos(\phi - \theta) + v\sin(\phi - \theta) \qquad (1.2.27)$$

Where ϕ is the phase angle between E_s and E_{lo}, while θ is the phase of the RF signal relative to the RF local oscillator. It can be seen from this that a suitable choice of θ will allow the components of the signal parallel to u and v to be observed independently.

Rotary Echoes

The other coherent transient used in this thesis is the rotary echo. Rotary echoes in the optical regime are very similar to those first found in NMR experiments (Solomon 1959). Experimentally it involves driving the ensemble of center for a period of time τ, less than T_2 and longer than one Rabi cycle, and then reversing the phase of the driving field. At time τ after the phase reversal of the driving field the transmitted signal will shows an oscillation in the detected intensity (see figure 1.2.1), this oscillation is the rotary echo.

Like photon echoes it is most easily understood using the geometrical interpretation of the optical Bloch equations (see figure 1.2.2). During the initial driving field the Bloch vectors of the ensemble rotate clockwise in the *vw* plane. During this time the transverse components of the Bloch vectors also experience dephasing according to their individual detunings, however this dephasing will vary with each π rotation of the Bloch vectors

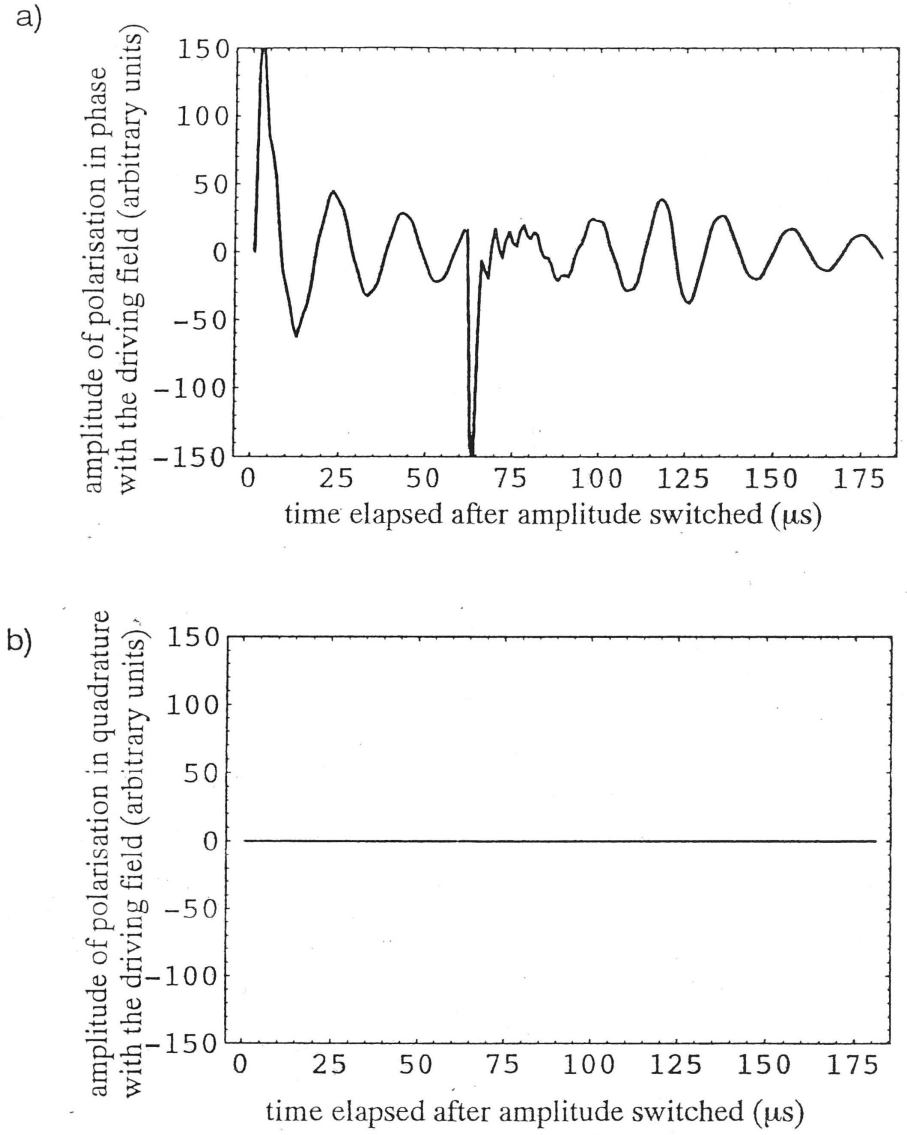

Figure 1.2.1: A numerical simulation trace showing the evolution of the in-phase (a) and in-quadrature (b) components of the polarisation during a rotary echo sequence. The phase was reversed after 60 μs, with the echo, seen as an increase in the peak to peak oscillation in (a), occurring at 120 μs.

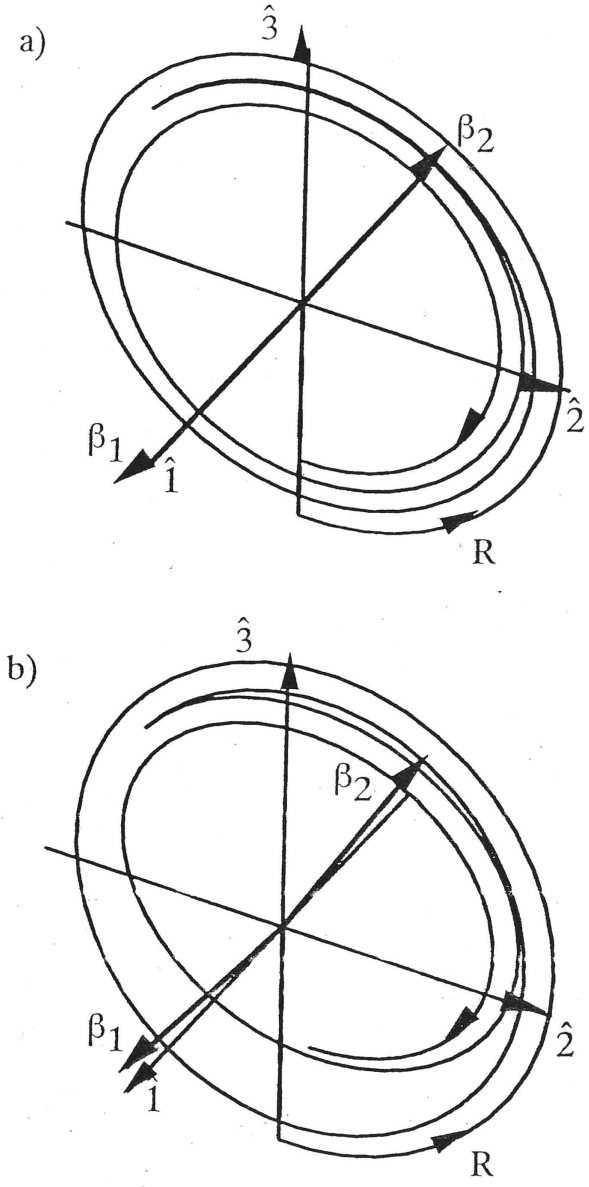

Figure 1.2.2: Evolution of the Bloch vector during a rotary echo pulse sequence. (a) shows the Bloch vector evolution for the on resonance case and (b) shows the evolution of a vector that is slightly off resonance. $\beta 1$ and $\beta 2$ respectively show the orientation of the Rabi vector before and after the driving field phase is reversed

about the *v* axis. When the phase of the driving field is reversed, at time τ, the Bloch vectors will rotate counterclockwise about the v axis, and the dephasing directions of the individual vectors will also be reversed. At time τ after the phase reversal, the Bloch vectors will have completely retraced their motion and will once again be aligned in a single direction, giving a net polarization. This is the source of the rotary echo signal. The oscillatory nature of the signal is due to the vectors rotating around the *v* axis at the Rabi frequency and thus the polarization is alternately along the positive and negative *u* directions.

The oscillation of a rotary echo is thus determined by the Rabi frequency and thus by both the applied field intensity and the dipole moment of the transition. By measuring the Rabi frequency experimentally both the pulse areas used and the dipole moment could be calculated. It should be noted however that because of the Gaussian distribution of intensity across a laser beam, the measured Rabi frequencies are only approximate.

Chapter 2 The Experimental System

2.1 Experimental Overview

The system used for the experiments described in this work utilized two important components that differed substantially from those used by most other TDOM researchers. These were an ultra high resolution stabilised dye laser and an optical interferometer for detecting the phase of the coherent transients and of the transmitted light. Both of these components are discussed in detail below. In addition, the system comprised a number of more typical components, which will only be discussed briefly.

To ensure suitable temperatures the sample was maintained in a liquid helium cryostat. The particular cryostat was equipped with a needle valve, which could provide a controlled amount of helium into the sample space. The sample space was also connected to a pumping system so that the vapour pressure and thus temperature of the sample space could be lowered. This system allowed the sample to be kept cold and also minimised the optical and vibrational effects of bubbles in the liquid helium. With the pump in action the cryostat contained enough helium for a maximum of 18 hours operation. The cryostat also contained a superconducting magnet capable of generating DC magnetic fields of up to 5 Tesla. Initially the sample was mounted within a copper coil within the cryostat. This was used for the experiments requiring direct RF application to the sample, however the coil was found to enhance the transmission of vibrations to the sample and so the sample was subsequently mounted on a solid copper block.

The laser used was a Coherent 699 dye laser with Rhodamine 6G dye, pumped by a Coherent Innova Argon ion laser. Where possible the beams of both lasers were enclosed to minimise the effects of atmospheric disturbances. The operation of the dye laser in the high resolution mode is described below, however the laser could also be used at the lower resolution as originally constructed. This was useful for certain experiments such

as burn and scan holeburning as in the high resolution mode the laser frequency was difficult to scan.

Pulse generation and data collection was done using a personal computer, which had been equipped with a pulse generator card and a data acquisition card. The software for these was written in house using Visual Basic. Alternatively the data acquisition was sometimes done with a digital oscilloscope.

2.2 The High Resolution Laser System

A substantial proportion of the experiments described in this work rely on the use of a highly stable, high resolution laser light source. Free running dye lasers have linewidths of about 10 MHz, and commercially available stabilized lasers have linewidths of the order of 1 MHz. This limits any spectral holes formed using these lasers to linewidths at least as wide as the laser linewidth, regardless of the actual homogeneous linewidth of the material studied. In the case of time domain memory applications, the MHz laser linewidth means that any techniques that rely on controlling either the phase or frequency of the input light are limited to a timescale of the order of microseconds. This is orders of magnitude shorter than the coherence times of some of the rare earth materials suggested as desirable for such memory usage. Consequently a laser source with considerably higher resolution and phase stability is necessary.

The laser used in this work was a commercially available Coherent 699, which has been modified in several ways to improve its frequency and phase stability. Specifically the laser has
been locked to a high finesse external reference cavity, with additional electronics incorporated to enable it to relock when it loses the reference locking signal. The laser has also been externally intensity stabilized. Modification of the laser has been an ongoing project within the laboratory, with the major contribution of the current work being the high precision measurement of the laser performance through the use of phase sensitive detection of coherent transients, and the consequent fine tuning of the system. Further details of the laser stabilization are available in (Sellars 1995, Pryde 1999), whereas details of the high precision measurement of the laser performance are described this thesis in Chapter 5. A schematic diagram of the stabilization setup is shown in figure 2.2.1.

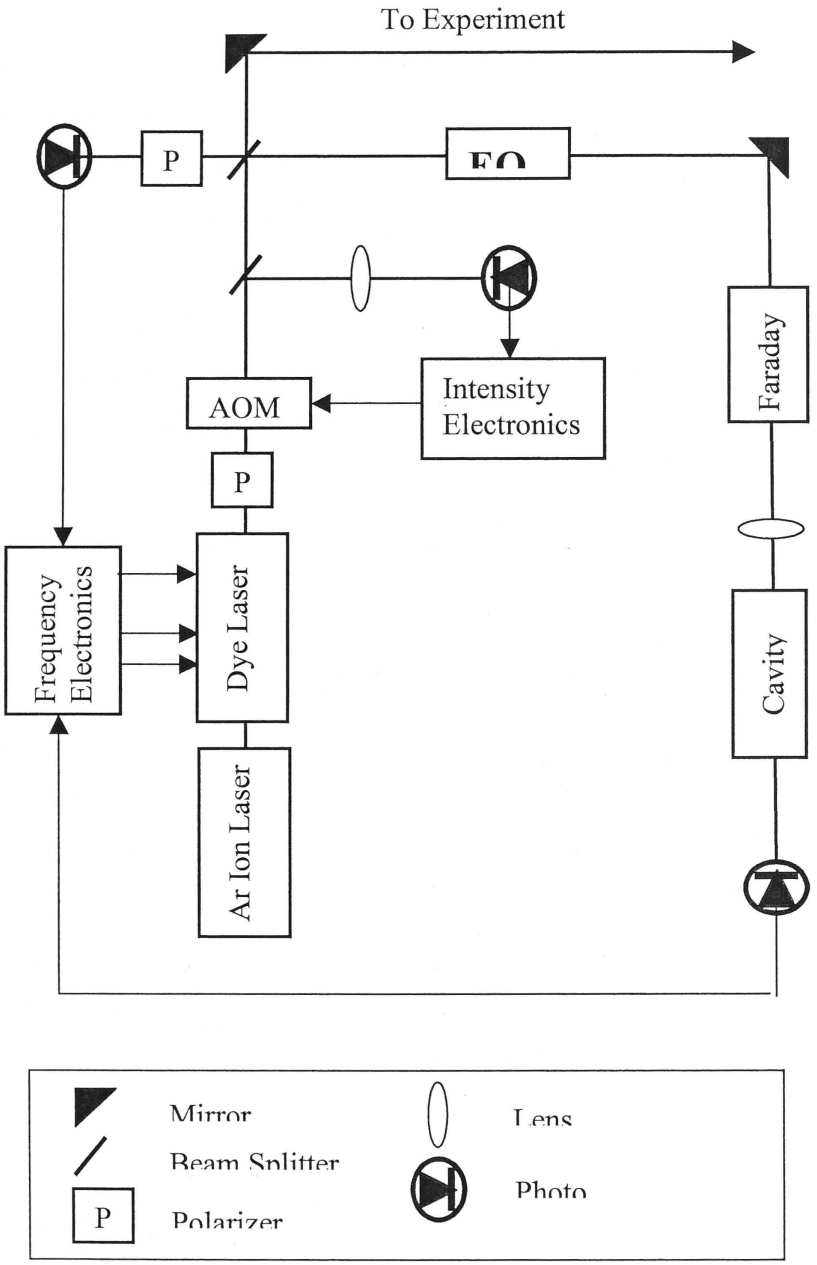

Figure 2.2.1: Schematic diagram of the high resolution laser locking setup. AOM represents an acousto optic modulator, EOM represents and Electro optic modulator, Faraday represents a polarization rotator, and cavity represents the high finesse external cavity.

Laser Locking system

The laser was locked to an external high finesse cavity that was custom made by the Commonwealth Scientific and Industrial Research Organisation (CSIRO) Australia. The cavity consisted of a non-confocal arrangement based around a drilled-out rod of "Zerodur". To reduce the effects of environmental changes the cavity was suspended from thin wires within an evacuated chambers. Both the cavity and the other optical elements were designed to also reduce the effect of vibrations. The cavity was gently heated to about 313K, to reduce the impact of thermal variations, with the temperature monitored and controlled using a feedback system. During the course of the work the thermal shielding of the cavity was also considerably improved. The finesse of the cavity was about 300, giving a FWHM of 1 MHz and a free spectral range of approximately 300MHz.

A Pound Drever technique (Drever 1983) was used to generate an error signal from the light reflected form the cavity. This was done by using an 8 MHz electro optic phase modulator to produce sidebands on the beam incident onto the cavity. The beam was then coupled into the cavity so that one of the sidebands was preferentially absorbed, and consequently the reflected beam was amplitude modulated at 8 MHz. This reflected beam was heterodyne detected using a photodiode, and the resultant signal mixed with the 8 MHz RF driving signal to produce an error signal with an in quadrature and in phase component as shown in figure 2.2.2 (a) and (b) respectively.

In the unmodified Pound Drever locking system that was originally used, the in quadrature signal was used with some negative feedback electronics to provide a locking signal to the laser. Using this error signal the laser frequency was corrected using an intracavity electro-optic phase modulator, a laser mirror mounted on a piezo electric disk (the tweeter mirror in the original Coherent 699 configuration), and a Brewster plate. These three devices provided correction in the bandwidths of 100 kHz, 1 kHz, and 100

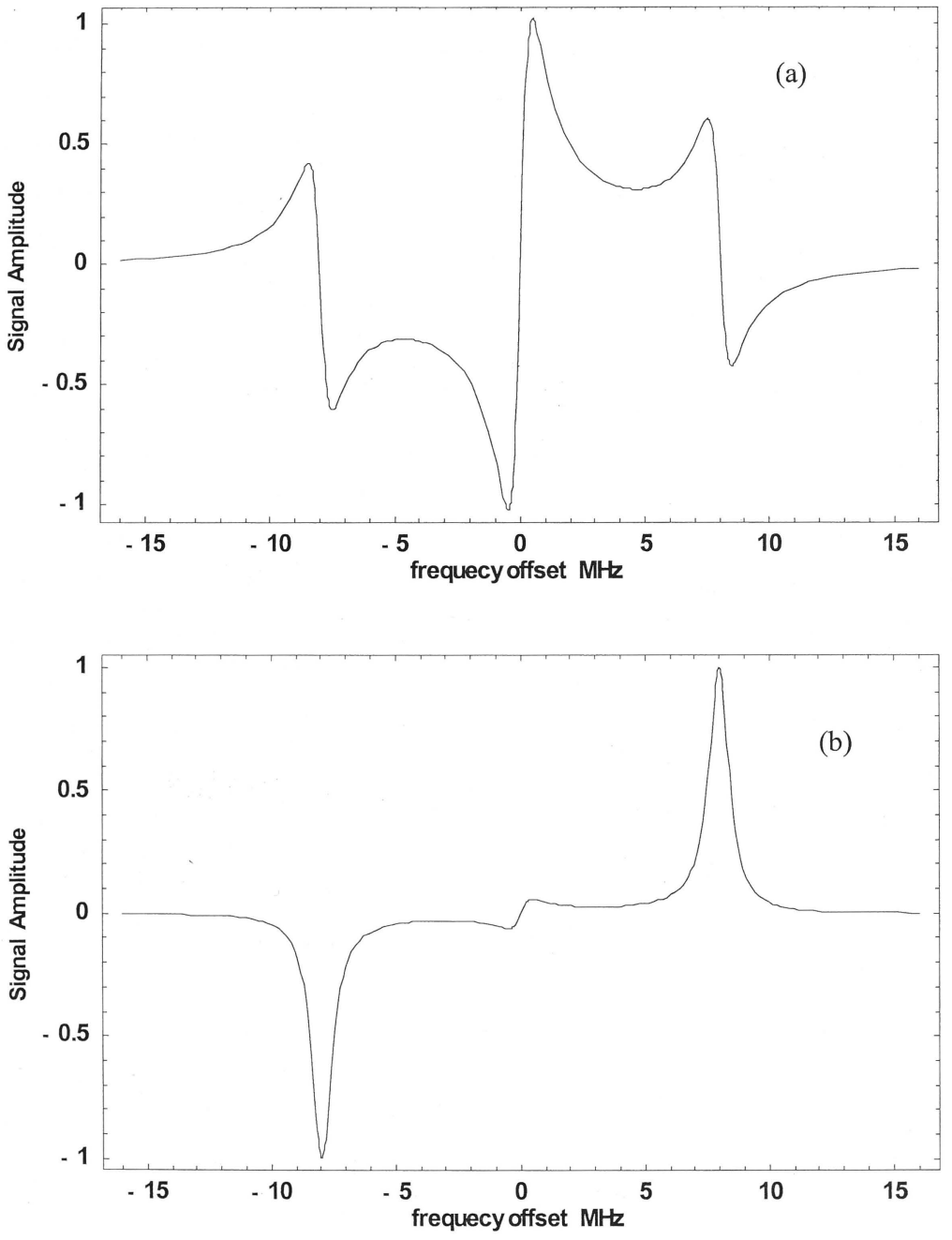

Figure 2.2.2: The in quadrature (a) and in phase (b) heterodyne detected error signals from the reflected light from the high finesse cavity.

Hz respectively. When the error signal was such that the laser frequency was effectively stabilized, the laser was considered "locked".

As can be seen from figure 2.2.2 (a), the unmodified Pound Drever system has a tight locking region of about +/- 0.5 MHz, where the sharply dispersive portion of the error signal crosses the zero point. The full locking region extends out to +/- 8 MHz where the sign of the error signal remains appropriate to push the laser frequency back into the tight locking region. However frequency excursions of more than 8 MHz away from the centre are not compensated for. To compensate for this, the error signal was electronically modified so that the total locking region extended to +/- 300 MHz (the free spectral range of the cavity). This was achieved by using the absorptive or in phase component of the error signal, shown in figure 2.2.2 (b), as a trigger to determine when a laser frequency excursion deviated by more than 8 MHz from lock. A DC override voltage then replaced the error signal until a second trigger indicated a return to the locking region, when the unmodified error signal was again utilized. The differing signs of the high and low frequency peaks of the in phase component allowed the direction of the frequency excursion and thus the restoring voltage to be determined. A theoretical example of the modified error signal, with the frequency scanned from high to low is shown in figure 2.2.3.

Despite the above improvement, the laser still occasionally dropped out of lock, for example, when the triggering signal was not detected during a substantial excursion. This was monitored by detecting the beam transmitted through the locking cavity. When the laser was detected to have been out of lock for a set time, usually > 0.5 seconds then the error signal voltage was overridden and set to the value recorded from the last time the laser was locked. This was usually sufficient to relock the laser, and was only necessary once or twice an hour.

The other valuable modification of the laser was the incorporation of intensity stabilization. A stable laser intensity is useful both because it improves the reliability of the experiments and also because variations in the intensity can be interpreted, via the

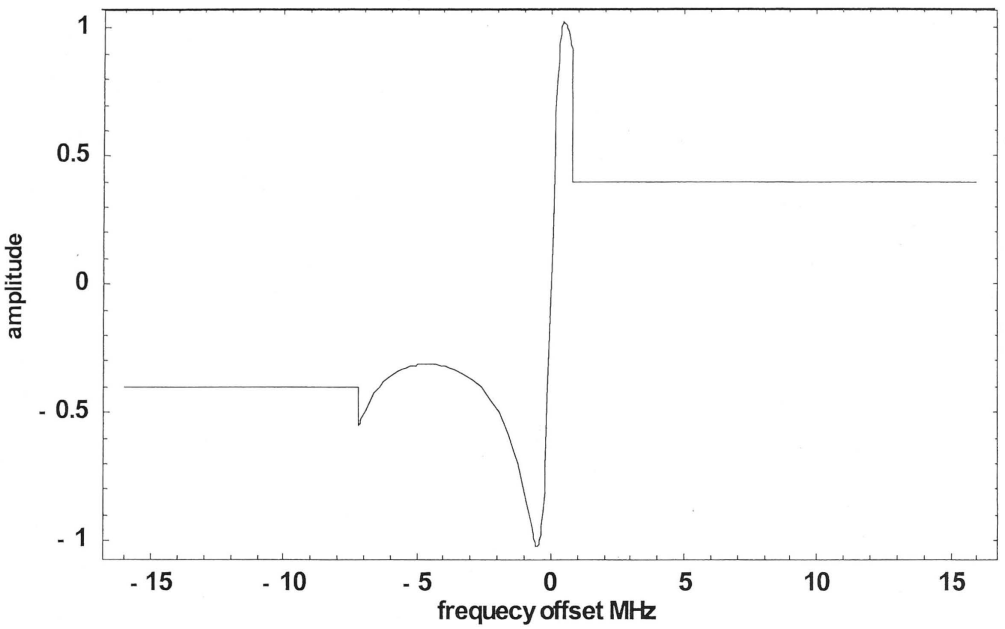

Figure 2.2.3: The modified form of the frequency locking error signal, as used to correct for frequency fluctuations larger than 8 MHz. The electronically added +/- 0.4 offset ensures that when the laser becomes unlocked, it will relock to its original position, and not to a side mode. This trace is shown scanning the frequency from high to low.

detector monitoring the optical error signal, as changes in frequency, and thus produce anomalous results from the frequency locking system. The implementation of the intensity stabilization is shown in the schematic diagram for the laser system of figure 2.2.1. The intensity stabilizer consisted of an acousto-optic modulator (AOM) placed immediately after the laser output, with the zero order beam being retained. Immediately after this a beam splitter directed a beam to a photodiode and the signal from the photodiode was used to control the RF driving the AOM. Thus as the laser power increased, so did the driving RF to the AOM, pushing more of the laser power into the higher orders and reducing the intensity of the main beam, and vice versa for lower intensity. The AOM was tuned to diffract some of the beam into the higher orders at the desired intensity, to allow for decreases in the laser intensity. This system could correct for intensity fluctuations up to 200 kHz, and the subsequent residual variation was around 1%. The intensity stabilizer could compensate for variations of up to 20%, which was sufficient for most of the variations which occurred, however in some cases bubbles in the dye jet would briefly interrupt the beam, dropping the intensity to zero and dropping the laser out of lock. In these cases the relocking scheme described above was required.

Detailed measurements of the laser frequency stability are given in chapter 6, however it is worth noting here that when the research described in this work commenced the laser frequency stability was typically a few kHz at short timescales, and several hundred kHz at longer timescales. As discussed below the achievable stability at the completion of this work was better than 200 Hz on a 5 ms timescale and better than 1 kHz/s at longer times.

2.3 Phase Sensitive Detection

A number of the experiments described in this work were only feasible because of the introduction of phase sensitive detection of the coherent transient signals, into the optical system. For example the observation of the signal phase allowed a direct interpretation of the response of the system to changes in the relative phase of the optical input signal, such as with the selective data erasure described in chapter 4. The separation of the two orthogonal signal phases also allowed the exploitation of new and potentially valuable memory techniques such as those described in chapter 5.

The phase sensitive detection (PSD) system was constructed around a modified Mach Zehnder interferometer, with the modification referring to the introduction of a heterodyne detection scheme. This system is similar to that used by Muramoto et al (Muramoto 1981) A schematic diagram of the PSD system is shown in figure 2.3.1. The optical local oscillator beam was produced by inserting a 5% beam splitter into the main beam. A second beam splitter was used to recombine this beam with the main (signal) beam after the main beam had been transmitted through the sample.

Before reaching the sample the main beam was passed through two acousto-optic modulators (AOMs), with the first-order diffracted signal being retained in each case. The first AOM shifted the frequency of the beam by 80 MHz, while the second sifted the beam frequency by 90 MHz in the reverse direction. The result was that the beam reaching the sample was shifted by –10 MHz from the beam exiting the laser, and thus also from the optical local oscillator. In consequence, once the signal was recombined with the optical local oscillator signal, the result was a beat at 10MHz. A third AOM was included in the system after the transmitted beam and the local oscillator beam had been recombined to enable selective attenuation of the light reaching the detector, and thus protect the photodiode.

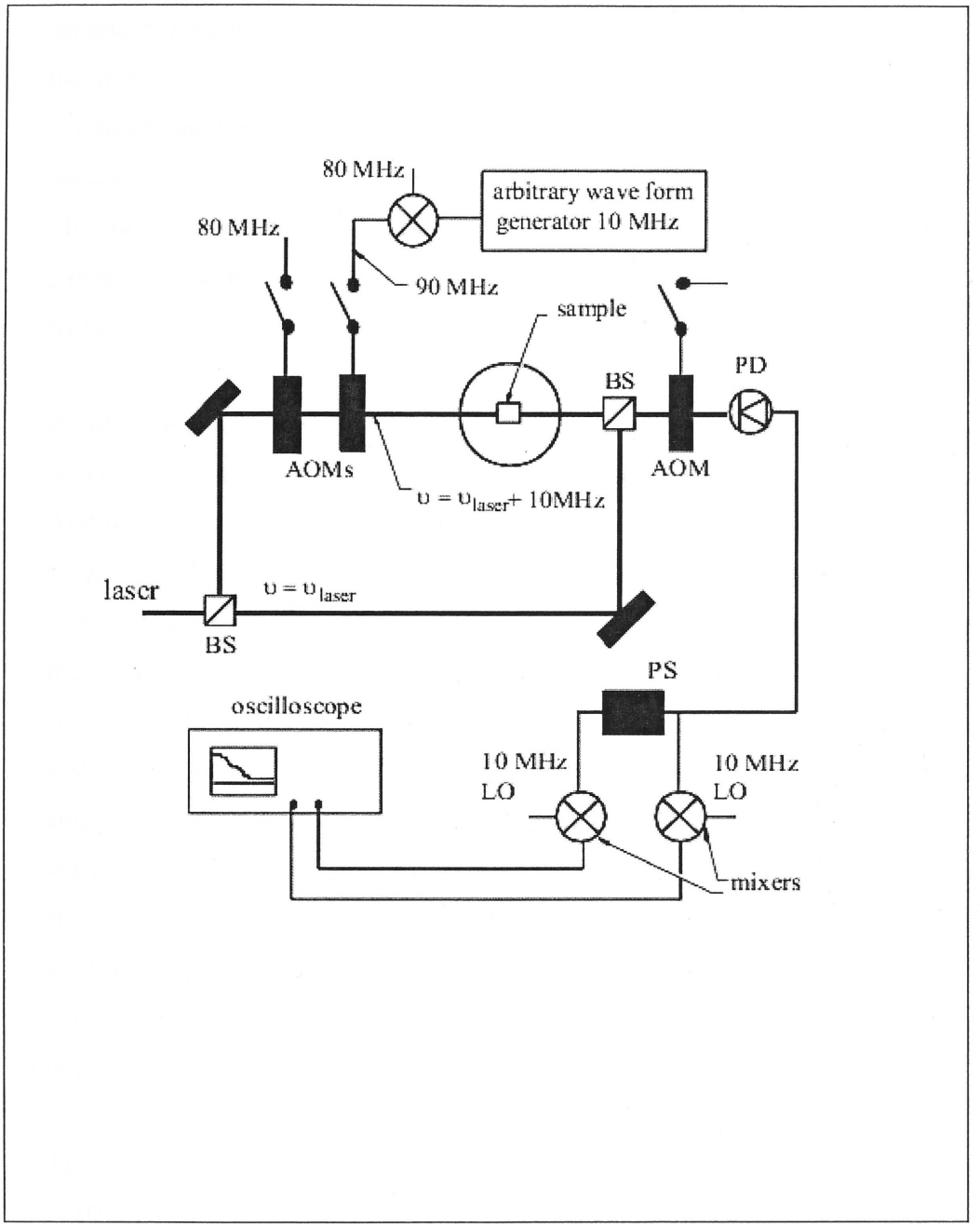

Figure 2.3.1: Schematic diagram of the Phase Sensitive detection system. AOM refers to Acousto optic modulators, BS refers to optical beamsplitters, PS refers to the phase shifter, and PD refers to photodiode detectors.

In addition to providing a reliable frequency shift to the transmitted beam the two pre-sample AOMs were used to control the amplitude of the transmitted light, by controlling the amplitude of the RF driving each AOM. This was used to determine both the amplitude and timing of pulses reaching the sample and, by switching both AOMs together, the light could be suppressed by better than 60dB when the light was set to off. The rise times of the AOM responses was approximately 10ns, which was approximately 2 orders of magnitude less than the 1 μs length of the typical short pulses used in this work.

Another important function of the pre-sample AOMs was the control of the relative phase of the light incident on the sample. By changing the phase of the RF driving one of these AOMs, the phase of the beam transmitted through it is also changed by the same degree. With suitable switching of the RF, the relative phase of the transmitted signal can thus be accurately controlled. For the majority of the work described the RF signals for both of the AOMs was produced by repeated frequency doubling and mixing of a single very stable 10MHz signal, with phase control achieved through the use of rf delay lines. This system was constructed in house. In some cases where more complex modulations of the amplitude and/or phase of the input signal was required, a single fixed frequency 80MHz signal was used to power the first AOM and mixed with a 10MHz signal from a high stability synthesized function generator. This synthesizer could be used to produce arbitrary amplitude and phase modulation of the AOM driving field, without the need for external delay lines. This method was more versatile, but it did allow an additional source of phase noise through the use of two RF generators.

The effect of the interferometer was that the signal at the detector was a heterodyne beat at 10 MHz. A 2 MHz bandpass filter centred at 10 MHz was used to reduce the noise, then the electronic signal was converted to DC using a dual double balanced mixer. The other input for the mixer was a 10 MHz local oscillator signal from the same RF source used to drive the AOMs. The mixer produced two orthogonal outputs, representing the two phase components of the signal. The phase of the transmitted light, for example the

readout pulse used for an echo sequence, was used to provide a relative reference for the phase of the signal.

A heterodyne detection scheme was used because it allowed excellent signal to noise to be obtained. For a suitably high intensity ratio between the local oscillator beam and the signal beam, shot noise limited detection can be achieved. (Yariv, 1985). This is possible because the heterodyne detected signal is proportional to both the transmitted signal beam intensity and the local oscillator beam intensity. When the intensity of the local oscillator beam is increased, the signal strength increases proportionately, whereas noise from sources other than the laser noise do not. Thus for sufficient oscillator intensity the quantum laser noise dominates.

To measure the system detection efficiency the sample was removed and the intensity of the signal light reaching the detector was measured used to calibrate attenuation provided by the pre-sample acousto-optic modulators. This was done at –10dB (3mW) and –21dB (0.24mW) attenuation. The laser was then set to produce 1μs pulses, and the attenuation was reduced to determine the minimum power at which the pulses could be discerned from the surrounding noise. During this process the power of the local oscillator beam was kept constant. The minimum detectable power was at –100dB. This corresponds to a minimum of 20 photons at 2MHz bandwidth as the minimum detectable signal, and thus a detection efficiency of 10%.

In addition to the stability of the laser good phase stability from the interferometer was essential to obtain accurate results. To check this the output from the laser was used in continuous wave mode and the phase sensitive detector output was fed into a spectrum analyzer. From this, the frequencies of the dominant noise sources were determined. Initially all of the optical mounts were replaced with 2.5cm diameter optical pillars, and a plastic curtain was used to reduce bulk air turbulence and dust particles. Subsequently specific noise sources were identified using a piezo-electric microphone to localize specific vibrations and separately a frequency generator and small speaker to induce

resonance with the noise sources. This allowed the stability of the interferometer to be improved considerably.

Chapter 3 Rare Earth Material Studies

3.1: Rare Earth Ions and the Holeburning Mechanism

The optical memories described in this thesis are based on a physical process termed spectral holeburning. Spectral holeburning requires an optical transition that is inhomogeneously broadened, subsequent irradiation of this transition with a narrow band laser excites a subset of centres, namely those resonant with the laser frequency. A fraction of these excited centres decay into states other than the original ground state (such as other hyperfine ground states or even states formed through photo-chemical or photophysical mechanisms). The net effect of this process is that once all of the excited centres have decayed from the excited state, there are less ground state centres remaining at the resonant frequency of the laser and thus there is a decrease in absorption at that laser frequency. For a sufficiently narrow laser bandwidth, relative to the inhomogeneous width of the transition, this decrease in the absorption will be seen as a (spectral) hole in the absorption profile, relative to the rest of the inhomogeneous lineshape. Depending on the alternative state that the centres decayed into, a spectral hole can have a very long lifetime. If the presence or absence of a spectral hole at a particular frequency is used to code for a bit of information then such spectral holeburning provides the basis for an optical memory system. The methods of utilising this memory capacity is presented in chapter 4, this chapter will be restricted to a discussion of some holeburning materials and the specific holeburning processes that occur within these materials, as well as an analysis of their suitability as a memory material.

The centres of interest to this work are trivalent rare earth ions in crystals. The reason for the interest is that they can give narrow optical transitions arising from optical transitions associated with well-screened electron configurations. The transitions are within the open shells of $4f^n$ electrons which are screened by lower energy s and p electron shells and in a

crystal field the energy levels are only slightly perturbed from the free ion energies, see figure 3.1.1.

The intra-configuration transitions are nominally forbidden and only weakly induced by odd-parity crystal fields. However, as dynamic crystal fields are also small the transitions are largely electronic with not much evidence of vibrational sidebands. Also broadening of the electronic transitions by vibrational processes is readily eliminated by lowering the temperature and at low temperatures the magnetic effects become the dominant interaction in determining the line widths. Thus, for narrow homogeneous linewidth one must identify transitions between meta-stable states, identify states that are less susceptible to magnetic effects and eliminate as far as possible magnetic moments from the lattice.

The materials initially selected have relevance for optical memories but largely because they exhibit the relevant phenomena rather than the material offering particular promise. The narrowest homogeneous lines will be between states of rare earth ions with no first order electronic moment. Two transitions that meet these criteria are the $^7F_0 - ^5D_0$ transition of Eu^{3+} and the transition between the lowest crystal field levels of the $^3H_4$ and $^1D_2$ states of the Pr^{3+} ion occupying a non-axial site in a crystal. One material selected was CaF_2 and this was largely because of the availability of Eu^{3+} and Pr^{3+} crystals of reasonable optical quality. The crystal exhibited optical transitions associated with numerous different defect centres but in the case of Eu^{3+} centres all of the centres had been studied previously. However, in the case of Pr^{3+} after a heat treatment a "new" centre was identified and with a preference for original work a study of this centre is presented in the next section. This is followed by study of Eu^{3+} in a stoichiometric material $EuCl_3.6H_2O$ a material which exhibits some novel spectroscopic characteristics. These initial Pr^{3+} and Eu^{3+} studies allowed us to identify some of the more desirable characteristics of a memory material and a promising material Y_2SiO_5: Eu^{3+} became available. Thus the final section of this chapter deals with a study of Y_2SiO_5: Eu^{3+}. The parameters associated with the material are determined and its suitability as an optical memory material is assessed.

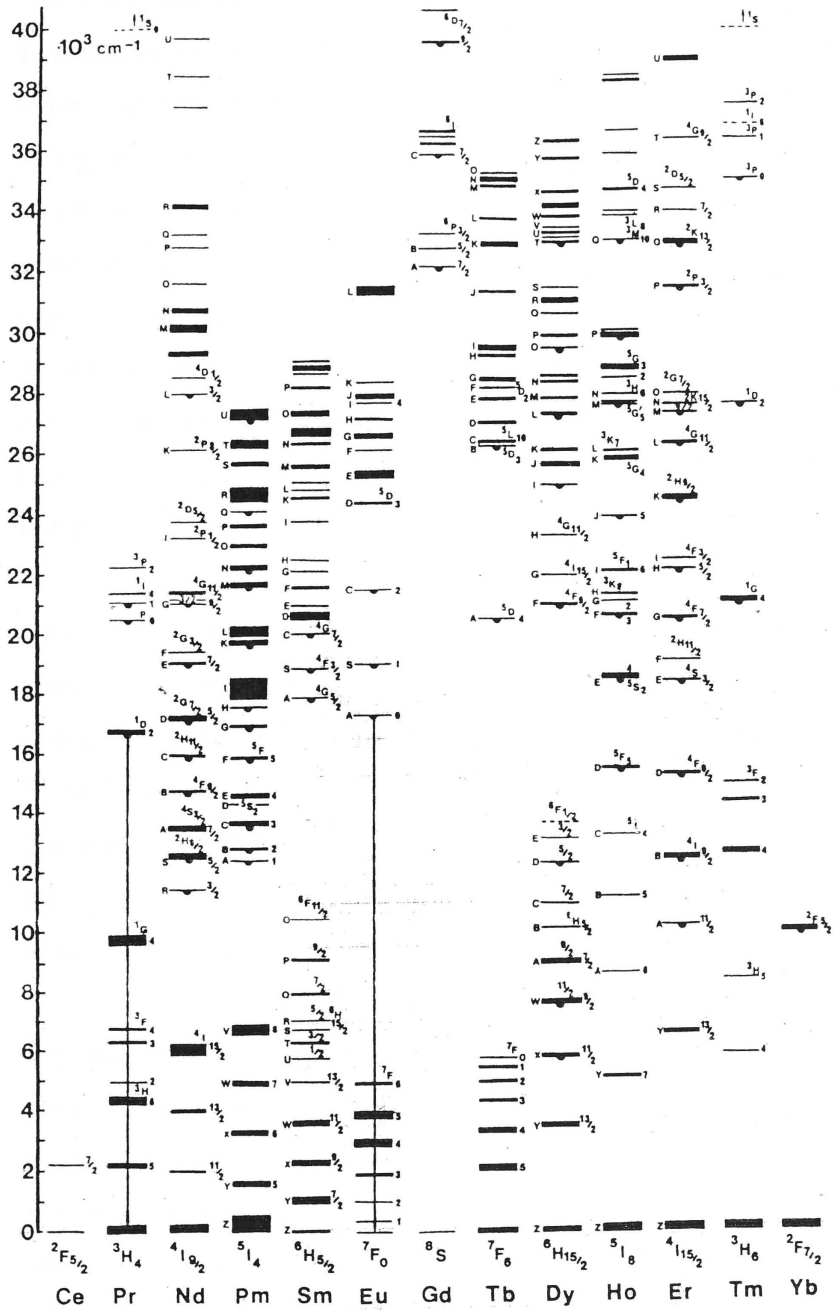

Figure 3.1.1: Classic 'Dieke diagram' showing energy levels for the free trivalent rare earth ions (Macfarlane 1987). The optical transitions directly excited in this study are indicated.

The same basic holeburning mechanism is involved in all three rare earth centres studied. The processes involved are well established and thoroughly described in the literature but as these are fundamental to the development of the holeburning memory we give a brief description.

The three centres have low symmetry such that all electronic degeneracy is lifted and, hence, the optical transitions are between non-degenerate electronic levels. However, there is hyperfine splitting associated with a nuclear spin of $I = 5/2$ in each case and the quadrupole splitting of the hyperfine levels is greater than homogeneous linewidth of the optical transition. Thus, individual centres involve transitions between three ground state hyperfine levels ($\pm 1/2$, $\pm 3/2$ and $\pm 5/2$) and three excited state hyperfine levels as shown in figure 3.1.2.

Optical transitions will conserve the nuclear spin but as a consequence of the low symmetry the orientation of the quadrupole will be different in the ground and excited states. Hence the nuclear eigenstates will differ and many of the nine possible optical hyperfine transitions will be allowed. Exciting one hyperfine transition may decay via a different hyperfine transition and, the optical cycle result in a change in occupation of the ground hyperfine level. The hyperfine lifetime may be long and the system will remain in the second hyperfine level. This is the basis of the memory process.

Imperfections in the crystals cause a variation in the optical frequencies from centre to centre and this inhomogeneous distribution of frequencies is much larger than the optical homogeneous width and usually larger than the quadrupole splittings (the $EuCl_3.6H_2O$ system studied is an exception). When a laser is tuned to a frequency within the optical inhomogeneous line it only excites a subset of centres. It will only excite centres for which there is a transition coincident with the laser frequency. For a given centre it can be any one of the hyperfine transitions and when considering all optical centres there will be examples of each of the optical hyperfine transitions. The laser will cause a redistribution of the population in the ground state hyperfine levels and this gives rise to a decrease in absorption (hole) at some frequencies and an increase (antihole) at other frequencies. All possible transitions have then to be considered to determine the

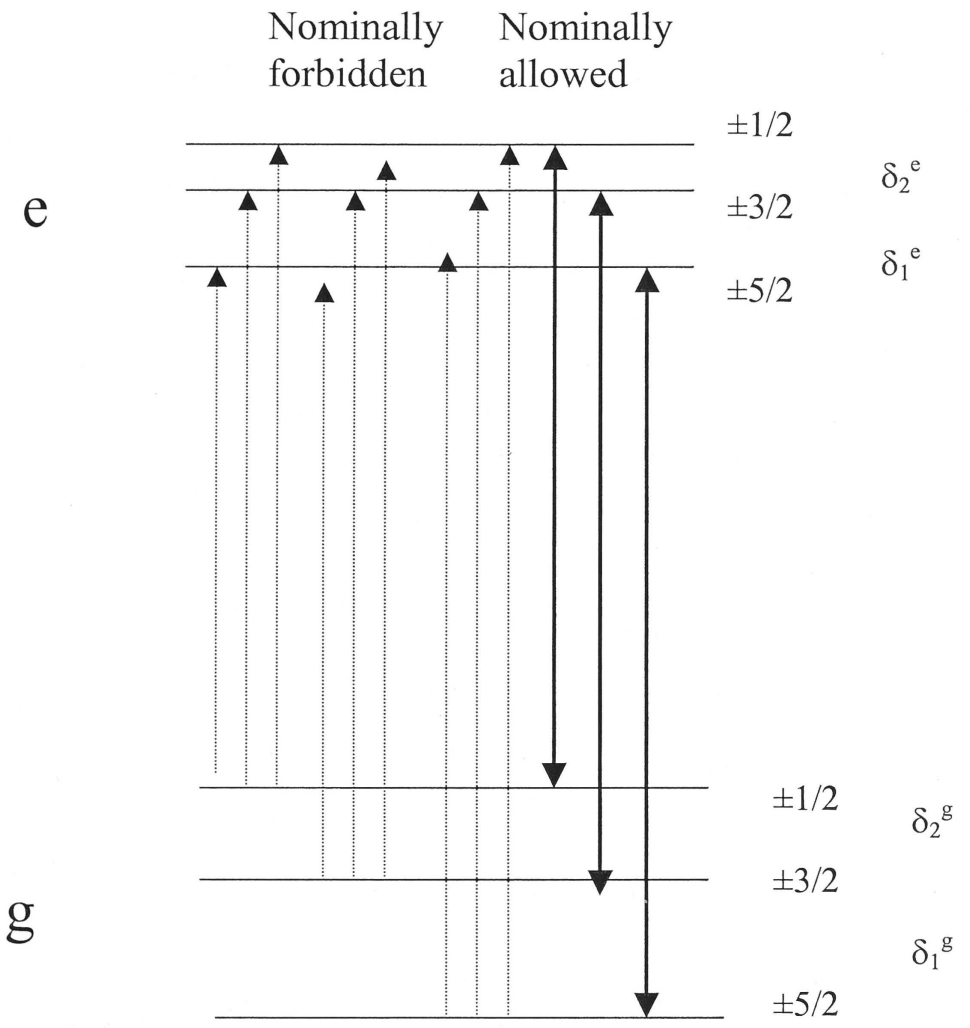

Holes at: $\pm\delta_1^e$, $\pm\delta_2^e$, $\pm(\delta_1^e+\delta_2^e)$

Anti-holes at: $\pm\ \delta_1^g$, $\pm\ \delta_2^g$, $\pm(\ \delta_1^g+\delta_2^g\ )$

$\pm(\ \delta_1^g\pm\ \delta_1^e)$, $\pm(\ \delta_2^g\pm\delta_2^e)$, $\pm(\ \delta_1^g\pm\ \delta_2^e)$, $\pm(\delta_2^g\pm\delta_1^g)$

$\pm(\delta_1^g\pm(\delta_1^e+\delta_2^e))$, $\pm(\delta_2^g\pm(\delta_1^e+\delta_2^e))$

$\pm(\delta_1^g+\delta_2^g)\pm\delta_1^e$, $\pm(\delta_1^g+\delta_2^g)\pm\delta_2^e$, $\pm(\delta_1^g+\delta_2^g\ )\pm(\delta_1^e+\delta_2^e)$

Figure 3.1.2: Schematic diagram of trivalent rare earth center hyperfine levels. Shows allowed transitions (bold arrows) and the nominally forbidden transitions (dotted arrows). The predicted positions of the spectral holes and antiholes are given in terms of the differences between the hyperfine energy levels.

frequencies of the holes and antiholes. It can be established that they will be separated from the frequency of the burning laser at ground and excited state hyperfine frequencies and at sums and differences of these splittings (Macfarlane 1987) and many are seen in the case of $EuCl_3.6H_2O$ described below. The spectrum of holes/antiholes can obtained by measuring the absorption in a frequency range. This is usually achieved by subsequently sweeping the burn laser, perhaps with reduced intensity, and detecting the total emission as a function of laser frequency. This is the approach used here.

The holeburning spectrum can often be used to determine the quadrupole splittings. However, this is frequently combined with a second experimental technique that involves some of the same processes. A laser is held at fixed frequency at a frequency within the inhomogeneous line and as previously will cause spectral holeburning. An rf field is then applied to the crystal and is swept in frequency. When the frequency coincides with a ground state hyperfine separation it inhibits one of the holeburning paths and there is a reduction in the hole depth detected by an increase in emission. This optical/rf double resonance technique readily gives the ground state hyperfine splittings. It is termed optically detected nuclear magnetic resonance (ODNMR) or, as it is frequently applied with no applied magnetic field, optically detected nuclear quadrupole resonance(ODNQR). The technique gives essentially the same information as Raman heterodyne detected NMR (RH-NMR). ODNMR is an incoherent technique whereas RH-NMR is a coherent technique. The same fields are applied but the signal is detected in transmission as a beat frequency on the transmitted laser beam.

3. 2. Pr^{3+} Doped CaF_2

Previous studies

In Pr^{3+} doped calcium fluoride the trivalent ion substitutes for a divalent Ca^{2+} ion. To preserve charge neutrality an additional negative charge is need and there are two distinct ways this is achieved. In one a monovalent anion occupies the interstitial space adjoining the Pr^{3+} ion. In the other way a divalent anion substitutes for one of the monovalent F- nearest the Pr^{3+} ion.

Spectral holeburning studies have been made in both types of charge compensated centre. For example, the most common centre in Pr^{3+} doped CaF_2 crystal is of the first type where a fluorine ion in an interstitial position along a <100> direction acts as the charge compensation. This gives a tetragonal centre of C_{4v} symmetry and a transition between the lowest levels of the $^3H_4$ and $^1D_2$ multiplets allows emission and absorption at 594.1 nm wavelength. This transition is an A – E transition and the spectrum shows a resolved hyperfine splitting of 2.77 GHz. A holeburning study of this material was the first case where super hyperfine was involved (therefore, different to the energy levels and holeburning scheme discussed above) and the work still represents the most comprehensive study of such a system (Burum 1982, Macfarlane 1984). As well as obtaining holes and anti-holes on the separate hyperfine lines they obtained optically detected magnetic resonance (ODMR) signals at the hyperfine microwave frequencies of 2.77 GHz and separate ODMR at superhyperfine splittings of 9.20, 9.975 and 20.65 MHz. These latter signals are associated with spin flips of adjacent fluorine ions in two of the nearest neighbour sites and interstitial sites respectively.

An example of the second type of charge-compensated centre is an oxygen compensated centre. An O^{2-} ion can replace a F^- ion along a <111> direction from the Pr^{3+} ion and gives a trigonal C_{3v} site. This gives a transition between the lowest levels of the $^3H_4$ and $^1D_2$ multiplets at 593.5. It is assigned to an E – E but the line is broad (30 GHZ) and the hyperfine structure is not resolved. However, holeburning experiments establish the hyperfine splittings in the ground and excited states as 4.12 GHz and 4.06 GHz respectively. ODMR experiments gave the superhyperfine splittings associated with the three non-equivalent nearest neighbour fluorine of 10.5 MHz, 13.2 MHz and 20.2 MHz, respectively (Hasan 1987).

There have been studies of other centres in Pr^{3+} doped CaF_2. For example, Cockroft et al (Cockroft 1987) have studied centres where H^-, D^- or T^- replaces the F^- in C_{4v} charge compensated centres. In this case the holeburning mechanism is different in that it is photo-physical, as the compensating ion can move to an alternative compensating site. There has also been a study of an alternative oxygen compensated site (Masui 1967).

Indeed there are inconsistencies in the literature regarding the centres that occur for heat treatment in oxygen or moist air. As a consequence, although the site symmetries of centres are established, the precise nature of the oxygen centres are not firmly established. The samples for this work were prepared in this way but this issue was not investigated in detail.

Present study

These studies used a CaF_2 crystal doped with 0.1% Pr^{3+} for which the dominant spectrum was the C_{4v} , F^- compensated centre. The crystal was heated in moist air at a temperature of 800°C for 8 hours and this introduced new centres into the crystal. The excitation spectrum of this crystal, monitoring red filtered fluorescence, is shown in figure 3.2.1

The measurements are for a crystal at pumped helium temperatures of ~2 K. The photomultiplier was gated open 10μs after a 20ns pulse from a N_2 pumped tunable dye laser and all emission in a ~1ms period detected. The two strong lines at 593.6nm and 594.1 nm are associated with the C_{4v} , F^- centre whereas the line at 593.5 nm is associated with the C_{3v} , O^{2-} compensated centre. When investigated with a CW narrow band (1 MHz) tunable dye laser both the C_{4v} and C_{3v} centre exhibit spectral holeburning as described previously. The only other line to exhibit spectral holeburning was that associated with the unassigned centre giving the sharp excitation line at 596.4 nm. This centre was studied in this work.

Selective emission establishing the position of some of the levels associated with the unidentified centre was achieved by exciting at 596.4nm and scanning a monochromator to determine the emission spectrum shown in figure 3.2.2.

In this way the following levels were established associated with the $^3H_6$ (4316 and 4247 cm-1), $^3H_5$ (2241 and 2232 cm^{-1}) and $^3H_4$(0 and 48 cm^{-1}) multiplets. Also subsequent selective excitation established that a level at 16797 cm^{-1} in the same centre gives rise to the absorption line at 595.3 nm in figure 3.2.1. The selective excitation also established

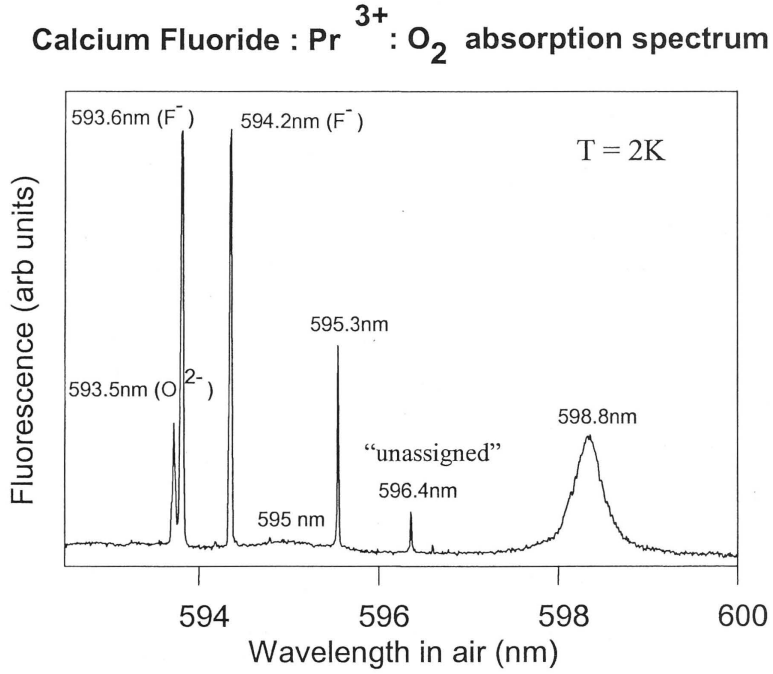

Figure 3.2.1: Excitation Spectrum of $CaF_2:Pr^{3+}:O_2$ sample in the $^1D_2 \rightarrow {}^3H_4$ transition region. Sample temperature 2K. Peak Assignments are labeled where known. The spectrum was obtained from scanning a nitrogen laser pumped dye laser and detecting sample fluorescence using a broadband red filter and a photo-multiplier.

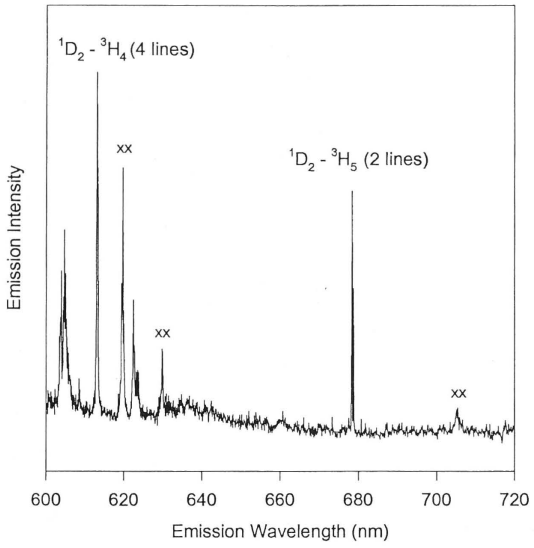

Figure 3.2.2: The emission observed while exciting the 596.4 nm absorption line. Peaks due to the assigned transitions within the center are labeled. The peaks marked "xx" are due to exciting an overlapping center which has an absorption peak at 595 nm.

that the other sharp line in the spectrum at 592.1nm is associated with another unidentified centre.

For the centre of interest the transition at 596.4 nm shows no structure beyond a single smooth peak. It has a linewidth of 10 GHz which. The C_{4v} F^- centre in the same sample can be used as an indication of the broadening due to strain in the sample and in this case the 2.77GHz structure is just resolved. It is inferred that any unresolved hyperfine splitting of this new centre is less than 1.7GHz in magnitude. Consistent with this the holeburning does not indicate the presence of any hyperfine structure. The 2K holeburning spectrum of the 594.6 nm transition is shown in figure 3.2.3.

The holeburning spectrum was recorded with the 1 MHz linewidth laser using a burn and scan technique and monitoring the fluorescence emission at 613 nm. The hole burnt rapidly and was 100% deep within one second. It also recovered quickly although 5% remained after 1 minute. Anti-holes can be seen in the wings of the central hole (upper trace in figure 3.2.3). No structure was observed at separations larger than the range shown, consistent with the lack of hyperfine structure. The lower trace shows a hole burnt in the 594.1nm line of the C_{4v} F^- centre. This hole is broader with a width of 30 MHz compared to the top trace with a width of 10 MHz. Macfarlane et al. (Macfarlane 1981) have recorded a holewidth of the C_{4v} , F^- centre of 9 MHz by reducing the intensity of the read beam. In the present study the holes have been burnt and read all under the same conditions which can partially explain the larger holewidth. However, it is clear that the O^{2-} centre (596.4 nm) gives narrower holes than the C_{4v} , F^- centre. This is attributed to higher symmetry of the C_{4v} centre where the orbital degeneracy can be lifted and, hence, the centre will be more susceptible to strain. There is no hyperfine associated with the levels involved with the O^{2-} centre and the levels are non-degenerate. The transition is likely to be less susceptible to strain.

Measurements of the ODNMR spectrum were made with the laser frequency fixed in resonance with the 596.4 nm line, and the emission monitored as an rf field was applied

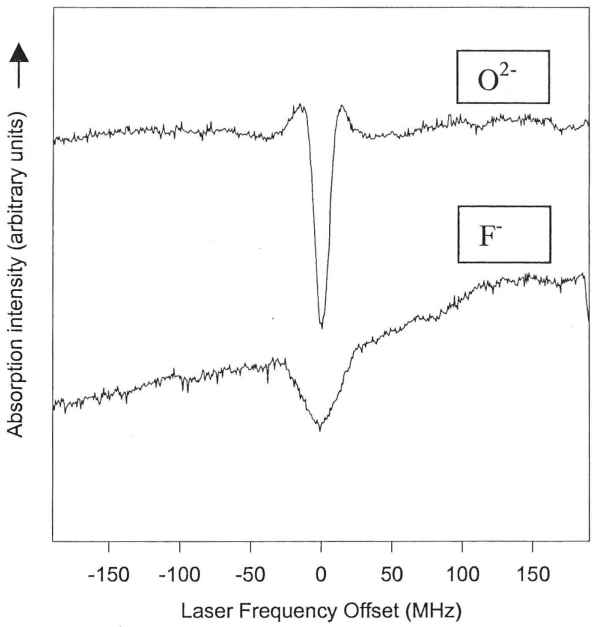

Figure 3.2.3: The spectral hole burnt in the 596.4 nm absorption line, observed by a burn scan technique. For comparison the lower trace gives a spectral hole burnt in the 594.2 nm resonance of the same sample shown on the same scale.

to a coil wound round the sample. The field was swept in the 0 – 100 MHz range and the resultant spectrum is shown in figure 3.2.4.

Two peaks were observed at 22 ±1 MHz and 43±1 MHz. For fluorine crystal lattices a strong correlation exists between the local magnetic field, the fluorine nuclear spin flip frequencies and the homogeneous linewidth of luminescent centres (Sellars 1995). This correlation supports the suggestion that the narrow spectral hole observed for the 596.4 nm transition is absorption from a singlet ground state where the small local magnetic fields would produce low fluorine spin flip frequencies. The resonances observed are consistent with that due to transitions between pseudo-quadrupole levels of the I = 5/2, Pr^{3+} nucleus. In this case the one to two ratio of the hyperfine frequencies and the absence of a resonance at the combined frequency of 65 MHz are characteristic of a centre with near axial symmetry.

Reeves and Macfarlane (Reeves 1993) have analysed the pseudo-quadrupole splitting of the ground state in the multi-hydrogenic modification of the C_{4v} centre, relating the energy of the first resonance to the quadrupole splitting between the two lowest electronic levels. The quadrupole splitting parameter, D, is given by

$$2D = 2\, A_J^2\, |\langle \phi^+ |\, J_z\, | \phi^- \rangle|^2 / \Delta. \qquad (3.2.1)$$

The J_z matrix element was derived from the C_{4v} centre g-value and was found to be in excellent agreement for all of these centres. If a similar analysis is used here for the 596.4 nm centre with the same value for the matrix element and using the ground sate splitting of 48 cm^{-1}, we find that the calculated hyperfine splitting is too small by a factor of 2. However, it is more closely related to the C_{3v}, O^{2-} centre associated with the line at 593.5 nm. The g-value of this centre has been measured to be g = 5.9 (Boonyarith 1992). If this value is used for the derivation of the matrix element then the calculated lower hyperfine splitting is 22.6 MHz, in excellent agreement with experiment. Thus it is suggested that the present centre studied is a distorted O^{2-} centre distorted from trigonal symmetry.

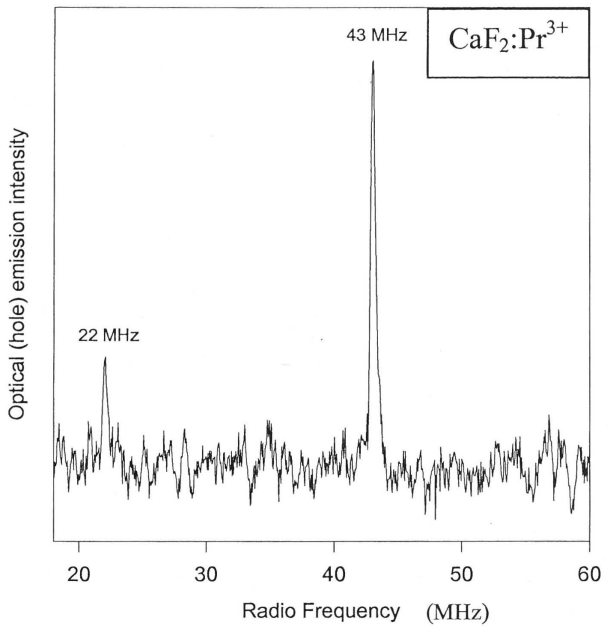

Figure 3.2.4: The optical – RF double resonance spectrum observed from spectral holeburning of the 596.4 nm absorption transition. Measurement errors are estimated to be +/- 1 MHz.

Thus, in the present studies of spectral holeburning of an unidentified centre we have been able to make some deductions regarding the likely character of the centre. The main purpose of the study was to obtain an understanding of both the experimental procedures and the processes involved in spectral holeburning and for this the study was successful. For the longer term project of developing an optical memory the material is readily recognised as being unsuitable. All of the reasons for this unsuitability need not be accurately detailed here but some more notable aspects that are undesirable are the wide hole width (10 MHz), the very shallow persistent hole and the low percentage absorption. The oxygenation treatment of calcium fluoride also leaves a crystal with a cloudy appearance and this makes the sample unsuitable for coherent transient measurements in transmission and no echo measurements were attempted.

3.3. $EuCl_3.6H_2O$

The second material studied was a sample of europium tri-chloride. These studies were undertaken with others and have been published with five co-authors. I have been involved in all aspects of the work although not always as principal investigator. When grown out of aqueous solution the stoichiometric chloride is associated with six water molecules. The Eu^{3+} ion lies at a site of C_{2h} symmetry made up of a surrounding distorted dodecahedron with triangular faces. The transition of interest is the $^7F_0 - {}^5D_0$ transition at 580.2 nm. From excitation measurements the transition had a line width of 600 MHz. This is a remarkably small inhomogeneous broadening and reflects the fact that in a stoichiometric material there is no strain introduced by impurities. The narrow linewidth is also a consequence of the interaction between Eu^{3+} ions being weak as well as the low lattice distortion in the crystal as compared to samples doped with impurities. The reported inhomogeneous linewidth in other stoichiometric samples varies from 170 MHz in $Eu(OH)_3$ to several GHz in EuP_5O_4.

Because of the high density of Eu^{3+} the sample must be thin to avoid distortions due to re-adsorption and for the same reason it was also advantageous to detect the fluorescence from the front surface of the crystals. However, with these precautions it was found that not only was the excitation line at 580.21nm narrow but it also had structure. The hypothesis that the structure arose from the hyperfine splittings was investigated as part of the present study. The naturally occurring isotopes are ^{151}Eu and ^{153}Eu and they occur in very close to equal abundance. We were able to obtain isotopically enriched material, therefore, two sets of $EuCl_3.6H_2O$ crystals were grown from solution. (i) crystals with a 48:52 natural abundance ratio of ^{151}Eu and ^{153}Eu and (ii) crystals with a 1:99 abundance ratio. The general characterization measurements, such as selective excitation and emission, were made on the natural-abundance ratio crystal whereas the high-resolution techniques involved both crystal types. The material is prone to dissolving if it is left in a moisture-laden atmosphere. In practice this tendency to dissolve meant that an individual

sample was destroyed each time a cryostat was warmed up which was inconvenient as some observations could not be readily repeated with the same sample.

There is only one Eu^{3+} site and the energy levels are readily established through conventional emission and excitation and confirmed with selective emission and excitation. There are three degenerate levels in a $^7F_1$ multiplet but the degeneracy can be lifted by the crystal field. In an axial field two remain degenerate but here three transitions are observed, indicating all the degeneracy is lifted. The site, therefore, has low symmetry.

On excitation of the transition at 580.21 nm with a tunable high resolution laser and monitoring the $^5D_0 - {}^7F_2$ emission at 614 nm the narrow $^5D_0 - {}^7F_0$ optical excitation line shown in figure 3.3.1 was obtained.

The spectrum was measured for both crystal types (i) and (ii) and the intensity of the two spectra were scaled to give the same integrated area. The hyperfine structure is obtained in both spectra but there is also a shift in average position. Analysis of the difference between the two experimental optical transitions shown in figure 3.3.1 for the two different isotopic mixtures gives an isotope shift of 0.15(±2) GHz for the ^{153}Eu transition compared to that for ^{151}Eu. This corresponds to a shift per unit mass of 2.5×10^{-3} cm^{-1}. This is similar to optical transitions for Nd^{3+} in $LaCl_3$ of 6.5×10^{-3} cm^{-1} (Pelletier-Allard 1984) and Er^{3+} in $YLiF_4$ of $2.74\ (\pm 7) \times 10^{-3}$ cm^{-1} (Pelletier-Allard 1985).

The natural abundance sample was investigated using optically detected nuclear quadrupole resonance (ODNQR). Four lines were obtained. The signals at 26.98 and 29.02 MHz were assigned to the hyperfine transitions of the ^{151}Eu ions, and those at 70.07 and 74.57 MHz were attributed to the hyperfine transitions of the ^{153}Eu ions. The spectrum was measured at five different laser frequencies across the inhomogeneous line shape (as marked A-E) on figure 3.3.1. The results are shown on figure 3.3.2.

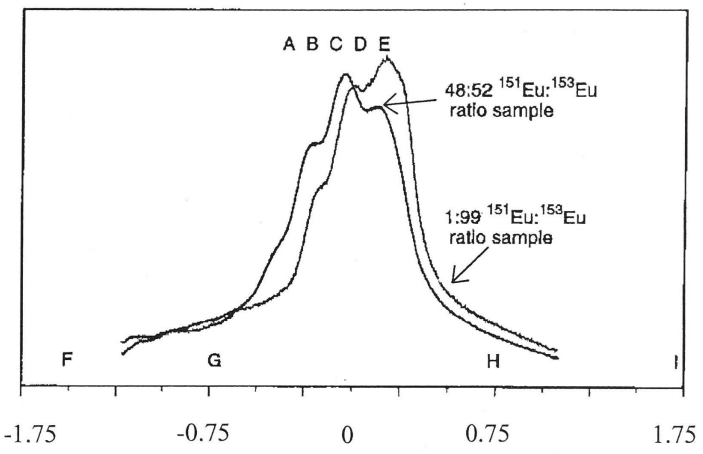

Figure 3.3.1: The $^7F_0 \rightarrow {}^5D_0$ transition for two samples of $EuCl_3.6H_2O$ of different Eu isotope composition. A, B, C, D, E, are the optical frequency positions used for the ODNQR experiments. F, G, H, I are the optical frequency center positions used for the burn scan holeburning measurements. The curve from the 99% ^{153}Eu enriched sample is the one frequency shifted to the right.

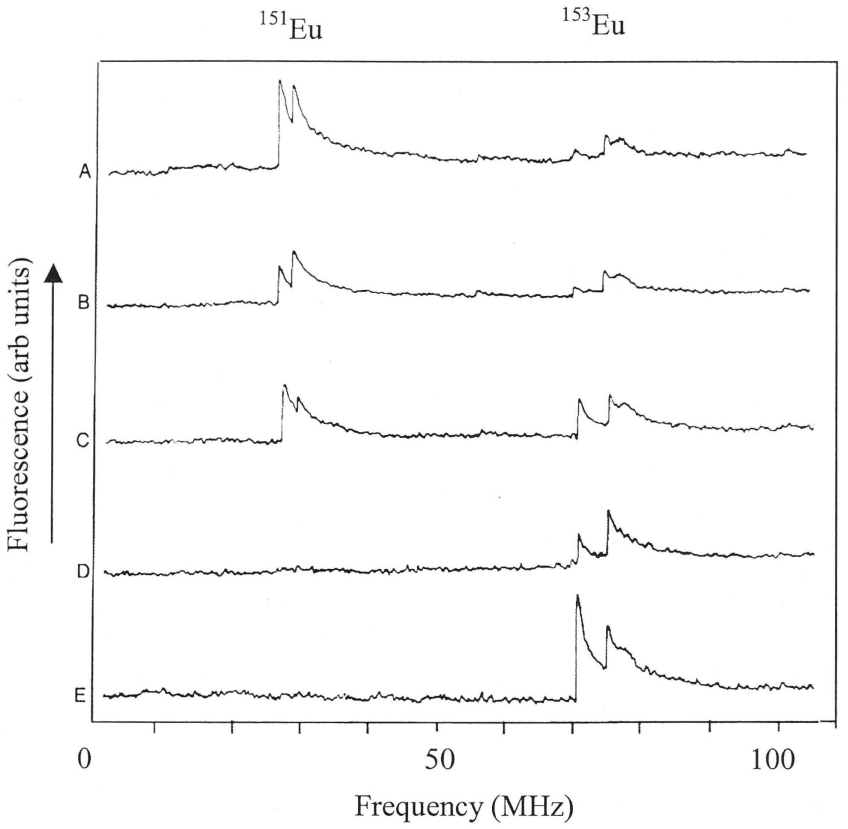

Figure 3.3.2: $EuCl_3.6H_20$ natural Eu isotope abundance sample, ODNQR signals with scanned RF, and the laser fixed at the frequencies shown as A, B, C, D. E in figure 3.3.1.

It is clear that the signals associated with the ^{151}Eu isotope are only present on the lower side of the naturally abundant sample whereas the signals associated with the ^{153}Eu occurs over a wider spectral region. Consistent with this observation the ^{153}Eu isotopically enriched sample only gives the 70.7 and 74.57 MHz signals. For the ^{153}Eu isotope it can be seen that there are changes of the relative strengths of the two hyperfine components depending on the excitation wavelength. The variation in intensity of the signals is consistent with the above isotope shift and the change of relative intensities will later be shown to be consistent with the assignments of the optical transitions for the various hyperfine components. The same resonances were obtained with CW Raman heterodyne detection and the RH-NMR lines used to provide more accurate hyperfine frequencies. Raman heterodyne signals could also be obtained in the wings of the line and used to confirm that, although the signals were weaker (and varied in sign) the frequencies were not changed with excitation wavelength.

The ODNQR gives the hyperfine splittings in the ground state. Holeburning can give the hyperfine splittings in the excited as well as ground state. However, no persistent holeburning was obtained in the centre of the zero-phonon line at the laser frequencies A-E used to give the ODNQR spectra. Persistent holes were obtained in the wings and are shown in figure 3.3.3 (a) for frequencies F - I indicated in figure 3.3.1. Given the higher spectral density of centers at the central frequency, the absence of persistent holeburing at that frequency is likely to be due to a dominance of instantaneous spectral diffusion effects.

Holeburning spectra could be obtained even with the laser detuned by up to ±1.5GHz and it is clear that the optical line has larger contributions in the wings than expected for a simple Gaussian line shape. The occurrence of holeburning in the wings of the line (where the holes had a lifetime of minutes) is attributed to the lower concentration of excited ions at these frequencies, near the line centre the concentration of ions excited is considerably greater. The failure of holeburning in these regions suggests that instantaneous spectral diffusion is occurring frequently when neighboring excited ions

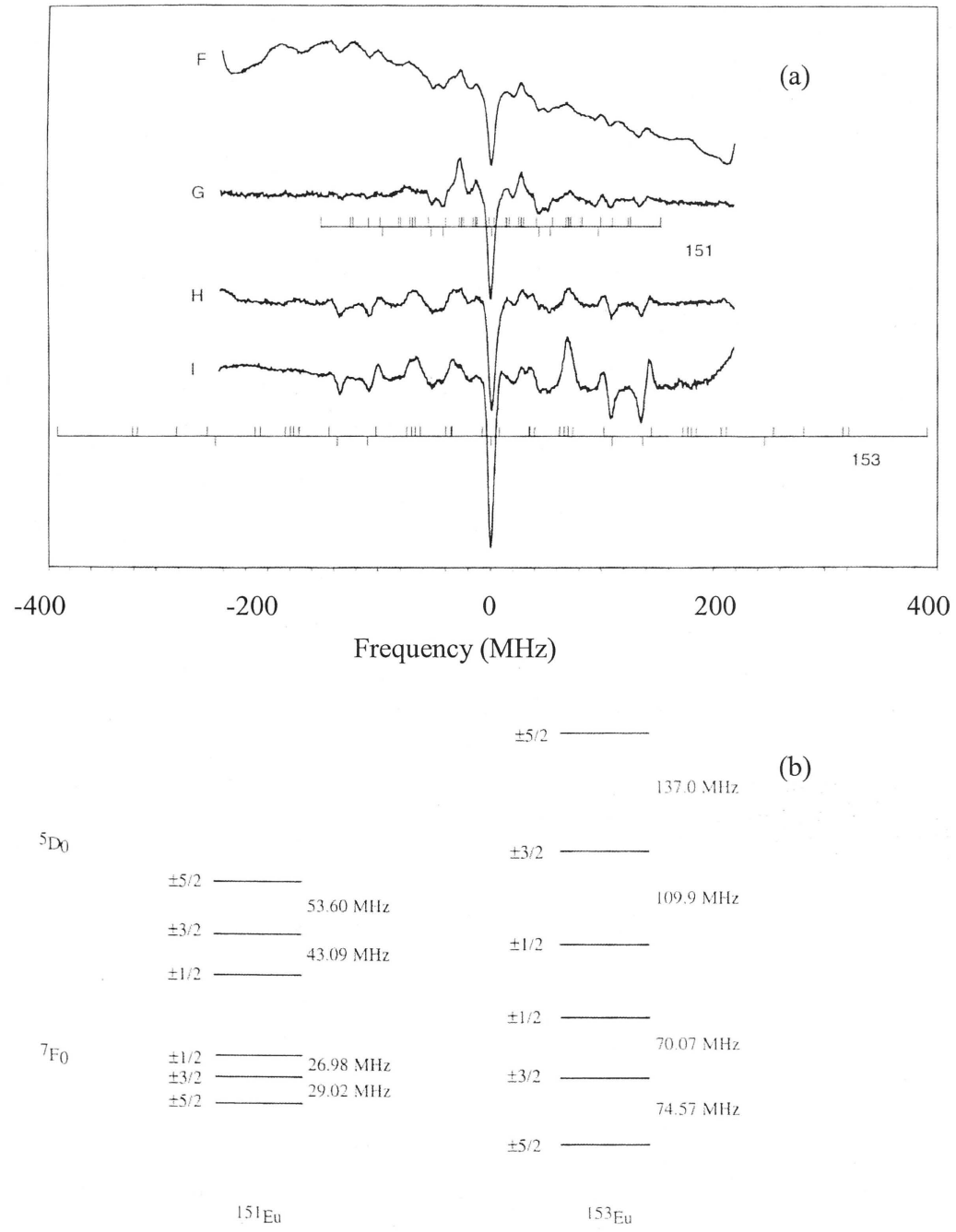

Figure 3.3.3: (a) Variation of hole and antihole structure from burn and scan measurements at different frequencies across the $^7F_0 \rightarrow {}^5D_0$ transition, using a natural isotope abundance sample. F G H I are frequency positions are marked on figure 3.3.1. (b) $^7F_0$ and $^5D_0$ hyperfine energy level structure, as calculated from burn-scan experiments and ODNQR observations.

interact, thus damping the holeburning signal. Instantaneous spectral diffusion (ISD) is the term used to explain the dephasing effects caused by the change in the local crystal field around a centre when a nearby centre is optically excited. This is equivalent to standard spectral diffusion, which results from the coupling of a centre with nearby centres, however it is referred to as instantaneous because the excitation of the coupling centre occurs through the same applied field as the target centre. For this reason ISD is more pronounced when there are high spectral and physical densities of target centers, such as at the spectral line centre of a highly concentrated sample.

With the knowledge of the ground state hyperfine splittings an analysis of the holes and anti-holes structure gives the hyperfine splittings in the excited $^5D_0$ state for both the ^{151}Eu and ^{153}Eu isotopes. The hyperfine splittings are given in figure 3.3.3(b), and the predicted position of holes and anti-holes for such frequencies are indicated in figure 3.3.3 (a). Several comments can be made regarding the hyperfine splittings.

(i) The ratio of the hyperfine splittings (between ½ - 3/2 and 3/2 –5/2) in all cases is far from a ratio of ½ for an axial site indicating a low symmetry site consistent with the earlier conclusion.

(ii) The ^{151}Eu / ^{153}Eu ratio of quadrupole splittings in the $^5D_0$ state 2.56 (± 0.12) agrees with the accepted ratio of quadrupole moments of 2.553 (± 0.001) (Silversmith, 1992).

(iii) In the $^7F_0$ state the ratio can differ from that of the moments due to admixture with the $^7F_1$ and $^7F_0$ states. The effect appears small as the ratio is 2.57.

(iv) The relative peak heights due to each of the two isotopes in the holeburning spectrum varies with laser wavelength. This variation was not fully explored, however some qualitative comments can be made. The isotope ^{151}Eu has smaller hyperfine splittings and consequently gives absorption over a narrower spectral range than that of the ^{153}Eu. The ^{151}Eu ensemble also has a lower average energy (higher wavelength) than that of ^{153}Eu

(v) Using the hyperfine splittings given in figure 3.3.3(b) the position and strength of the nine optical transitions between the three ground and three excited state hyperfine levels can in principle be predicted.

The inhomogeneous linewidth of the individual optical transitions are taken to be 150 MHz and following the prediction of (v) above the optical transition can be modelled. For the ^{153}Eu isotope the three principal hyperfine transitions give peaks roughly consistent with the spectrum of the isotopically enriched sample. (Note the order of the hyperfine levels are reversed to account for the ~300 MHz peak separations). The other six transitions have significant oscillator strength but the inhomogeneous broadening is still too large to provide any test of the correctness of the model. In the case of the ^{151}Eu isotope the hyperfine splitting is less than the inhomogeneous linewidth and will give a single optical line only marginally broader than the inhomogeneous width. The superposition of this single line with the partially resolved hyperfine structure for the ^{153}Eu isotope is sufficient to account for the small red shift of the naturally abundant sample.

The material was not selected as a candidate for a memory material but it is worth noting some of the aspects learnt as a consequence of the studies.

(i) Samples of poor physical stability are inconvenient for experimentation and would be prohibitive for a commercial memory system.

(ii) High absorption can be desirable but if the total absorption is excessive then optical readsorption can both distort the emitted signals as well as reducing the total signal strength. Reducing the physical thickness of the samples may address this, but the delicacy of such thin samples can introduce manufacturing and handling problems.

(iii) The high concentration of optically active centres can easily result in instantaneous spectral diffusion negating any holeburning and, hence, memory capability.

(iv) The laser limited holewidth of this material showed the need for a system with higher stability that available with commercial systems.

3. 4: $Y_2SiO_5:Eu^{3+}$

The figure of merit for the largest storage capacity, as noted previously, is given by the ratio of the homogeneous to inhomogeneous line width of the holeburning optical transition. It is, hence, advantageous to strive for narrow homogeneous linewidth and to achieve this is necessary to eliminate or minimise spins in the crystal. This minimisation involves the following considerations. Firstly there are the ions of the host lattice. Ideally they should not involve ions with electron or nuclear spin. Secondly there should not be any impurity ions in the crystal with electron or nuclear spin and likewise there should not be vacancies or defects with electron spins. The fourth aspect involves the incorporation of the rare earth ion, specifically the ion site within the lattice must lack inversion symmetry to induce electric dipole transitions and the symmetry should be non-axial for efficient holeburning. During the course of this work crystals matching these conditions namely crystals of $Y_2SiO_5:Eu^{3+}$ became available. The crystals could be grown with high optical quality free from defects and other impurities. The naturally occurring oxygen and silicon only contain small percentage of isotopes with non-zero spin (oxygen, 0.1% of I= 1/2) and silicon, 0.5% of I =1/2) whereas Y although 100% of I = ½ the magnetic moment of ^{111}Y is small (= 0.21 kHz/G). The material was developed by a group in University of Montana interested in optical memories and they and others have reported some of the characteristics. These are summarised in the next section.

Published work.

$Y_2SiO_5:Eu^{3+}$ crystal is monoclinic. It belongs to the C_{2h}^6space group with eight molecules per unit cell and two types of inequivalent Y^{3+} sites each with C_1 symmetry. The Eu^{3+} substitutes for the Y^{3+} and the $^7F_0 - {}^5D_0$ zero-phonon line associated with these two sites are at 579.88nm (termed site 1) and 580.05 laser wavelength (termed site 2) (Yano 1991, 1992).

(i) Inhomogeneous line width and polarisation

The inhomogeneous line widths of the two sites are slightly different. However, for the same nominal concentration of 0.1% Eu different values are given by Yano et al (Yano 1991, 1992)and Equall et al (Equall 1994, 1995a, 1995b). For site 1 the values

quoted are 8.6 GHz and 4.1GHz by Yano and Equal respectively. For site 2 the equivalent values are 5.6 and 3.8GHz. However the line broadens almost linearly with concentration such that the absorption at line centre is almost constant, and these different observed linewidths surely reflect small variations in concentration. Our sample had a linewidth of 10 GHz for site 1.

There is no marked polarization dependence of the site 2 transition and Equall et al has obtained a peak absorption coefficient of 1.4 cm^{-1} corresponding to an oscillator strength of 3.1×10^{-8}. They also obtained a smaller absorption coefficient for site 1 and smaller oscillator strength of 1.2×10^{-8}. However, the absorption of site 1 is polarised and in the preferred direction has an approximate oscillator strength of 8.8×10^{-8}, Equall et al did not specify which direction they used for their measurement.

(ii) Energy levels

Many of the levels of the ^7F manifold have been obtained by Yano et al (Yano 1991, 1992) from selective emission measurements. For site 1 the levels are as follows $^7F_1$: 203, 418 and 508 cm^{-1} and $^7F_2$: 864, 880, 924 1086 and 1283 cm^{-1} and site 2 the levels lie at $^7F_1$: 224, 409 and 493 cm^{-1} and $^7F_2$: 896, 1003, 1074,1132 and 1183cm^{-1}.

(iii) Lifetime

The measurements of T_1 for the two sites have been reported and are in reasonable agreement. Yano et al. (Yano 1991) giving values of 2.0 ms and 1.7 ms for site 1 and site 2 respectively and Equall et al.(Equall 1994) giving values of 1.9 ms and 1.6 ms.

(iii) Holeburning and holeburning lifetimes

The holeburning has been reported by Yano et al (Yano 1991) for both sites. They obtain a clear spectrum with six side holes on either energy side of the central hole plus thirteen anti-holes each to the high and low energy sides of the main hole. The hole spectrum can be readily analysed (see section 3.1) to give the excited splittings of the two naturally occurring Eu isotopes. For site 1 these are 75 and 102 MHz for ^{151}Eu and 194 and 260 MHz for ^{153}Eu. For site 2 the splittings are 63 and 108 MHz for ^{151}Eu and 160 and 274 MHz for ^{153}Eu.

The lifetime of the holes are stated to be longer than 1 hour at liquid helium temperatures.

(iv) Optically detected magnetic resonance has been reported by Yano et al (Yano 1992). The measured ground state splittings were 34.5 and 90.0 and 29.5 and 57.2 MHz for site 1 and site 2 respectively.

(v) Homogenous linewidth – spectral diffusion & instantaneous spectral diffusion

For time domain memory the most relevant measurements are the long holeburning lifetime and long optical coherence times. The long coherence times was first reported by Yano et al (Yano 1991) and gave values of the optical dephasing T_2 as 477 μs and 822 μs respectively for site 1 and site 2 respectively. They also compared the linewidth measurement as a function of storage time and found that there was little change in the linewidth observable. (This contrasted strongly with the behaviour of $YAlO_3:Eu^{3+}$, which has a T_2 of the order of 300 μs for short storage times, but less than 50 μs once the storage time increases beyond a millisecond) The significance is that $Y_2SiO_5:Eu^{3+}$ does not exhibit line broadening due to spectral diffusion.

Equall et al. (Equall 1994) subsequently reported dephasing studies of $Y_2SiO_5:Eu^{3+}$ and noted that the rate was dependent on the measuring light intensity. In extrapolating to zero light intensity they found that site 1 had a zero field T_2 of 1.5 ms, which increased to 2.6 ms in the presence of a 100 G static magnetic field. Site 2 had a zero field T_2 of 1.1ms, also increasing with a 100 G field to 1.9 ms. The dependence on the excitation power due to instantaneous spectral diffusion - an effect due to the local crystal field changing with the excitation of neighbouring Eu^{3+} ions. Instantaneous spectral diffusion accounts for why the values differ from that of Yano et al.

In the literature the emphasis in developing new materials for TDOM has been on the coherence time and the inhomogeneous line width. There are a number of other parameters which will impact on the performance of a TDOM. In the next section parameters for $Y_2SiO_5:Eu^{3+}$ are determined under our experimental conditions and this material is assessed for use as a data storage material. The main reason for performing this analyses is develop an understanding of the practical limitations of TDOM's.

Assessment of the $^7F_0 \Leftrightarrow {}^5D_0$ transition in $Y_2SiO_5:Eu^{3+}$ for use in a time optical memory

When assessing a particular optical transition's suitability for use in a TDOM the following parameters need to be considered:

1) The lifetime of the optically excited state T_1. The excited state lifetime impacts on the memory in a number of ways. The most direct is that, for a transition without a "permanent holeburning mechanism, it represents the lifetime the memory. It also sets the upper limit for the coherence time T_2 and is a critical parameter in determining the efficiency of the memory readout (see below).

2) The transition oscillator strength of the transition to be driven by the laser. This determines spectral bandwidth for the memory that can be achieved for a given laser intensity. The larger the oscillator strength the shorter the excitation pulses that can be used and hence the larger the bandwidth.

3) The absorption coefficient. This determines the proportion of the input light that is available for memory storage within the material.

4) The branching ratio of the emission out of the excited state via the transition driven by the laser. As discussed below this can be calculated from the oscillator strength and the excited state lifetime. As it is only the light emitted at the same frequency as the laser excitation that will be coherent, the branching ratio gives the upper limit of the fraction of the light emitted by the sample that will be coherent. Multiplied by the absorption level of the sample it gives the maximum readout efficiency of the memory, which will be defined here as the fraction of the reference pulse intensity that is scattered into the data pulse on readout.

5) The coherence time of the transition, T_2. The coherence time determines the maximum length of the data pulse that can be stored.

6) The inhomogeneous broadening of the transition. Neglecting issues of the transition strength and available laser intensity, the inhomogeneous linewidth of the transition determines the maximum bandwidth of a signal that can be recorded.

For persistent spectral holeburning materials two further parameters are important

7) The holeburning efficiency: the fraction of the ions that when optically excited will relax to metastable states that are out of resonance with the laser.

8) The lifetime of the spectral hole which is given by lifetime of the metastable states.

Determination of parameters for $Y_2SiO_5:Eu^{3+}$

All the parameters were determined from measurements made at or below 2.2 K and exciting the transition at 579.879 nm corresponding to the absorption of site 1. The laser excitation was linearly polarized and along the C_2 axis of the crystal. Along the C_2 axis of the crystal the sample used was 4 mm long. Site 1 was chosen over site 2 because of the higher absorption of the site1 transition. The observed higher absorption level of site 1 transition was at least in part due to it being nearly perfectly linearly polarized, maximised along the axis used for the experiments in this thesis Site 2 was not fully characterised, as the information is already available in the published literature. Also note site 2 did not offer any characteristic superior to that of site 1 and hence no measurements are reported for site 2.

i) Excited state lifetime

The lifetime of the excited state was measured by exciting the transition with a laser pulse 500 μs long and then monitoring the emission at 614 nm. The laser was tuned into

the wings of the inhomogeneous line to avoid effects due reabsorption of the emitted 579.879nm wavelength light,and the subsequent instantaneous spectral diffusion effects that this could produce. The time dependence of the emission is shown in Figure 3.4.1. The observed value of the lifetime of 1.9 ± 0.1 ms is consistent with the value of Equall et al. (Equall 1994) of 1.9 ms.

ii) Transition dipole moment and branching ratio

The transition dipole moment was determined through measurements of the nutation frequency induced on the transition at a known laser intensity. The relationship between the Rabi frequency χ and the dipole moment $\langle a|er|b\rangle$ is given by Levenson, (Levenson 1988)

$$\chi = \langle a|er|b\rangle |E|/h \qquad (3.4.1$$

Were E is the amplitude of the electric field component of the laser excitation and whose magnitude can be determined from the laser intensity using

$$|E| = \sqrt{\frac{2I}{c\varepsilon_0}} \qquad (3.4.2$$

The nutation frequency used a rotary echo as is shown in figure 3.4.2. The observed nutation frequency was 40.0 ± 1 kHz. The laser power used was 40 mW and the beam diameter on the sample was 1.0 ± 0.1mm, resulting in a laser intensity of 5.1 W/cm^2. From equation 3.4.2 magnitude of the oscillating electric field incident on the sample was therefore (6 ± 1)x 10^3 Cm^{-1}. Substituting into equation 3.4.1 the observed nutation frequency and the incident electric field the magnitude of the transition dipole moment is found to be

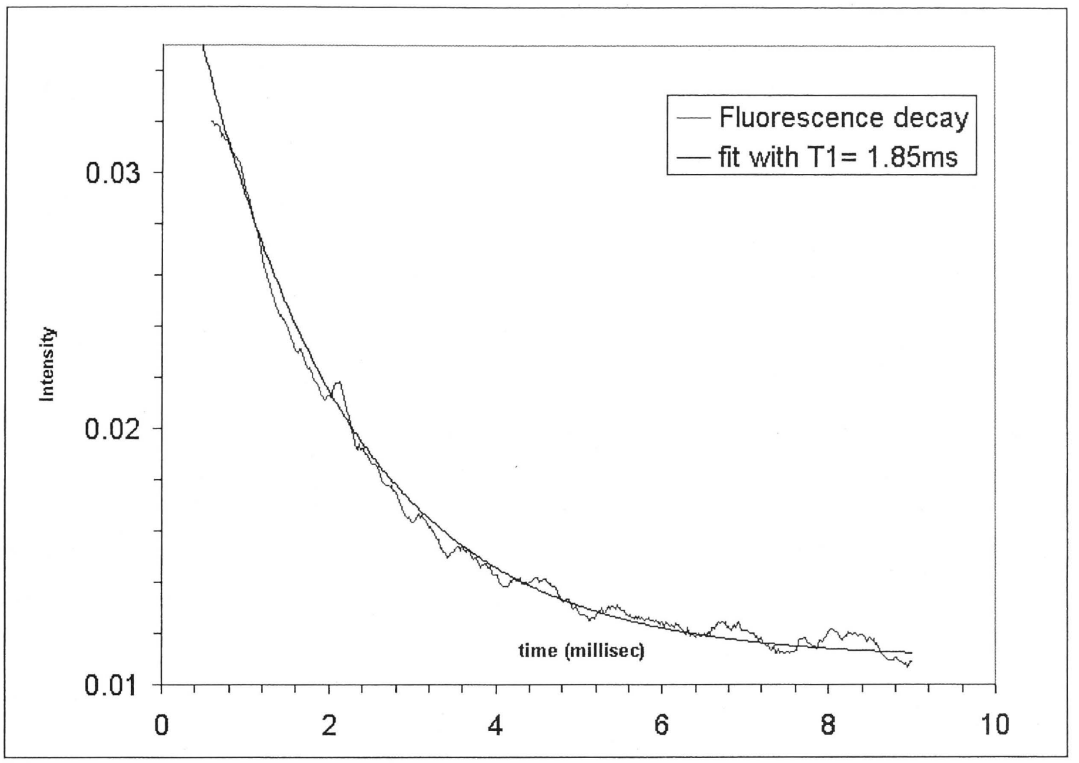

Figure 3.4.1: Fluorescence decay from the $^5D_0$ excited state of $Y_2SiO_5:Eu^{3+}$, the data was fitted to an exponential to give a T_1 of 1.9 +/-0.1 ms. The residual non-zero value at the end of the decay is due to ambient light falling onto the detector, this ambient has an essentially constant value and was subtracted away during curve fitting.

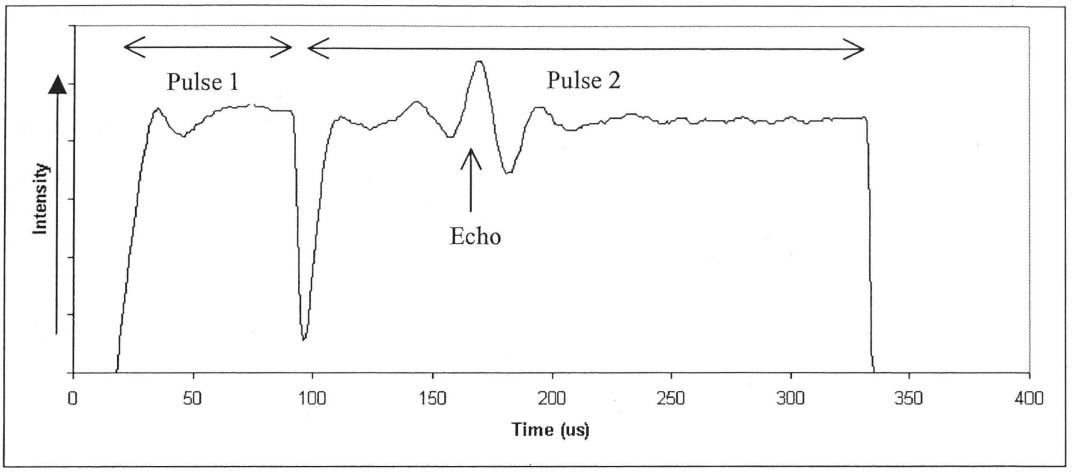

Figure 3.4.2: Rotary echo of $Y_2SiO_5:Eu^{3+}$, site 1, using 40 mW laser power and 80 μs pulse then 240 μs phase reversed pulse. The echo is the oscillation observed during the second pulse with a measured Rabi frequency was 40.0 +/- 1kHz. The zero intensity at the start and end of the sequence is due to the drop in intensity when the pulses are gated off. Since an intensity detection scheme was used this drops the signal to zero.

$$\langle a|er|b\rangle = 9 \pm 1x10^{-33}\ cm \qquad (3.4.3$$

The Einstein A coefficient can be calculated from the transition dipole moment using (Thorne 1988)

$$A_{ab} = \frac{16\pi^3 \nu^3 |\langle a|er|b\rangle|^2}{3\varepsilon_0 hc^3} \qquad (3.4.4$$

On substituting the value for the dipole moment given in equation 3.4.4. A_{ab} was found to be $10 \pm 1\ s^{-1}$.

The branching ratio B_r is given by the product of Einstein coefficient A_{ab} the lifetime of the excited state. (Thorne 1988).

$$B_r = A_{ab} T_1 \approx 0.02 \pm 0.004 \qquad (3.4.5$$

iii) ***Absorption coefficient***

To avoid saturation effects the peak absorption of the inhomogeneously broadened line was measured by comparing the transmission of a weak laser pulse 10 μs long (pulse area $< \pi/100$) on resonance with the transition with an identical pulse tuned well off resonance (greater than 20 GHz). The intensity of the transmitted on resonance pulse was found to be $20 \pm 2\%$ of the off resonant case. This gives a total absorption of $80 \pm 2\%$ and an absorption coefficient of $4.0 \pm 0.1\ cm^{-1}$.

For this sample the upper limit for readout efficiency, given by the product of the total peak absorption and the branching ratio, is 0.02 ± 0.004. This result indicates that even with for data stored with an 100% modulation in the transition's absorption the maximum

percentage of the readout pulse that can be expected to be scattered into the output data pulse is 2%.

iv) ***Coherence Time (T_2)***

Two series of photon echo measurements were performed using different laser intensities and pulse lengths. For the series (a) shown in figure 3.4.3 the "$\pi/2$" pulse was 20 μs long with a laser power of 0.4 mW. For series (b) the pulse length was 3 μs long with a laser power of 4 mW. T_2 was found to be 1.1 ms for series (a) and 300 μs for series (b). Intensity dependent T_2 measurements have previously been reported by Equal et al above (Equall 1994) and is referred to as Instantaneous Spectral Diffusion (ISD) (Huang 1989, Graf 1998). In Eu^{3+}:Y_2SiO_5 the observed ISD is attributed to an electric dipole-dipole interaction between the Eu^{3+} ions (Graf 1998). The Eu^{3+} ions in the crystal possess a static electric dipole moment whose magnitude and direction is dependent on the electronic state of the ion. Hence exciting an ion will result in the electric field in the region close to the ion changing. The optical frequency of any ion in the vicinity of the excited will be Stark shifted. As the relative separation between the ions and hence the frequency shifts is random the interaction is seen as dephasing mechanisms for an ensemble of ions.

Even at the low intensities used in series (a) the value obtained for T_2 of 1.1 ms was lower than given by Equall et al.for site 1 of 1.5 ms[Equall 1995]. The difference is attributed to residual ISD in the current measurement.

v) Holeburning structure

Measurements confirmed the holeburning and ODNMR spectrum obtained by Yano et al. (Yano 1992). The holeburning spectrum is shown in figure 3.4.4.

The spectrum is dominated by side holes and the assignments are indicated (see section 3.1). The holeburning spectrum was obtained using a single shot burn scan technique, with the signal being detected by measuring the variation in the emitted fluorescence and

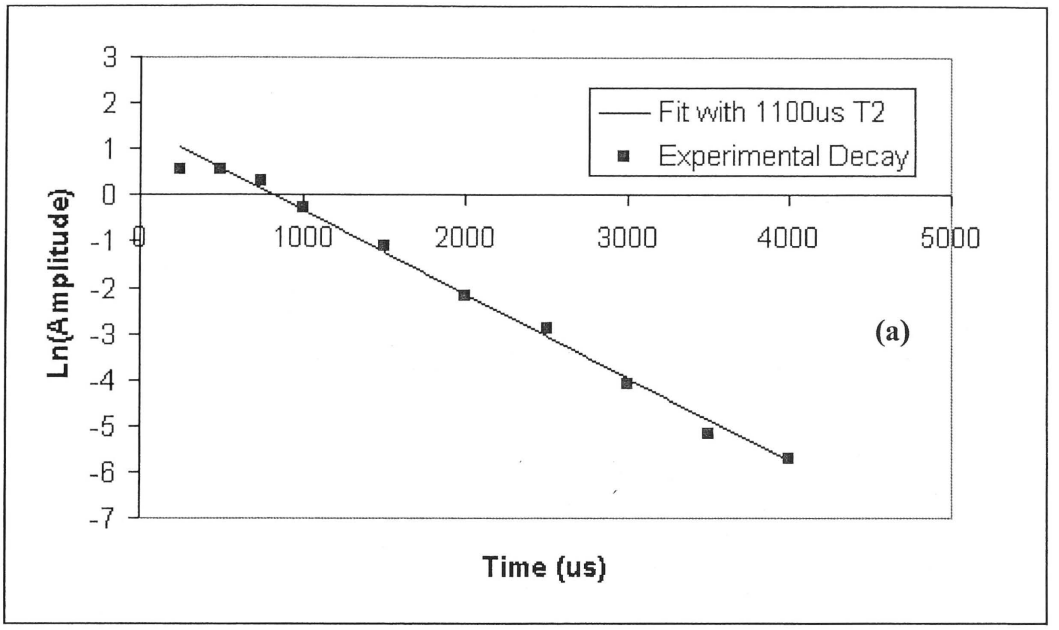

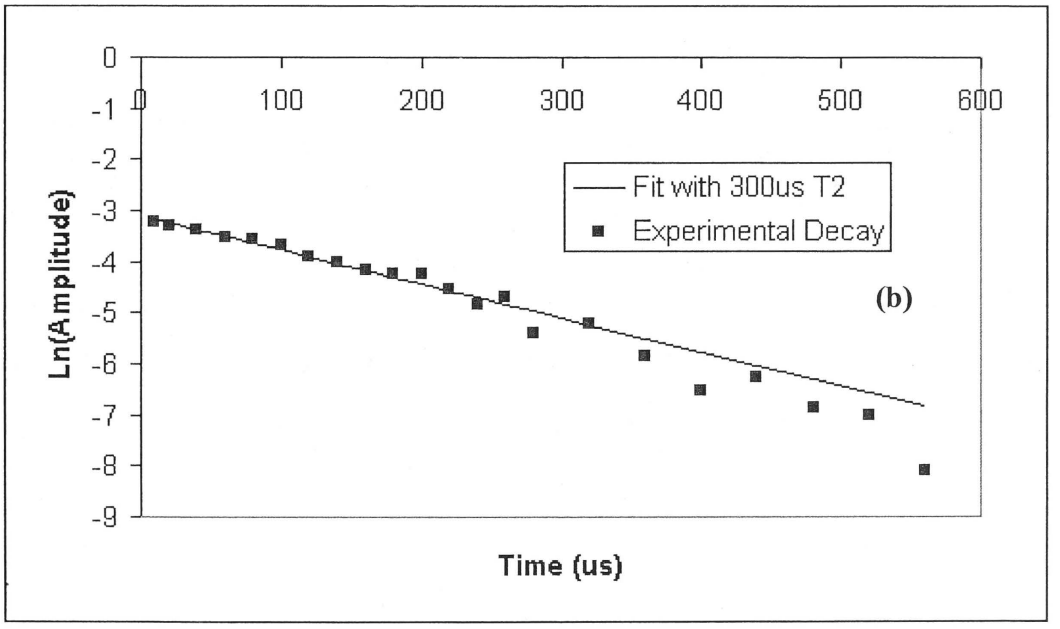

Figure 3.4.3: Two Photon echo T_2 measurements, and data fit. (a) T_2 is 1.1 ms, using pulse length 20 μs and power 0.4 mW, (b) T_2 is 300 μs using pulse length of 3 μs and power of 4 mW.

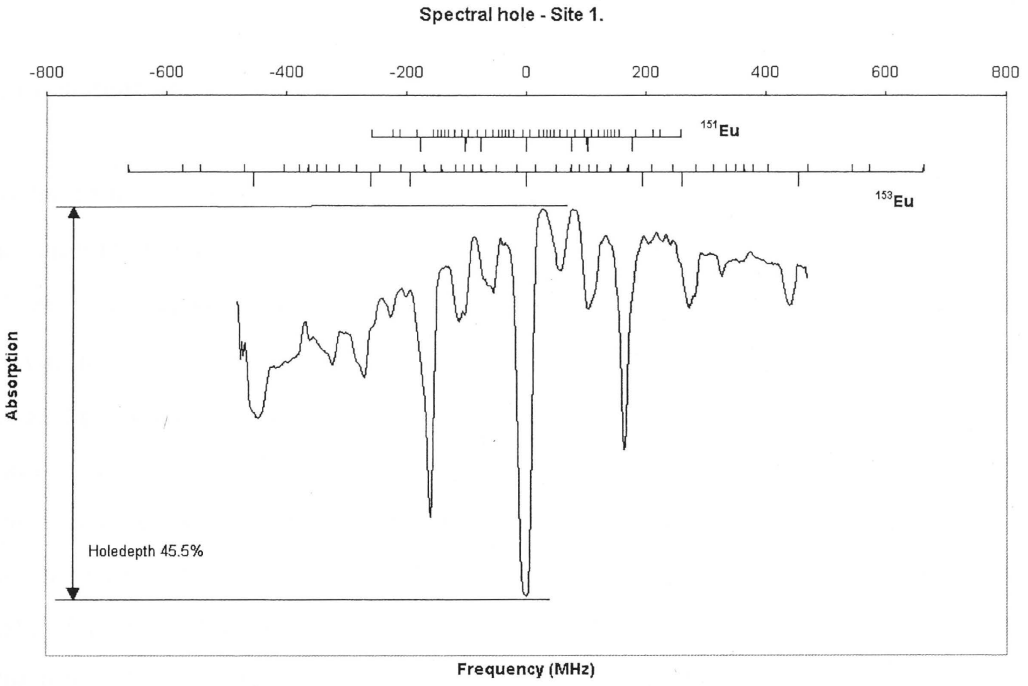

Figure 3.4.4: Holeburning spectra of $Y_2SiO_5:Eu^{3+}$, site 1. The positions of the expected side structure for the two isotopes is shown. The Side holes dominate the spectra.

the scanning beam being reduced in intensity to avoid additional holeburning during data collection.

v) Persistent holeburning efficiency

To determine the spectral holeburning efficiency a series delayed free induction decay measurements were made. The measurements use a saturation pulse of 100 μs and 1 W/cm^2 and readout pulses of 10 μs and 100 W/cm^2. An example of a DFID signal is shown in figure 5.1.2. Figure 3.4.5 shows the amplitude of the DFID 10 μs after the readout pulse was applied as a function of the delay between the saturation pulse and the readout pulse. The DFID signal is seen to decay by approximately 80% over the 15 ms. This initial decay component is attributed to the decay of the excited state (T_1= 1.85 ms). At delays over 10 ms the ions should have completely relaxed out of the optically excited state. The residual DFID signal is due to the persistent holeburning. As can be seen from equation 1.2.12 the amplitude of the DFID signal is proportional to the number of ions whose emission has been saturated. The holeburning efficiency is given by the ratio of the amplitude of the two (initial and 15 ms delay) DFID signals. The observed ratio of the amplitudes of the two DFID signals measured immediately after the readout pulse was found to be 20%.

vii) Lifetime of persistent hole
A hole was burnt and measured periodically over a timescale of 12 hours. Typical measurements are shown in figure 3.4.6

Decay over the restricted period gives a hole lifetime of 10 days, 41 minutes
The decay is associated with relaxation of the hyperfine population, thus giving a measure of the hyperfine T_1 lifetime. The decay is plotted in figure 3.4.7

It is note that the decay curve did not seem to be a pure exponential. The decay curve appeared to show two distinct contributions with the first showing a rate of 6 hours, and the second was a slower decay of approximately 10 days. This experiment was repeated

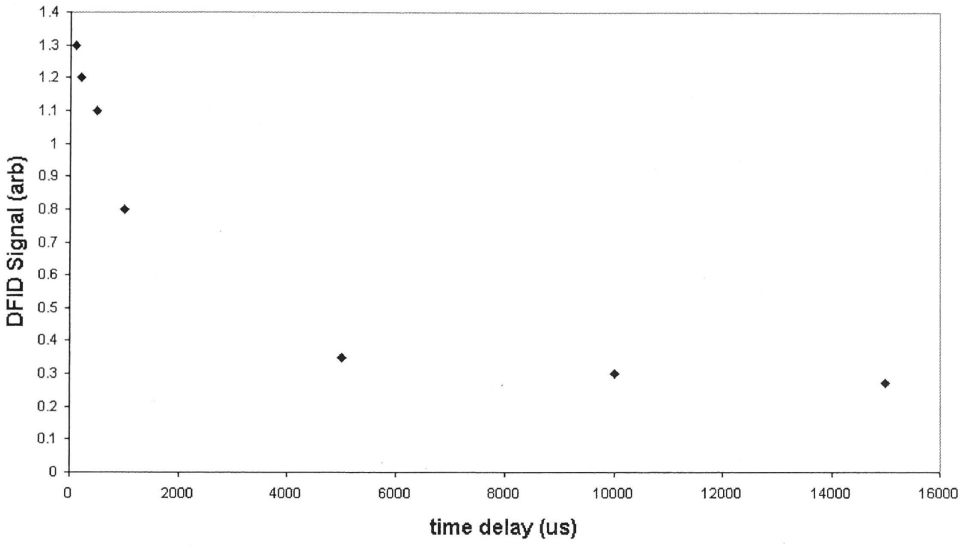

Figure 3.4.5: The initial height of the DFID signal from $Y_2SiO_5:Eu^{3+}$, site 1, with the delay between the burn and read pulse varied.

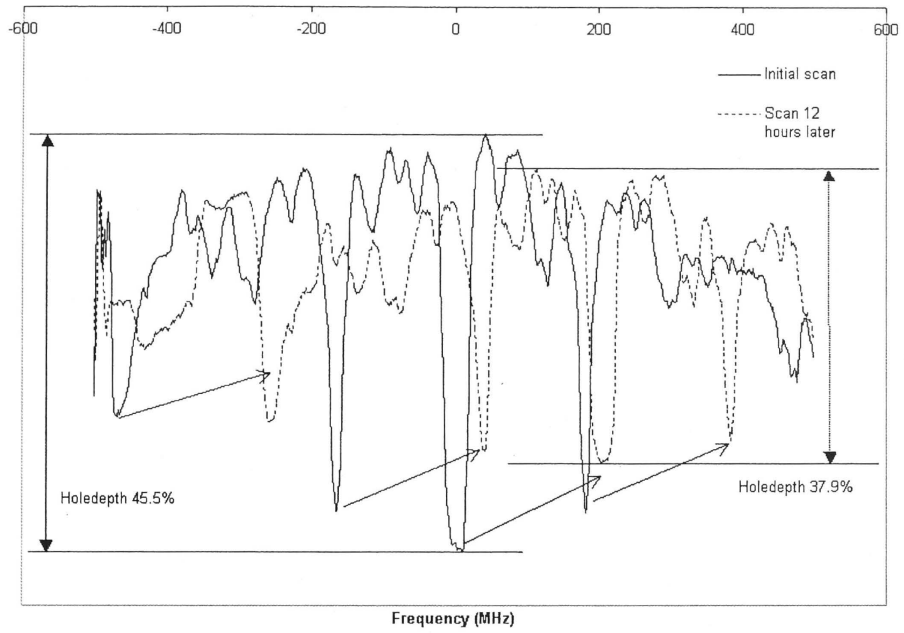

Figure 3.4.6: Two spectral hole scans taken 12 hours apart, both using the same initial burn pulse. The solid line is the initial observation, with the dashed line later. The drop in hole depth over the time period shows the effect of decay from the persistent holeburning state back to the equilibrium state. The frequency shift apparent in the figure is the result of the laser frequency drifting over the 12 hours of the experiment. This drift is most likely due to slight thermal in the reference cavity.

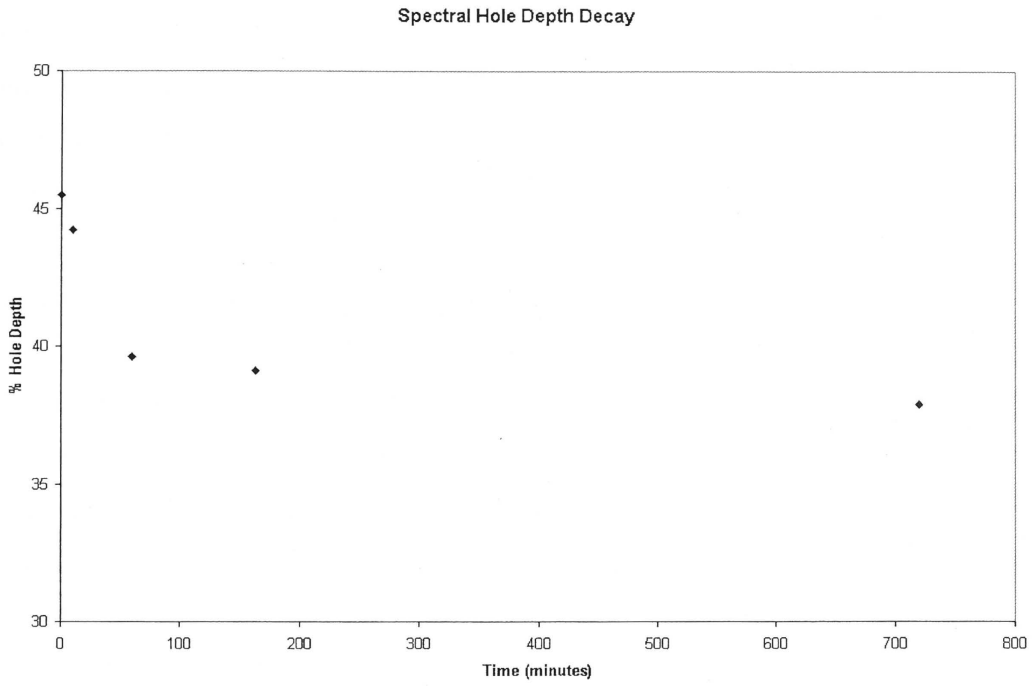

Figure 3.4.7: The observed spectral hole depth from repeated, time delayed scans after an initial burn. The longest delay was 720 minutes (12 hours).

with measurements taken over 5 hours and 12 hours. However in both cases measurements were taken more frequently in the early parts of the curves than during later times and the effect of the scanning laser was to artificially refill the spectral hole and probably accounts for the changing decay rate.
Note the holeburning burn-scan technique was preferred over echo measurements used by others (Babbitt 1987), as the technique is not sensitive to frequency drift of the laser.

Discussion and Conclusion

The outstanding features of $Y_2SiO_5:Eu^{3+}$.in regards to applications for TDOM's is it long coherence time and its long persistent holeburning lifetime. There are two characteristics of the material, which are likely to pose significant challenges in developing a practical memory device, namely the low branching ratio and the ISD. How these characteristics impact on the memory design can be appreciated by considering the energy requirements for a TDOM using $Y_2SiO_5:Eu^{3+}$.

The energy required to write a grating can be approximated as the energy required exciting half the ions in the desired volume and spectral bandwidth into the excited state. This energy is given by equation 5,

$$Energy = \frac{1}{2}\left(N(\vartheta) \times Bandwidth \times \text{int}eraction\ volume \times h\vartheta\right)/\left(1 - e^{-\alpha L}\right) \qquad (3.4.6$$

where α_v is the absorption coefficient, L is the interaction length, υ is the optical frequency, h is Planck's constant and $N(\upsilon)$ is the number density of Eu^{3+} ions per unit frequency. It is assumed that over the required bandwidth α_v and $N(\upsilon)$ are constant. The spectral density of ions $N(\upsilon)$ can be determined from the observed absorption coefficient and the transition's dipole moment. The absorption coefficient integrated across the inhomogeneous line is given by: (Thorne 1988).

$$\int \alpha_\nu d\nu = N_1 B_{12} \frac{h\nu_0}{c} \qquad (3.4.7$$

where N1 is the total ground number density of the ions. Assuming a α_ν is constant over the line, dividing equation 3.4.7 by the FWHM of the inhomogeneous line $\Delta\nu_{inhom}$ and rearranging, gives the spectral number density of the ions.

$$N(\nu) = \frac{c\alpha_\nu}{B_{12} h\nu_0} \qquad (3.4.8$$

where B_{12} is the Einstein absorption coefficient and is given by

$$B_{12} = \frac{2\pi^2}{3\varepsilon_0 h^2} \left| \langle a | er | b \rangle \right|^2 \qquad (3.4.9$$

substituting equation 3.4.9 into 3.4.10 gives N(ν) in terms of the dipole moment and absorption coefficient.

$$N(\nu) = \frac{3ch\varepsilon_0 \alpha_\nu}{2\pi^2 \nu} \left| \langle a | er | b \rangle \right|^{-2} \qquad (3.4.10$$

For the values of absorption coefficient, line width and dipole moment measured above and using equation 3.4.10 N(υ)is calculated to be 3.6 x 10^8 ions $Hz^{-1}cm^{-3}$.

A useful memory will be required to operate with a bandwidth of at least 1 GHz to be competitive with existing technology. To minimize the energy requirements we minimize the interaction volume by minimizing the beam diameter. Given the length of the sample (4 mm) it will be difficult to maintain a laser beam diameter of less than 10 μm through the length of the sample. Hence the beam volume is estimated to be (10 $\mu m)^2$ x 4 mm. On substituting these values for the density, beam diameter into equation 3.4.10 we obtain a value for the total laser energy needed to excite the grating of 150 nJ.

As discussed in chapter 1 the maximum time available to write the data in a TDOM is given by T_2. Dividing the require energy, calculated above, by T_2 (~1 ms) therefore gives the laser power required to write the grating which is 150 μW. This represents an easily achievable laser intensity given that commercially available lasers that operate at 580 nm typically produce about 1 W. With such laser power available it should be possible to scale the memory up by either increasing the bandwidth from 1 GHz or using multiple pixels.

One possible limitation to scaling the memory up is the need avoid heating once energy is absorbed. When the ion relaxes into one of the states in the F manifold it will decay to the ground state via phonon emission, giving heat. Given the mean energy of the F states of about 3000 cm^{-1} compared to the 17000cm^{-1} of the $^5D_0$ state we can expect somewhere between 10 and 20% of the absorbed light to be converted to heat. This represents a heat load of at least 30 μW GHz^{-1}/pixel.

The output signal level can be estimated from the branching ratio absorption level. The optimum readout reference pulse energy is the same as the energy given in equation 3.4.6 as it is the minimum energy needed to excite all the ions into a 50/50 superposition state. From the branching ratio, holeburning efficiency and the absorption level we know that at most 0.4% or 0.8 nJ of this pulse will be scattered into the readout data pulses. If maximum use of the data storage capacity is used there will be about 10^6 pulses emitted over a 1 ms time interval. Therefore the energy per data pulse will be 8 x 10^{-16} J. This is approximately 2000 photons/bit. This is considered an adequate signal level though a significant reduction from this level is likely to result in a intolerable bit error rate.

The effect of ISD will be to effectively shortening T_2 and hence the time available to write the grating. To avoid a significant performance drop it will be necessary to limit the density of excited ions to a level similar to that used in series (b) photon echoes shown in figure 3.4.5. For a memory utilizing a 1 GHz bandwidth it will be necessary to decrease the total density by a factor of 300 (1 GHz x 3 μs) to compensate for the

increase in the bandwidth excited. To retrieve the total optical absorption will require the interaction length to be correspondingly increased. The volume of our pixel will therefore be 4×10^{-6} cm^3. Given that the $\sim 10^6$ bits can be stored per pixel the data storage density is approximately 2.5×10^{11} bits cm^{-3}. This could possibly be achieved with the use of either wave-guide structures or multi-pass cells. It is ISD which will sets the limit on the volume capacity of the memory.

On the basis of the example above it can be seen that a practical TDOM using $Y_2SiO_5:Eu^{3+}$ is feasible. The laser power requirements and the heat load are reasonable. The main difficulty with this material is the light induced interactions between the Eu^{3+} limiting the material's storage density.

Chapter 4: Memory Applications of the High Stability Laser

The preceding chapter of this thesis utilised the phase stability of the laser system to explore effects that are likely to be detrimental in a fully functional memory system. In contrast this chapter demonstrates two capabilities that will be very valuable in a functional memory, but which were only possible to realise because of the phase stability of the laser system used. The two capabilities are data reinforcement and data erasure. The experiments also demonstrate the value of using PSD when developing an understanding of the physical processes involved in these operations.

4.1 Reinforcing Data Echoes.

One of the difficulties that TDOM systems have frequently encountered is the problem of "crosstalk". This is the description given to the occurrence of stimulated echoes that are stored by the interaction of two data pulses, rather than the write pulse and one data pulse. In practical terms crosstalk echoes act as non-random noise within the echo memory sequence, and could easily produce erroneous results in a working system. There have been a number of proposals regarding how the crosstalk signals might be minimized.

One approach, which has been demonstrated by (Hesselink 1979, Hesselink 1981, Carlson 1983, Kim 1987) is to use data beams that are spatially distinct from the read and write beams. In other words to use one beam for the write and read pulses and another which overlaps the first beam at the sample but which has a different incident angle. Because photon echoes are a holographic phenomena the spatial character of the two storage pulses will also be stored in the memory. Thus when the data is recalled, the desired data will be emitted collinear with the read and write beams, whereas the crosstalk echoes will be emitted collinear with the input data beam. This method requires

a more complex optical layout as well as excellent alignment of the two beams at the sample, and while it may prove to be a desirable technique, it has not been further pursued in this work.

Another approach is to incorporate a delay between the write pulse and the first data pulse that is longer than the total length of the data pulse train. The effect of this is to cause all of the crosstalk echoes to occur before any of actual data echoes occur. In this way the crosstalk echoes are temporarily separated from the data echoes. This method has been used in some experiments in this thesis because it is experimentally simple and provides easily interpretable results. However, it is not likely to be satisfactory for a functional memory system as it throws away the first half of the data storage window. In addition to losing half of the storage capacity, the first part of the storage window has the best signal to noise due to the effect of T_2 decay, and the fastest retrieval times, because it occurs soonest after the read pulse.

A third approach is the use of data pulses that are significantly weaker than the write and read pulses. The echo signal strength scales as the product of the amplitude of the pulses, at least for small area pulses. Thus the effect of this method is to significantly reduce the intensity of the crosstalk echoes as compared to the data echoes. This allows data echoes to be determined based on relative signal strength. Since it will also reduce the absolute signal strength of the data echoes the requirement of good signal to noise is a drawback of this method. This is because the f^n-f^n rare earth transition strengths in materials such as $Y_2SiO_5:Eu^{3+}$ are weak. It is also because the holeburning efficiency, which measures the conversion of excited centres into storage centres is inefficient. This was demonstrated in chapter 3 where these values were measured for $Y_2SiO_5:Eu^{3+}$. As a result of this, persistent photon echoes in rare earth systems are usually weak and difficult to detect.

An obvious solution to this difficulty is to increase the signal strength of the output echoes. This can be done by increasing the intensity of the input pulses, either all the pulses or just the write and read pulses. This works reasonably well to a point, but, as the results of the previous chapter show, it is limited by the distortions that occur with pulses

larger than π area. It is also limited by the increase in instantaneous spectral diffusion (ISD) that shortens the effective T_2 of more intense pulses (Huang 1989). Using longer pulses to increase the area rather than more intense pulses reduces the impact of ISD, but it also reduces the bandwidth and the operating speed of a memory system.

Another way to increase the signal strength is to use multiple writing of the data. A schematic representation of the generic pulse sequence used for this is shown in figure 4.1.1, where the use of repetitions of the write-data part of the pulse sequence act to reinforce the data. This type of reinforced echo was first described in the literature as accumulated echoes (Hesselink 1979, Hesselink 1981), with the same study noting the importance of maintaining a consistent phase relationship between successive pulse sequences. To date most accumulated echo results have been obtained using a pulsed laser system, where the pulses are split and converted into a pulse pair by means of optical delay lines (da Silva 1993). Such methods however are limited to small delays between the two pulses of a pulse pair due to the use of the optical delay lines, and are unable to take advantage of the long coherence times of materials such as $Y_2SiO_5:Eu^{3+}$. The Commercially available CW dye laser systems with typical bandwidths of around 1 MHz are also inadequate for these longer timescales.

The current demonstration shows that with a sufficiently stable laser system, such as the one used, reinforcement of photon echo data is a viable option for improving the signal strength of stored data. There are several criteria that this system needs to meet. The first is that the phase noise of the input pulses needs to be smaller than 90^o over a timescale of the coherence lifetime of the storage centres, which for $Y_2SiO_5:Eu^{3+}$ is in the range of a millisecond. The second is that the frequency of the laser needs to be stable over the whole time in which the repetition sequences are stored. The minimum timescale for this will be determined by the length of a single sequence, multiplied by the number of repeats required, along with a factor of two to ensure that repeat pulse sequences do not interact and thus produce additional unwanted echoes. For $Y_2SiO_5:Eu^{3+}$ this is of the order of 10's of milliseconds. The difficulty with frequency drift is that it introduces an unwanted ramping of the input phase across the length of the individual input sequence,

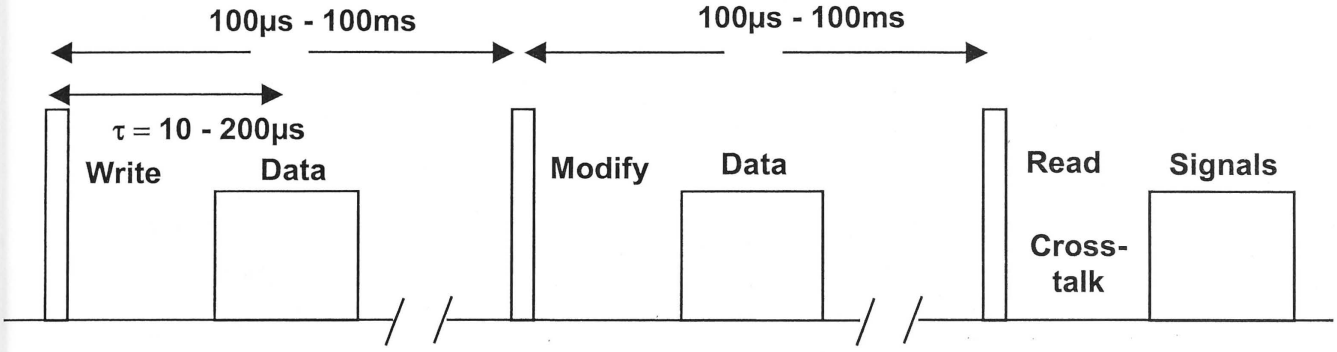

Figure 4.1.1: Schematic diagram of the generic input pulse sequence for bit-by-bit data storage or appending data.

as was described in Chapter 1. Thus effective reinforcement of data stored in the first 100 μs after a write pulse required the laser shift to have been less than 2.5 KHz. Given that the aim of reinforcement is merely to increase the signal strength, rather than to achieve a specific value, the technique is insensitive to intensity variations of the input pulses. This is one reason that the technique has worked well with pulsed lasers.

It is worth noting that with the phase sensitive detection system described in chapter 2 in use the actual relative phase variation of the input pulses and also of the final output data were measured directly. This not only allowed the discrimination of reliable versus coincidental reinforcement, but it also functioned as a probe to assist with finding and minimizing laser phase noise.

As a control and also as a phase jitter check we first stored two individual data echoes at 50us delay (data bit A) and 40us delay (data bit B). These times were chosen because they were well within the ISD shortened coherence time, and thus gave clear echo signals, but were also long enough to provide a useful demonstration of the system. The signal to noise is also why data pulses were of equal area to the write and read pulses. Figure 4.1.2 demonstrates the storage and retrieval of echoes A and B individually, as well as the retrieval of the combined signal. For comparison the quadrature component of the signal is shown below the in-phase signal. As can be seen the quadrature signal is minimal, indicating that the phase jitter and frequency drift of the system is also low at these timescales. The delay between the two sequences was 300 μs.

Figure 4.1.3 (a) then shows the equivalent retrieval output obtained when echoes A and B are stored as part of the same sequence. The presence of the cross talk echo 10 μs after the read pulse is clear. Figure 4.1.3 (b) shows the effect on the signal of using a second sequence to reinforce echo B. As desired the output signal strength of echo B is approximately double that of either echo A or the crosstalk echo.

From this it is clear that with suitably stable systems, reinforcing of the data becomes a viable consideration in the design of TDOM systems. As an aside it is apparent from a

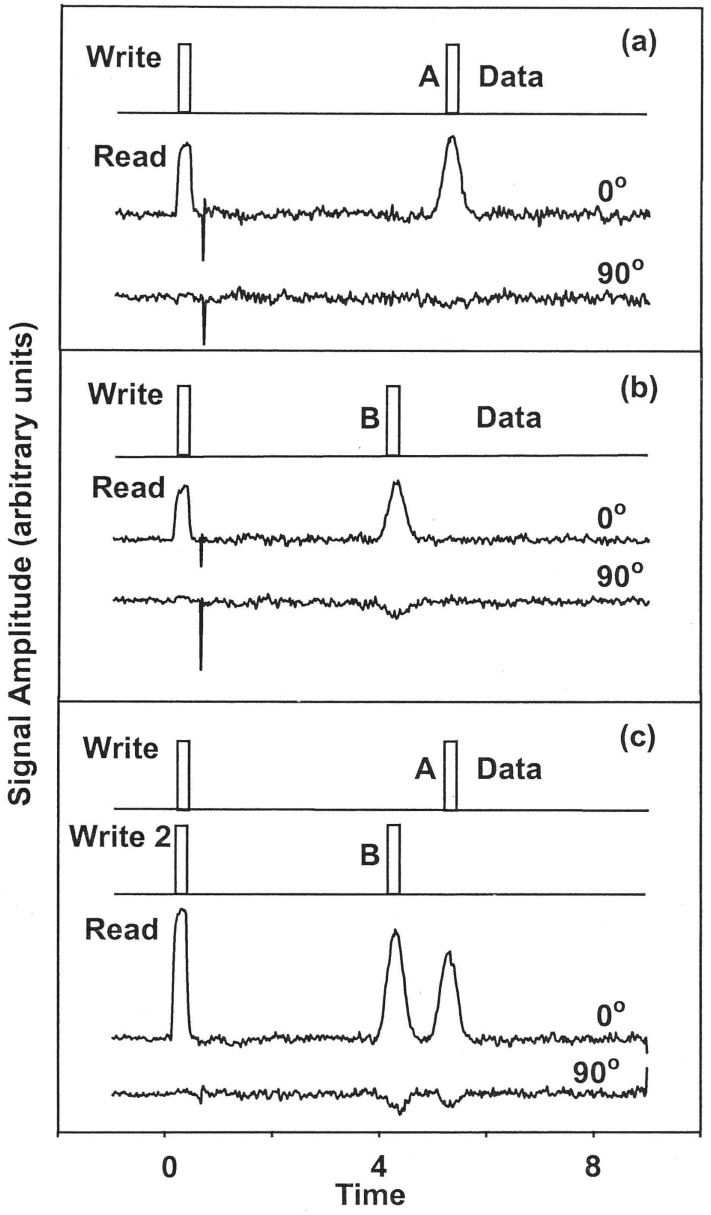

Figure 4.1.2: Experimental demonstration of bit-by-bit data recording. Data bit A is recorded in sequence (a), then data bit B is recorded in sequence (b), then both are recorded sequentially in sequence (c). In quadrature (90°) signals are shown to indicate the phase stability of the system. Five shots were collected for each trace and signal averaged.

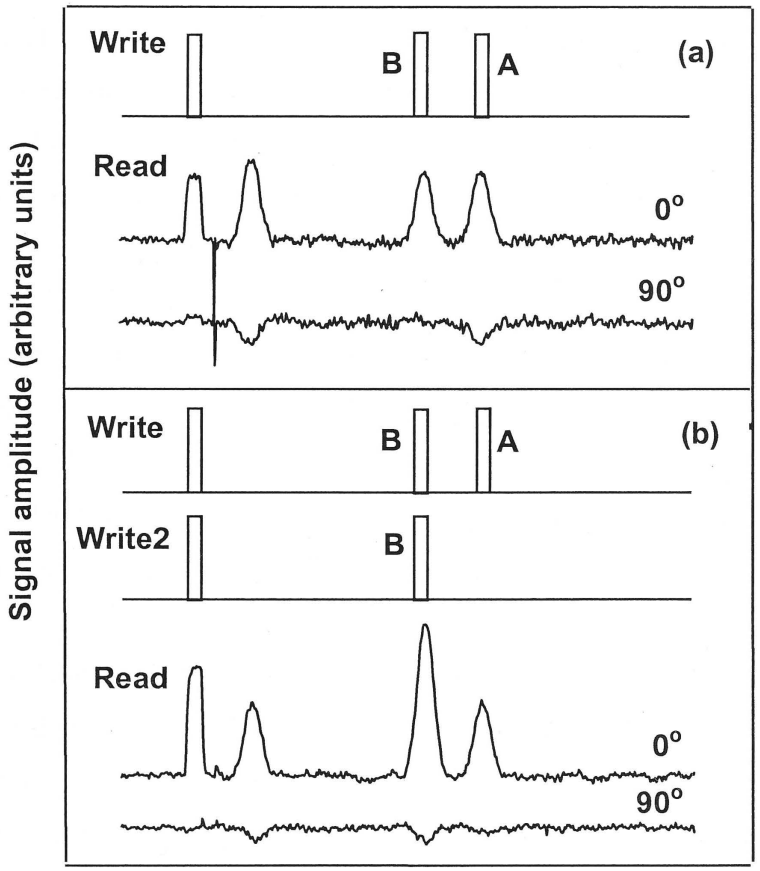

Figure 4.1.3: Experimental demonstration of data reinforcing. Data bits A and B are both recorded in sequence (a), then data bit A is recorded again in sequence (b), which then shows an increase in the signal for bit A. In quadrature (90°) signals are shown to indicate the phase stability of the system. Five shots were collected for each trace and signal averaged.

the absence of a crosstalk echo in figure 4.1.2 as compared with figure 4.1.3 that if necessary, crosstalk could be eliminated by writing the data one bit at a time. This would however reduce the speed of such a memory to that of a frequency domain method.

These results show the potential of coherently reinforcing data to improve the holeburning efficiency and thus output signal to noise. However, for a functional system, both multiple rewrites of the data as well as delays between writing sequences of considerably longer than the material T_2 are desirable. In addition it is desirable to use data delays approaching the coherence time, although this will be constrained by the effects of ISD.

For this reason, figures 4.1.4 and 4.1.5 relate to a more realistic reinforcement memory configuration. Five data pulses are used in each sequence. The data pulses have 1/3 of the input intensity of the write and read pulses, thus allowing the signal from crosstalk to be minimized. The data pulses occur at 20, 40, 60, 90 and 115 μs, using a substantial part of the ISD limited coherence time data window.

Figure 4.1.4 shows the single shot retrieval signals from this sequence. Figure 4.1.4 (a) shows the readout when the laser was used with the commercial stabilisation components only, while figure 4.1.4 (b) shows the output when the stabilisation features described in chapter 2 are used. Figure 4.1.5 then shows the observed effect on these two scenarios of rewriting the data five times, at an interval of 5ms. Note that the first and second data echoes also have a contribution from 2 and 1 crosstalk echo respectively.

While reinforced or accumulated echoes have been reliably used in pulsed laser experiments for some time, the short timescale limitation enforced by the use of optical delay lines reduces the value of this method for high volume optical memory purposes. Accumulated echo techniques have also been used for signal enhancement reasons in demonstrating hybrid memory applications (Mitsunaga 1991, Elyutin 1979). This method is similar to that used in the current work to produce the accumulated echoes using the commercial performance laser. Such a method tends to produce a statistical distribution

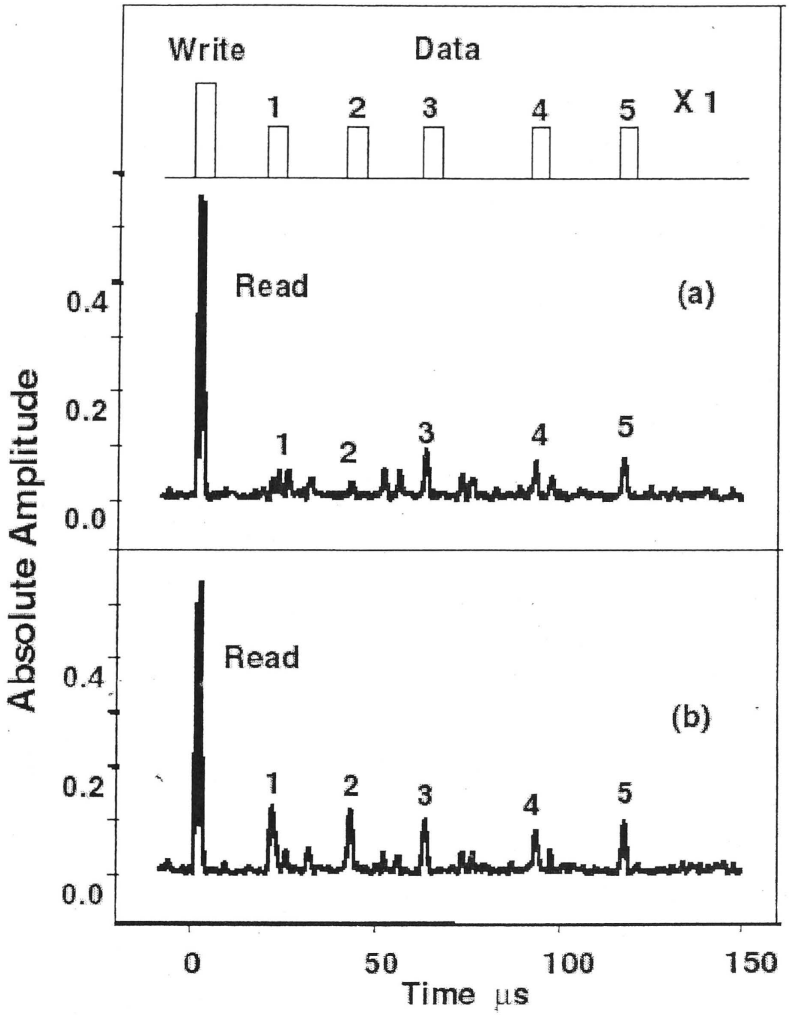

Figure 4.1.4: Single shot write and recall of 5 bit data pulse sequence. The schematic of the sequence is shown on top, all pulses are 1μs long, with the data pulses 1/3 intensity of reference pulses. Sequence delays were 20, 40, 60, 90, 115 μs (a) is the output observed using the laser in commercial (1 MHz) resolution mode, data echoes are marked 1-5. (b) the same experiment using the laser in phase stable mode. Smaller crosstalk echoes are visible but not marked.

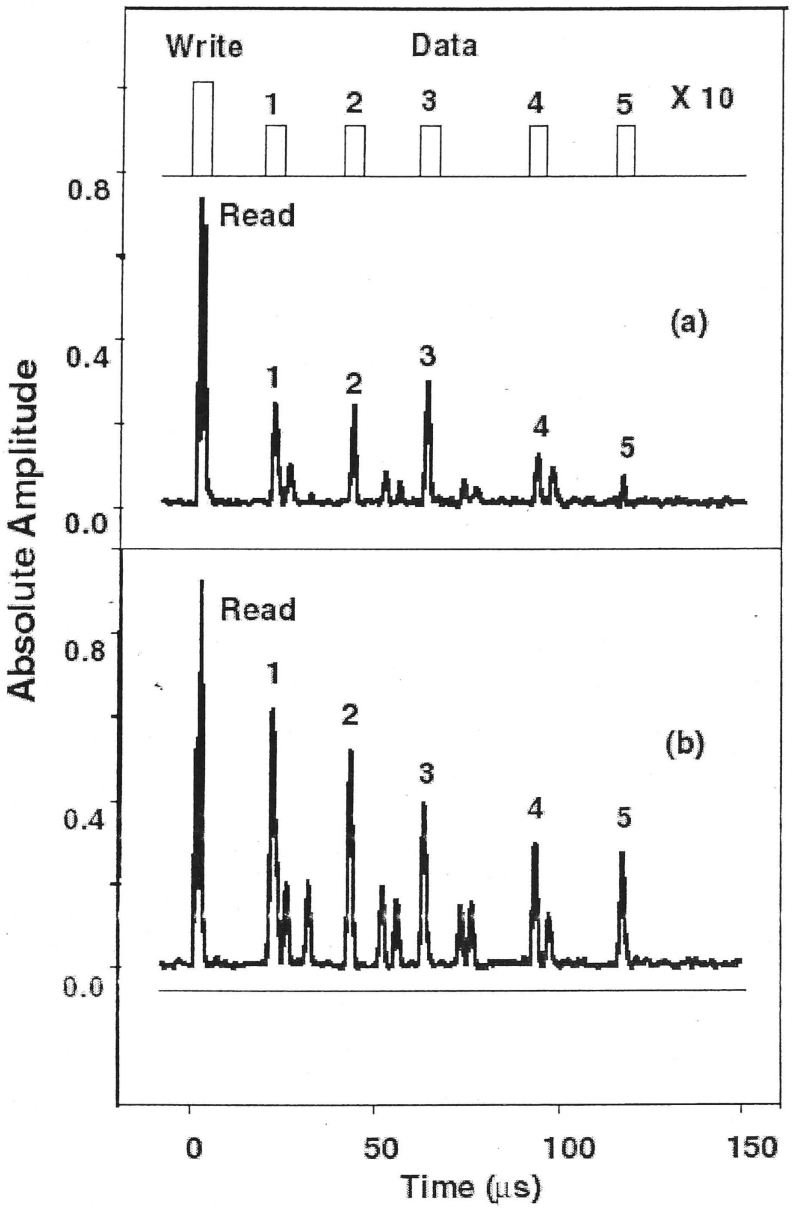

Figure 4.1.5: Single shot write and recall of 5 bit data pulse sequence as per figure 4.1.4.The sequence has been reinforced 5 times at intervals of 5 ms. (a) shows the results using the laser in commercial resolution mode, and (b) shows the (clearly improved) results using the phase stable laser. Note that data echoes 1 and 2 are larger because they also receive some contribution from overlapping crosstalk echoes.

in the enhancement of the echo signal, with the majority of the signals being enhanced, and for some individual echoes the enhancement will approach that possible with coherent methods. Most memory applications however utilise a threshold approach to determining a data bit as present or absent. In this scenario the amount by which an echo exceeds the threshold is of little relevance. Conversely the height (and thus signal to noise level) of the smallest data echo becomes critical to the memory fidelity. With a system that produces a broad statistical distribution the probability that the height of the smallest data echo is significantly enhanced can be quite low. This strongly limits such systems.

With the system demonstrated in this work however, the system stability is such that the statistical distribution of enhancement experienced with lower stability systems has been converted into a regime where the enhancement of all the data echoes is approximately linear with the number of accumulations. This allows the low holeburning efficiency of rare earth doped crystals to be partially overcome, and thus allows the other useful properties of these systems to be better exploited for optical memory applications.

Reliable data reinforcing has another potential application that may be of more significance for future optical memories, and that is data refresh. With current methods the data storage lifetime is limited by the lifetime of the persistent state that the data is stored into. In the case of $Y_2SiO_5:Eu^{3+}$ the value of 10 days, measured in chapter 3, is very long, however if it becomes necessary to store data for longer than this it would be necessary to store the data into another physically separate memory. At best the data would be erased in bulk and then read back from the other memory, which for large volumes of data would be an onerous task. With phase reliable reinforcing demonstrated however it would be possible to read the data out, then read the signal directly back into the memory, without the need for the data to exist outside longer than the optical T_2 lifetime. This refresh would reinforce the data already stored, and thus effectively "reset" the memory lifetime limit. The data signal could be processed prior to being used for refresh if it was desirable to improve the signal to noise of the system. It is important to note that with this system the only data that would need to be stored externally would be

the bit stream being refreshed. For the non-refresh system the data from all spatial locations and, for hybrid memories all frequency segments, would need to be stored externally.

4.2 Data Erasure:

An extension of the data reinforcing concept is that of data erasure. This was first proposed by Akmediev in 1990 (Akmediev 1990). The principle of data erasure is very similar to data reinforcing, with two notable differences. The first is that the relative phase between the write and data pulse is 180° different for the second (erasing) data sequence as compared with the initial data sequence. The second is that a specific signal output value is required following the readout pulse, namely zero. A consequence of the second point is that only two data sequences are used, and the intensity of the two individual echoes needs to exactly cancel. This makes erasure a more demanding technique than reinforcing, where the relative intensities of the data is less relevant.

Previous experimental work on erasure has shown in principal success, but has also suffered from limitations that would limit its practicality. Arend (Arend 1993) demonstrated erasure using a pulsed laser and forming each pulse pair by splitting a single pulse and sending one along an optical delay line. This was very similar to the early pulsed laser experiments with accumulated echoes, except that the phase of one of the data pulses was shifted using an EOM in the beam path. This experiment was conducted on sodium vapor atoms on a timescale of approximately 30 ns.

With the focus for TDOM devices mainly centering on trivalent rare earth doped crystals, and the long coherence times that these centres offer, erasure at longer times was investigated. To avoid problems of intensity variation, Elman et al. (Elman 1996a) used a commercially stabilized CW dye laser, where the pulses were created by 'chopping' the beam in a similar manner to that used in the current work. Using a cryogenically cooled sample of Pr doped $YAlO_3$, they found that 99% erasure of a stored data echo could be achieved. This required a write-data pulse separation of 400 ns and write-rewrite pulse separation of around 3 μs. They noted that with write-data pulse separations larger than a few microseconds the erasure performance was poor. They attributed this to the phase stability of the optical system. They discussed that this appeared to be due to both stochastic phase variations and also the systematic effect of frequency drift during the

write-rewrite pulse delay. Elman (Elman 1996b) also used the statistical variation of echo erasure efficiency to profile the frequency and phase variation behavior of their optical system.

The same experimental setup as for the reinforcing shown above was used. The phase was controlled by changing the phase of the radio frequency driving the gating AOM. The RF phase changes were accomplished using radio frequency delay lines. Data traces were collected on a single shot basis, and the laser frequency was shifted by 300 MHz to allow access to a clean part of the inhomogeneous line before each shot. Where a greater signal to noise was required, multiple shots were averaged after they had been phase corrected as part of the data processing. The generic pulse sequence used is the same as that shown for reinforcing in figure 4.1.1.

Figure 4.2.1 shows the writing of two separate bits of data into the echo memory. Bit A is used as a control, while bit B is the bit that will be manipulated. The figures show schematics of the input pulse sequence, followed by traces of the in-phase and in-quadrature echo outputs. Only the in-phase component actually contains data, the in-quadrature component exists as a quality control. Figure 4.2.2 demonstrates the same process as figure 4.2.1, except that the phase of bit B has been shifted by 180°. This shows that data with both positive and negative phase can be stored into the system. For this demonstration the write-data delays were 50 μs and 40 μs for bits A and B respectively, while the delays between each write-data pulse sequence was 200 μs.

Figure 4.2.3 shows the effect of combining the two operations shown so far, that is writing both a positive and then a negative data echo at B. The resulting trace shows only bit A in the in-phase (or data) component, and small echoes representing both bit A and bit B in the in-quadrature component. Data bit B in the in-phase component has been erased to below the level of signal to noise. Figure 4.2.4 shows both the reinforcing and erasure procedures when the data for both A and B are written into the memory as part of the same sequence. In this context the crosstalk echo from the two initial data pulses occurs immediately after the readout pulse. In the erasure trace there is again no evidence

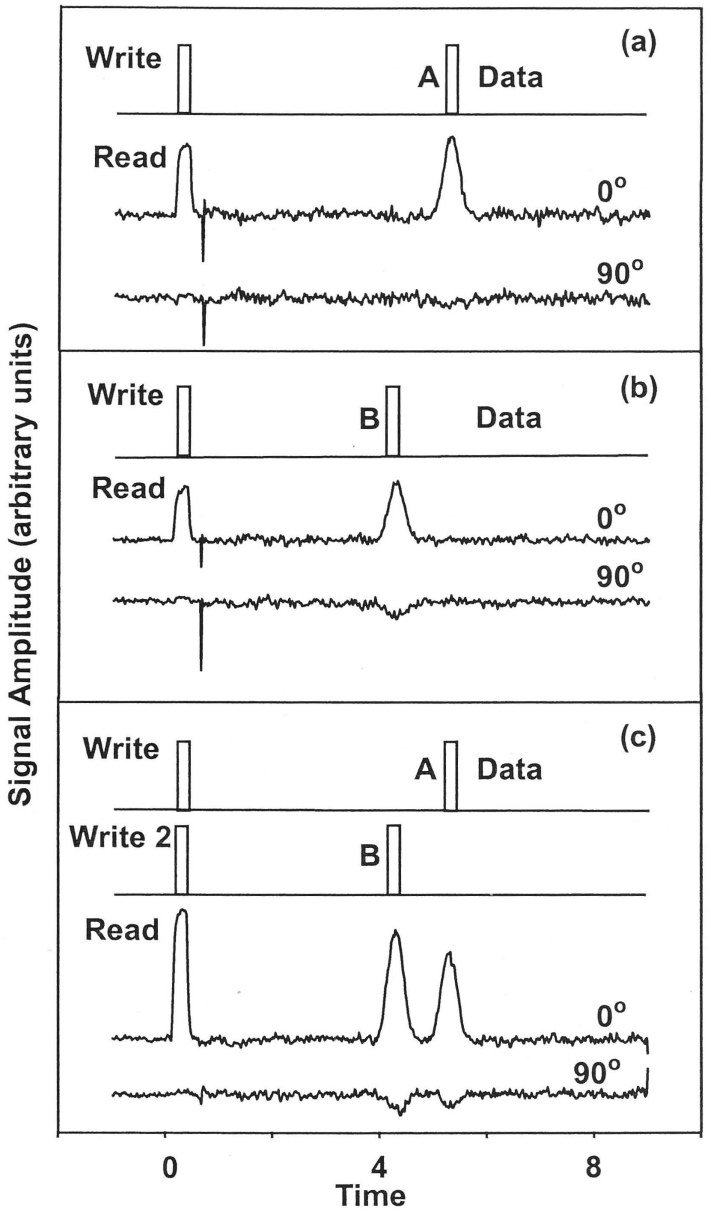

Figure 4.2.1: Experimental demonstration of bit-by-bit data recording. Data bit A is recorded in sequence (a), then data bit B is recorded in sequence (b), then both are recorded sequentially in sequence (c). In quadrature (90^{o}) signals are shown to indicate the phase stability of the system. Five shots were collected for each trace and signal averaged. This figure is the same as figure 4.1.2, and is given here for convenience.

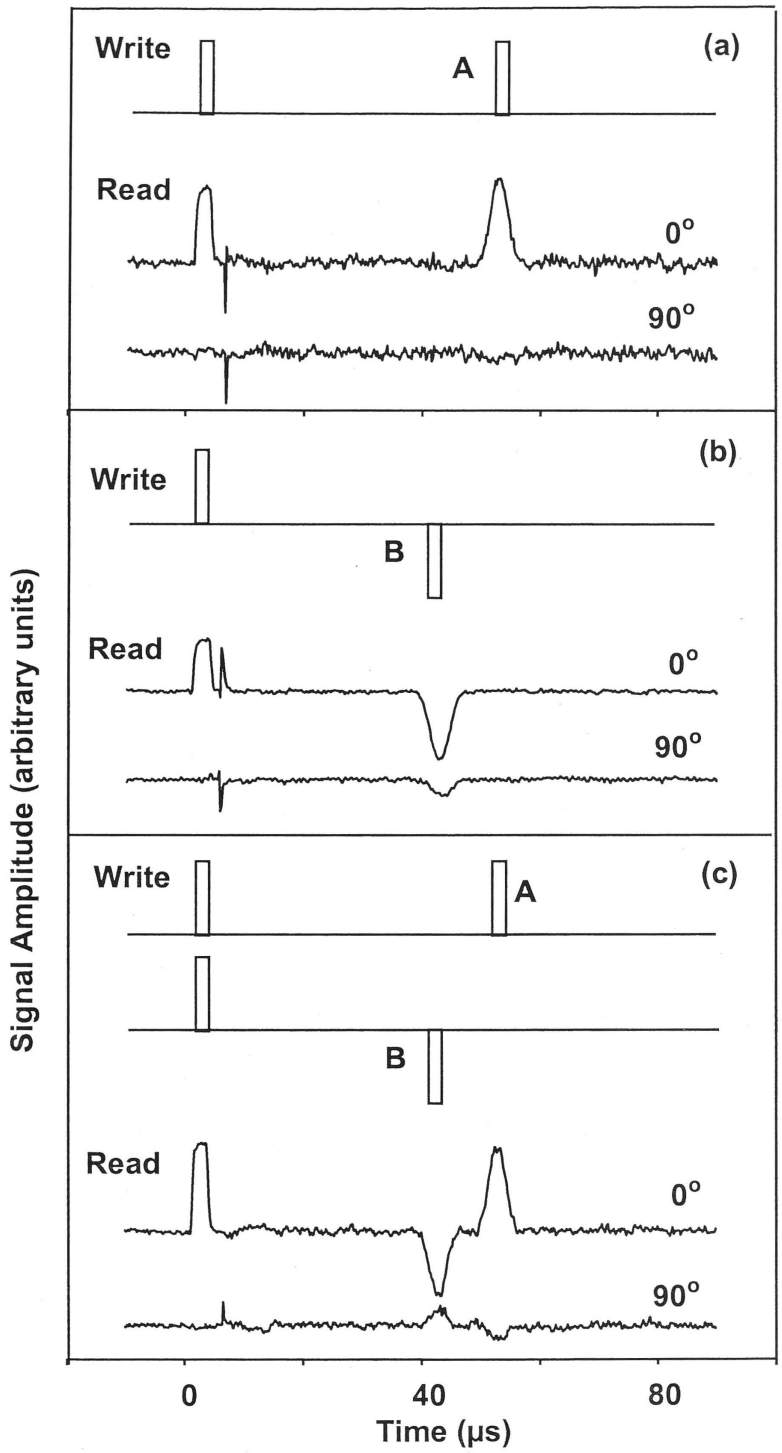

Figure 4.2.2: Experimental demonstration of phase sensitive bit-by-bit data recording. Data bit A is recorded in sequence (a), then data bit B is recorded in sequence with a 180° phase shift, and thus a negative value (b), then both are recorded sequentially in sequence (c). In quadrature (90°) signals are shown to indicate the phase stability of the system. Five shots were collected for each trace and signal averaged.

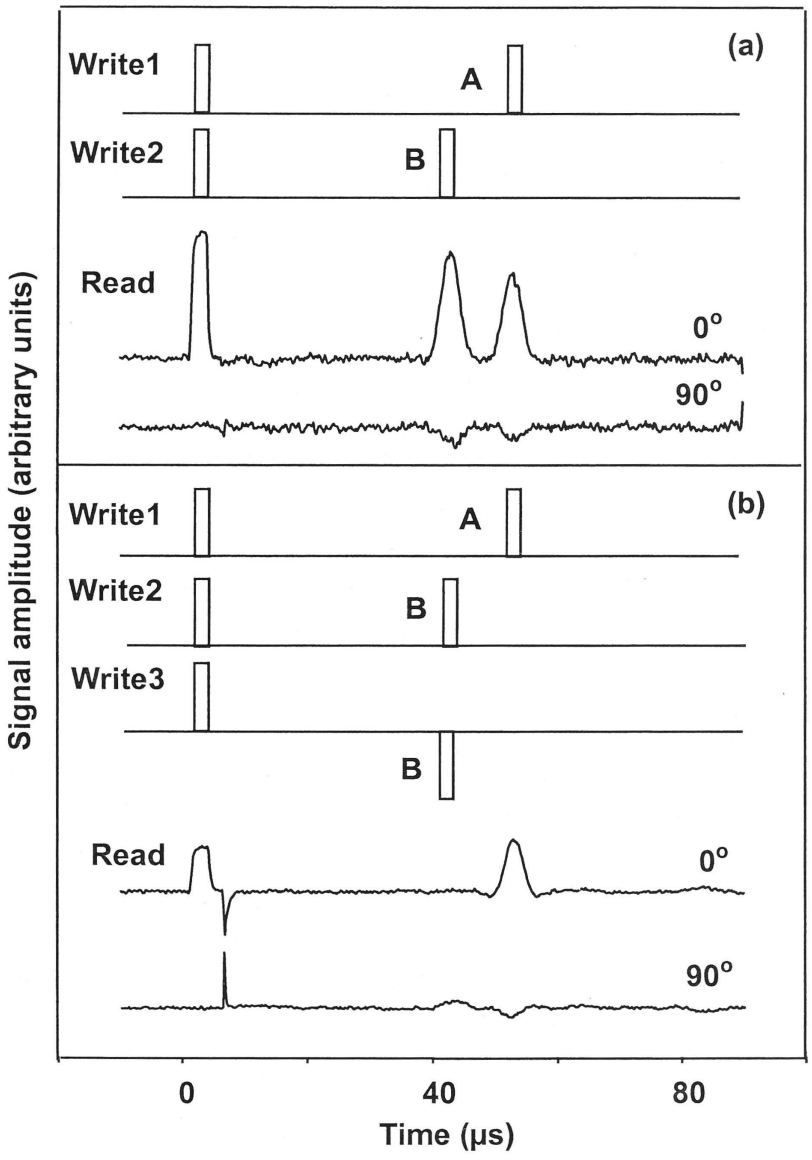

Figure 4.2.3: Experimental demonstration of combined bit by bit data storage followed by selective data erasure. Data bits A and B are recorded separately as shown in (a). Bit B is subsequently erased as shown in (c). In quadrature (90^{o}) signals are shown to indicate the phase stability of the system. Five shots were collected for each trace and signal averaged. Note that the cross talk echo does not appear.

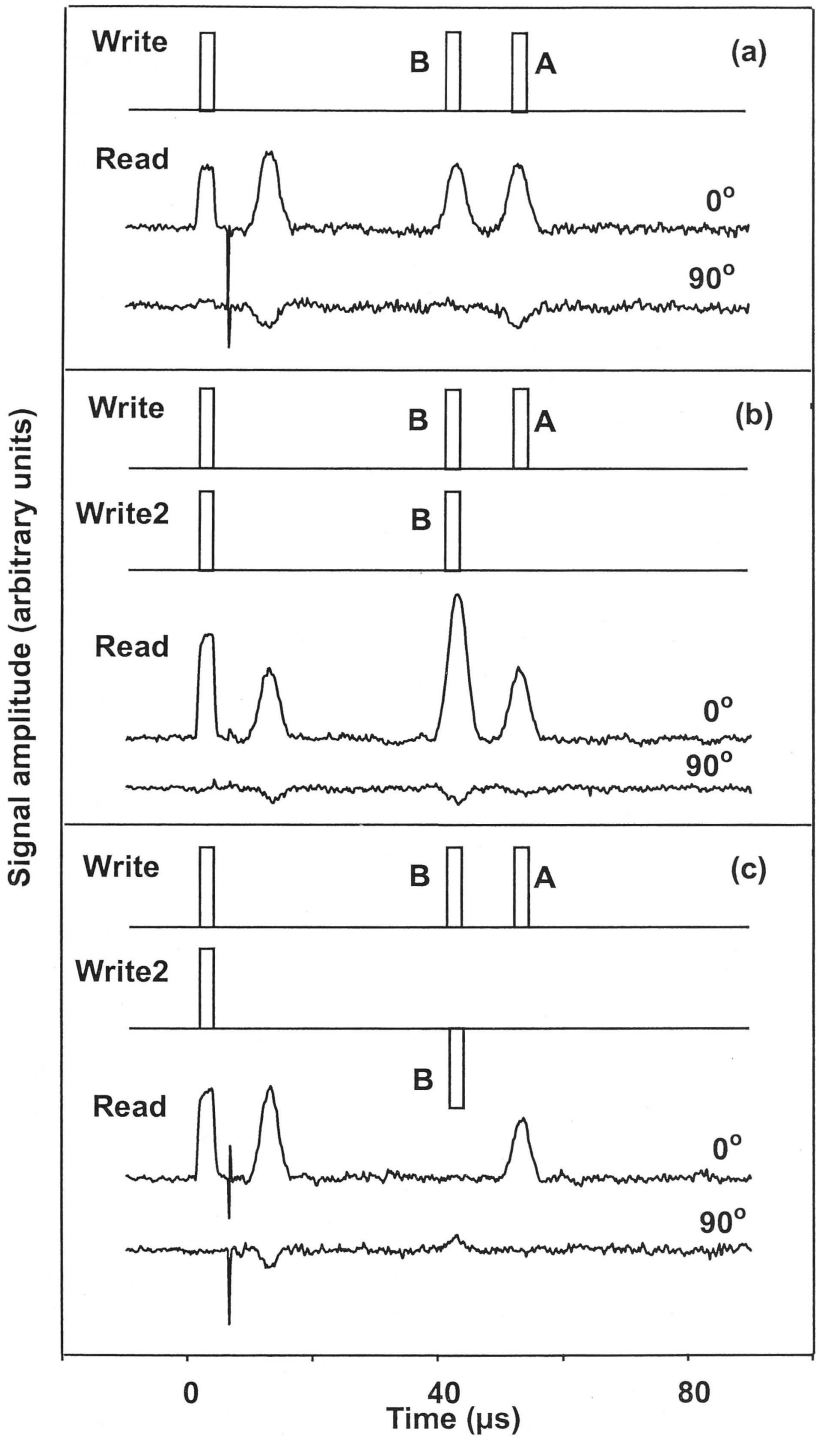

Figure 4.2.4: Experimental demonstration of selective data erasure. Data bits A and B are recorded in sequence (a). The reinforcing effect of the previous section is shown in (b) and the effect of reinforcing (erasing) with a 180o phase shifted pulse is (c). In quadrature (90^{o}) signals are shown to indicate the phase stability of the system. Five shots were collected for each trace and signal averaged. Note the appearance of the cross talk echo after the read pulse after erasure.

of the data echo B in the in-phase component, and only a weak signal in the in quadrature component. Note that the presence of the crosstalk echo clearly indicates that while data bit B is now erased, it was present originally.

The above demonstration clearly shows effective data erasure at timescales considerably longer than those previously achieved. However for practical memory systems it will be necessary to improve on this performance to include both longer time scales and more complex pulse sequences. For this reason an example of such a scenario is demonstrated in figure 4.2.5. In this case an initial data sequence of five data pulses was used. Complications arising from crosstalk echoes were minimized with the timing of the data pulses was chosen so that all the crosstalk echoes occurred prior to the data echoes. The gain of the system was adjusted using an AOM subsequent to the sample, and this was used to reduce the signal strength of the crosstalk echoes.

The five data pulses were written 10 μs apart from 50 μs to 100 μs after the write pulse. A manipulation sequence was then written using a single 180° phase shifted data bit, corresponding to one of the five initial data echoes. The delay between the data sequence and the manipulation sequence was 10 ms. The readout pulse was then applied another 10 ms after the manipulation sequence. Six traces were collected. The first consisted of a data set without any manipulation, and thus shows all five echoes. The next five traces show the single bit erasure of data bits one through five.

The data shows that good erasure can be achieved at these timescales. Although residual echoes above the signal to noise level can be seen following erasure. Because the in-phase component thus shows the degree of the erasure and also because of the increased complexity of the stored data, the in-quadrature components are not shown.

Discussion

The reliable manipulation of individual data bits at practical timescales, such as that demonstrated above, is highly significant for the further development of practical TDOM

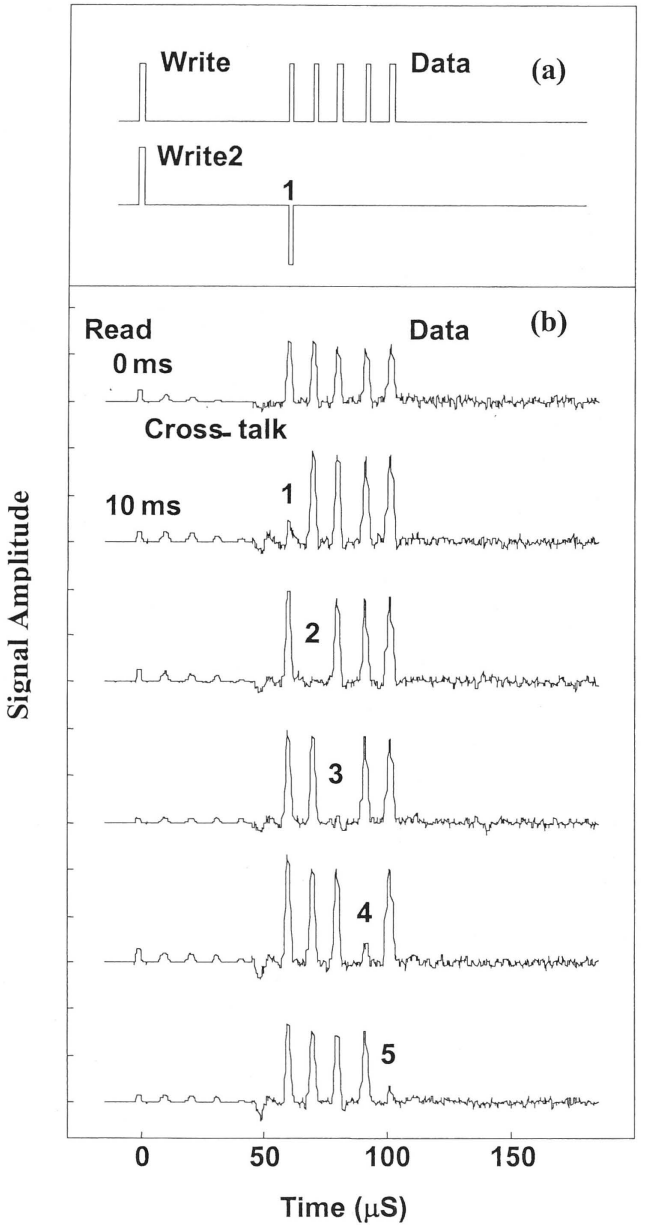

Figure 4.2.5: Demonstration of selective erasure from a multipulse data stream with 10 ms processing delays between data writing and data erasing. The data was written using the sequence shown in (a), and then erasure was performed on bit 1. The process was repeated for bits 2-5. The experimental traces in (b) show the effects. Crosstalk has been minimized using a reduced gain.

systems. Historically the ability to easily erase and rewrite specific sections within a stored memory has significantly increased the value of the memory system. This has been regardless of whether it was paper memories, magnetic memories or other optical memories such as CDs. Beyond this however there is also the possibility of using the erasure and reinforcing capabilities to produce Boolean optical data processors. A description of how this could operate was given by Kroll (Kroll 1993b).

It is clear from the results obtained that even with the considerably increased timescales demonstrated the limiting factor is still the frequency stability of the system. In the current case the frequency drift introduces something of a tradeoff between the maximum delay between write and data pulses, the maximum delay between subsequent write-rewrite sequences and the erasure or reinforcement efficiency. This is not an insoluble problem however and a suitable solution is demonstrated in the following chapter of this thesis.

Chapter 5: Memory Applications of Phase Sensitive Detection

Spectral holeburning methods such as TDOM have previously stored data using the frequency, timing, intensity, spatial direction and locations as discriminating elements (Mossberg 1982,Moerner 1988, Maniloff 1995). It is the combination of these that promise the high storage volumes that make these systems attractive. The capability of reliably storing and retrieving the phase of stored data adds another degree of freedom to this list.

The successful demonstration of data reinforcing and data erasure in the previous chapter relied upon the phase and frequency stability of the system. In that case the use of phase sensitive detection was simply a convenient way of observing the data quality. However in this chapter we show that phase sensitive detection of optical data is a valuable capability in its own right, and has the potential to extend the use of TDOM beyond the range available to intensity detected TDOM systems.

5.1 Direct Measurement of Laser Frequency Drift

The phase and frequency stability of the laser system is what has made the majority of the work demonstrated in this thesis possible. It is also one of the main factors limiting the potential of techniques such as data erasure. Further improvements in the short term phase and frequency stability of the optical system are quite attainable. Increased thermal insulation of the optical reference cavity, better damping of vibration sources, or replacing the inherently noisy dye laser with a solid state based laser system could all contribute to a more stable system.

Such improvements can reasonably be expected to enable a system to remain suitably stable over a period of seconds or perhaps minutes. As described above, the optical coherence lifetime of $Y_2SiO_5:Eu^{3+}$ is more than a millisecond. For a phase variation of

less than 0.1λ over this timescale the total frequency drift would need to be less than 100Hz. However, as was observed in chapter 3, the persistent holeburning lifetime for $Y_2SiO_5:Eu^{3+}$ at cryogenic temperatures is at least 10 days, and consequently it is desirable to have a frequency stable system over this timescale. Achieving this level of performance through improvements to the optical design alone would be a major technological undertaking.

Fortunately the very characteristics of rare earth doped crystals, such as $Y_2SiO_5:Eu^{3+}$, which require such high system performance, may also provide a solution. The key to this is that with phase sensitive detection of coherent transients, the entirety of the signal stored into a persistent holeburning memory is recallable. This means that at the time when a signal such as a photon echo or an FID is stored into the material, all of the input parameters of the input signal, such as the phase, amplitude and frequency are also stored, and can be recalled for comparison with a later signal.

To illustrate this a narrow spectral hole was burnt using a weak 3 ms pulse from the stabilised laser. The intensity of the beam was 0.5uW over a beam diameter of 0.7mm, and with an estimated Rabi frequency of 60 +/- 30 Hz. The free induction decay from this operation is shown in figure 5.1.1. The decay of the total amplitude is approximately exponential, with a decay time of 0.80 +/- 0.03 ms. Using the previously published values given for T_2 and T_1, of 2.6 ms and 1.9 ms respectively (Equall 1994), and the optical Bloch equations as described in chapter 1, a theoretical value for the FID decay time was calculated as 0.64 ms. This calculation also assumed an inhomogeneous broadening >> $1/T_2$, as is the case in $Y_2SiO_5:Eu^{3+}$, and a Rabi frequency of 30Hz. This theoretical decay time is notable because it is significantly shorter than the observed value, and may indicate that the actual value of T_2, in the low laser intensity limit, is longer than the published value. This may merit a more detailed study in the future, but for now it is relevant to note that only a very narrow frequency band (< 200 Hz) of centres has been excited.

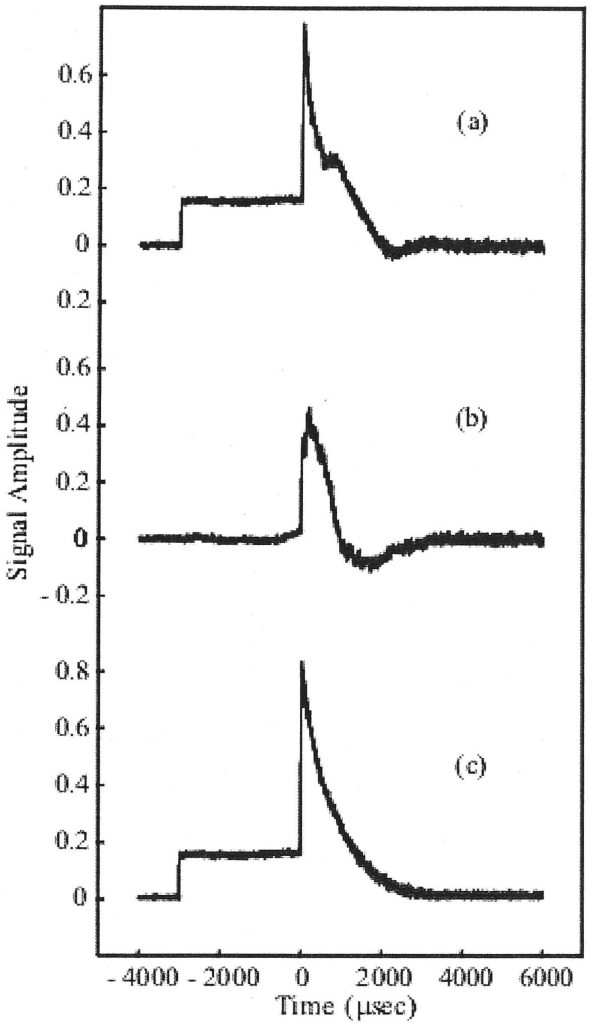

Figure5.1.1: Free induction decay measurement of Y2SiO5:Eu3+ following 3 ms weak laser pulse. (a) is the component in phase with the optical local oscillator, (b) is the component in quadrature with the optical local oscillator and (c) is the total amplitude, showing a decay time of 0.80 ms. The laser pulse preceding the decay was used to phase reference the signals. The gain was also reduced during the laser pulse.

It can be seen from the phase components of figure 5.1.1 that during the 2 ms of the decay, there is some phase fluctuation relative to the local oscillator. Such phase changes with respect to the local oscillator can arise from instabilities of the laser, variations in the interferometer or movements of the sample occurring at any time during the 5 ms of the excitation pulse and the subsequent free decay. This allows the phase performance of the system to be monitored, and it is clear that the total variation of the phase is less than 180° over the 5 ms timescale. It is also clear that the frequency stability of the system is better than 200Hz over this 5ms. From repeated observations of FIDs over this timescale it was consistently observed that during the first 120 μs the phase variation was less than 10 degrees. Along with the effects of instantaneous spectral diffusion, this was the reason that the majority of phase sensitive experiments demonstrated in this thesis, such as the data erasure demonstrated earlier, were performed within this time window.

While FIDs are suitable for investigating the system stability over the relatively short timescale of a few milliseconds, other techniques are needed at longer timescales. Both stimulated photon echo and delayed FID experiments can be used to produce a transient output signal at considerably delayed timescales, and both were used, although the DFID is the primary method used. The theory for both methods is the same; the initial storage of the transient via the holeburning process includes storage of the laser frequency at that time, this is then recalled at a later time and compared with the actual laser frequency at the recall time.

When using the DFID technique for example, the laser frequency was recorded by burning a narrow spectral hole using a long weak pulse. The subsequent application of a short readout pulse then initiates a coherent emission at the frequency of the hole (and thus the original laser frequency) with the decay rate of the emission determined by the linewidth of the spectral hole. Any difference in frequency between this coherent emission and the current laser can then be observed as a beat frequency in the phase sensitively detected signal, when the signal is combined with the local oscillator beam provided from the current laser output.

Figure 5.1.2 shows the delayed free induction measurement taken using a 3 ms delay between the end of the initial burn pulse and the read out pulse. The burn pulse was identical to that of the FID discussed above, with a 3 ms duration and intensity of 0.5 μW. The readout pulse was 20 μs long with a measured intensity of 1 mW. The total amplitude signal is given in figure 5.1.2 (c), and shows an exponential decay time of 400 μs, and a Fourier transform of this decay gives a corresponding spectral hole linewidth of 800 Hz. This is believed to be the narrowest optical spectral feature generated in a solid, although it is likely that it is still limited by the laser and not the material.

Both of the observed DFID phase components are shown as figure 5.1.2 (a) and (b), and it can be seen that there is negligible phase variation over the first 100 μs of the signal. The resolution obtained with this experiment is less than that from the FID, which is interesting, but nevertheless it can be concluded that the laser frequency drift was less than a few hundred Hertz over the total measurement time of 10 ms. This is consistent with the FID observations above.

To investigate longer times figure 5.1.3 shows the DFID measurements taken using a 30 second delay between the burning and readout pulses. The actual pulses were identical with those used for the shorter DFID measurement above. Looking at the total amplitude signal, there is no apparent change in the decay of the signal compared with the shorter delay of figure 5.1.2, with the measured decay still being 0.40 ms. This similarity implies that the linewidth of the spectral hole is unchanged over this time interval, a fact which in turn means that data stored in this material should have a high degree of data fidelity. Of significance regarding frequency drift is the obvious sinusoidal modulation of the two phase components of the observed signal. This modulation is the result of coherent emission beating with the local oscillator beam of the laser. The specific beat frequency and beat phase mean that the laser frequency has shifted by 5 +/-1 kHz during the 30 second time interval prior to the readout pulse.

With further repetitions of this experiment at a range of delays between 3 ms and 30 s, the drift rate of the laser was consistently observed to be less than 1 kHz /s.

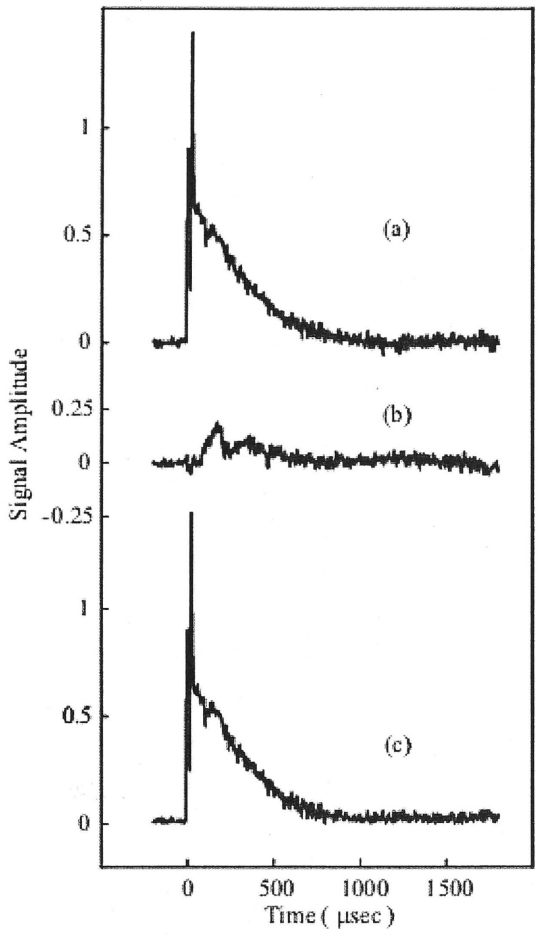

Figure 5.1.2: Delayed free induction decay excited by a 1μs pulse, 3 ms after an initial 3 ms long holeburning pulse. (a) is the component in phase with the 1μs pulse (visible at the start of the decay), (b) is the in quadrature component , and (c) is the total amplitude, giving a decay time of 0.40 ms

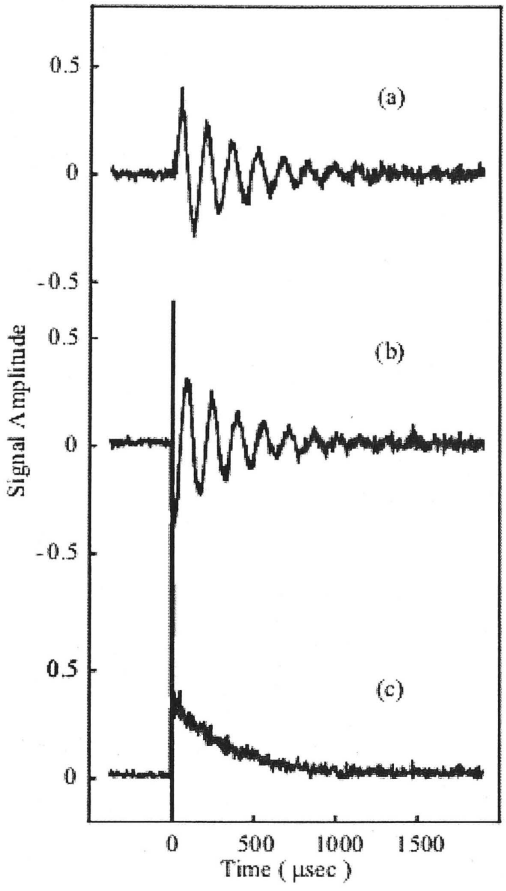

Figure 5.1.3: Delayed free induction decay excited by a 1μs pulse, applied 30 seconds after an initial 3 ms long holeburning pulse. (a) is the component in phase with the 1μs pulse, (b) is the in quadrature component , and (c) is the total amplitude. Oscillation visible in the phase components correspond to a + 5 kHz frequency shift between the frequency of the spectral hole and the frequency of the optical local oscillator. Decay time is 0.40 ms.

The above experiments were conducted towards the end of the research described in this work, after the performance of the optical system had been substantially improved, as described in chapter 2. As a comparison, figure 5.14 shows a photon echo based measurement of the frequency drift, taken relatively early in the work and thus also before some of the developments of the optical system. This measurement demonstrates the use of stimulated photon echoes rather than the DFID technique. The photon echo pulse sequence used consisted of 3 μs pulses each of approximately 10 μW, four pulses were used to store the data at separations of 10 μs, 10 μs and 30 μs, followed by the readout pulse 2 ms later. The laser frequency drift calculated from the variation of the phase of the photon echoes in this case was –15 +/-1 kHz.

As mentioned earlier underlying principle is the same whether using DFIDs or stimulated photon echoes. However the photon echo method only samples the beat signal at discrete points, rather than continuously. This means that unlike the DIFD method, beat frequency can only be determined accurately at when the frequencies are sufficiently low to allow at least two echoes to be used to sample each cycle (Skoog 1992). In addition replacing the single weak burn pulse used in the DFID technique with a string of short pulses typically requires that the short pulses have greater intensity in order to achieve respectable signal to noise levels. In rare earth crystals this increased intensity can lead to a reduction in the achievable resolution of the measurement due to the power dependence of the photon echo decay times. The appearance of crosstalk echoes can also complicate such photon echo measurements. Against this, the short pulses of stimulated echo method have a much wider bandwidth than the long burn pulse of the DFID. This allows a similar amount of pulse energy to be spread over a much wider spectral range, so it was not immediately clear which method was superior. The DIFD method was thus preferred for reasons of convenience.

For the purposes of developing time domain optical memories, the constraint of 100 Hz maximum frequency drift described above, combined with the DFID measurements made on the current system restrict the maximum useable storage times to less than 100 ms. As discussed this is well short of the potential timescales available from the material. Having

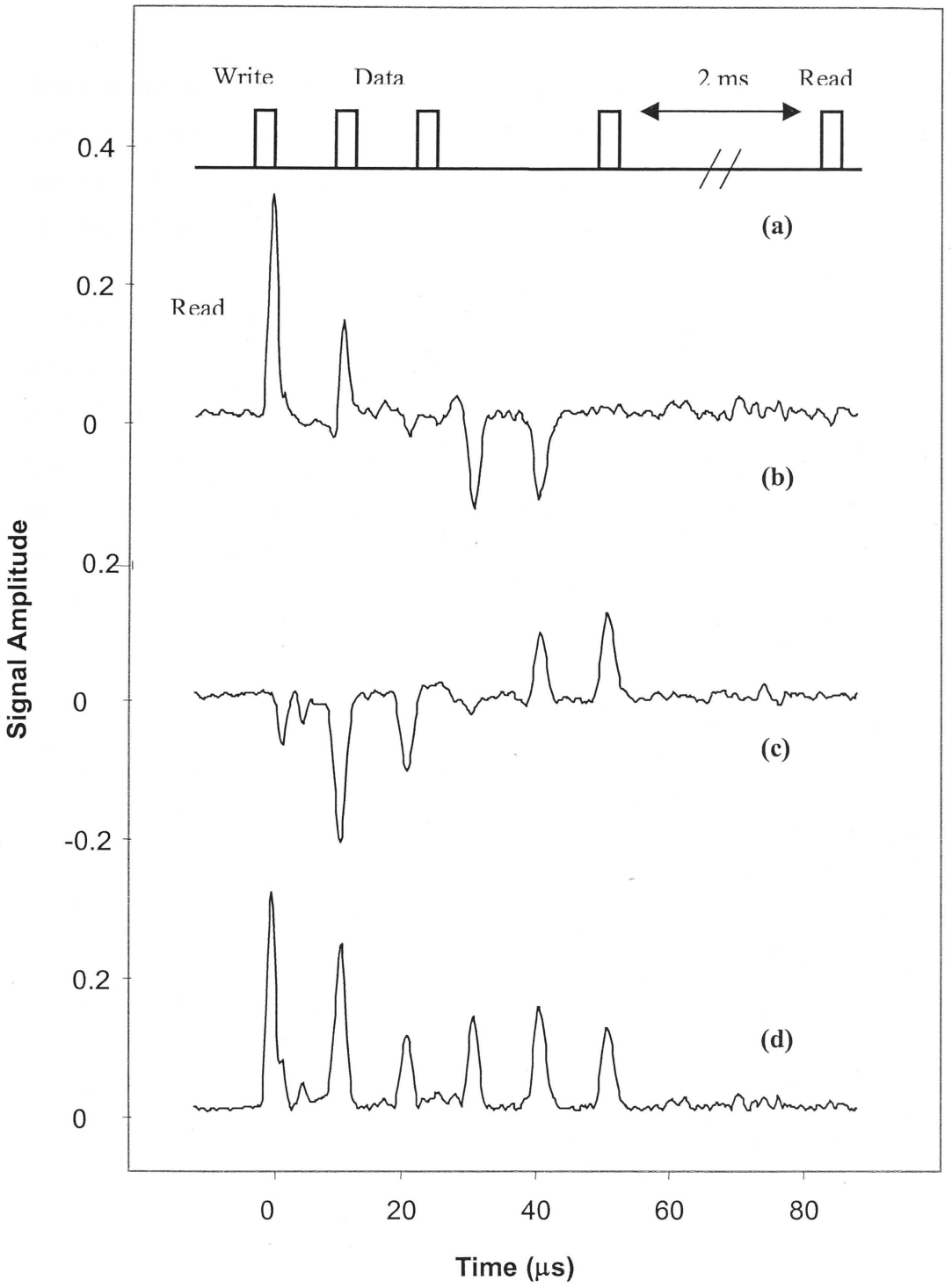

Figure 5.1.4: Photon echo trace demonstrating laser drift of –15 kHz. (a) shows the input pulse sequence used, pulse spacing was 10 μs, 10 μs, 30 μs, and the read pulse 2 ms later. (b) shows the observed component in phase with the read laser pulse, (c) shows the component in quadrature and (d) shows the total amplitude. The slope in the phase component echo contributions demonstrates the effect of laser drift on echo signals. This data was obtained prior to some of the laser improvements described earlier.

demonstrated the capability to accurately determine the frequency change, the next step will be to introduce a discrete frequency offset to reset the laser frequency back to the frequency of the stored spectral hole. In theory this procedure can be conducted at any time period less than the lifetime of the spectral hole.

There are two constraints on this resetting concept, with the first being the short term stability of the system during the actual measurement time. This will affect the accuracy with which the frequency can be measured. The second is the requirement that the stored hole remain within the Fourier width of the short readout pulse. For a readout pulse of 1μs long this width is approximately 1 MHz. The long term stabilisation of a system to within 1 MHz is quite feasible, and is unlikely to prevent this technique being actively used.

2.2 Eliminating Crosstalk Noise using Orthogonally Stored Data

In any practical TDOM system, "noise" echoes through crosstalk between data pulses is likely to be a serious complication. With the possible exception of using divergent reference and data beam directions, all of the methods used for minimizing crosstalk are compromises and reduce the efficiency of the memory system. In chapter 4 we demonstrated that one of the application of reliable data reinforcing was to reduce the signal to noise implications of using weak data pulses. In this section we demonstrate how the use of phase sensitive detection as a part of the memory system allows crosstalk echoes to be eliminated from the memory signal, without reducing the memory performance.

Specifically, if the signal is stored and recorded as two orthogonal phases then two independent channels become available. In simple terms this extra memory dimension doubles the possible memory capacity of a system. One elegant way to use these two channels is to put the desired data into one, and the crosstalk into the other, with only the data channel being sampled as part of the memory retrieval, this is the orthogonal echo method of crosstalk elimination.

The orthogonal echo method requires a phase shift of 90° between the write pulse and the subsequent data pulses. The consequence of this is that the data is stored with this 90° phase shift retained. The crosstalk echoes however , which are formed when one data pulse acts as a write pulse for a subsequent data pulse, do not experience a phase shift and are thus stored without the 90° phase shift. When the readout pulse is applied, this stored phase information is retrieved, relative to the readout pulse. Consequently the crosstalk echoes all appear in the in-phase component of the signal, while all of the data echoes appear in the in-quadrature component. If only the in-quadrature component is observed, using phase sensitive detection, then only the actual data is retrieved, without crosstalk.

This method is demonstrated in figures 5.2.1 and 5.2.2. Figure 5.2.1 was selected as a simple example that clearly shows both the crosstalk and data echoes separately in time. The 2 μs write pulse was followed by three 2 μs data pulses, phase shifted by -90^{o} from the write pulse. The 2 μs readout pulse was applied 2 ms later. Figure 5.2.1 (a) shows a schematic of this input pulse sequence, from which three data echoes and three crosstalk echos are expected. Figure 5.2.1 (b) shows the observed signal in phase with the readout pulse, and clearly contains the three crosstalk echoes immediately after the read pulse, with no sign of the data echoes. Figure 5.2.1 (c) shows the observed in quadrature component, which lacks any appearance of the crosstalk echoes, but clearly displays the three data echoes. Figure 5.2.1 shows the total amplitude of the signal and contains both the crosstalk and the data echoes, and is the signal that is retrieved if amplitude only detection is used.

While in figure 5.2.1 the data and the crosstalk is easily separated by the timing, figure 5.2.2 (d) shows the observed effects of the crosstalk on the total amplitude signal from the more complex data sequence of figure 5.2.2 (a). In this case the benefits of using orthogonal echoes is clear, with the in quadrature signal (figure 5.2.2 (b) giving a good reproduction of the data, while figure 5.2.2 (c) separates out the large amount of noise produced by crosstalk.

Providing that the phase and frequency stability of a system is sufficient, this method allows for the complete elimination of crosstalk noise from TDOM data, without the need to sacrifice either signal to noise or part of the storage time window. It could be readily incorporated into any phase sensitive TDOM system, with no apparent drawbacks.

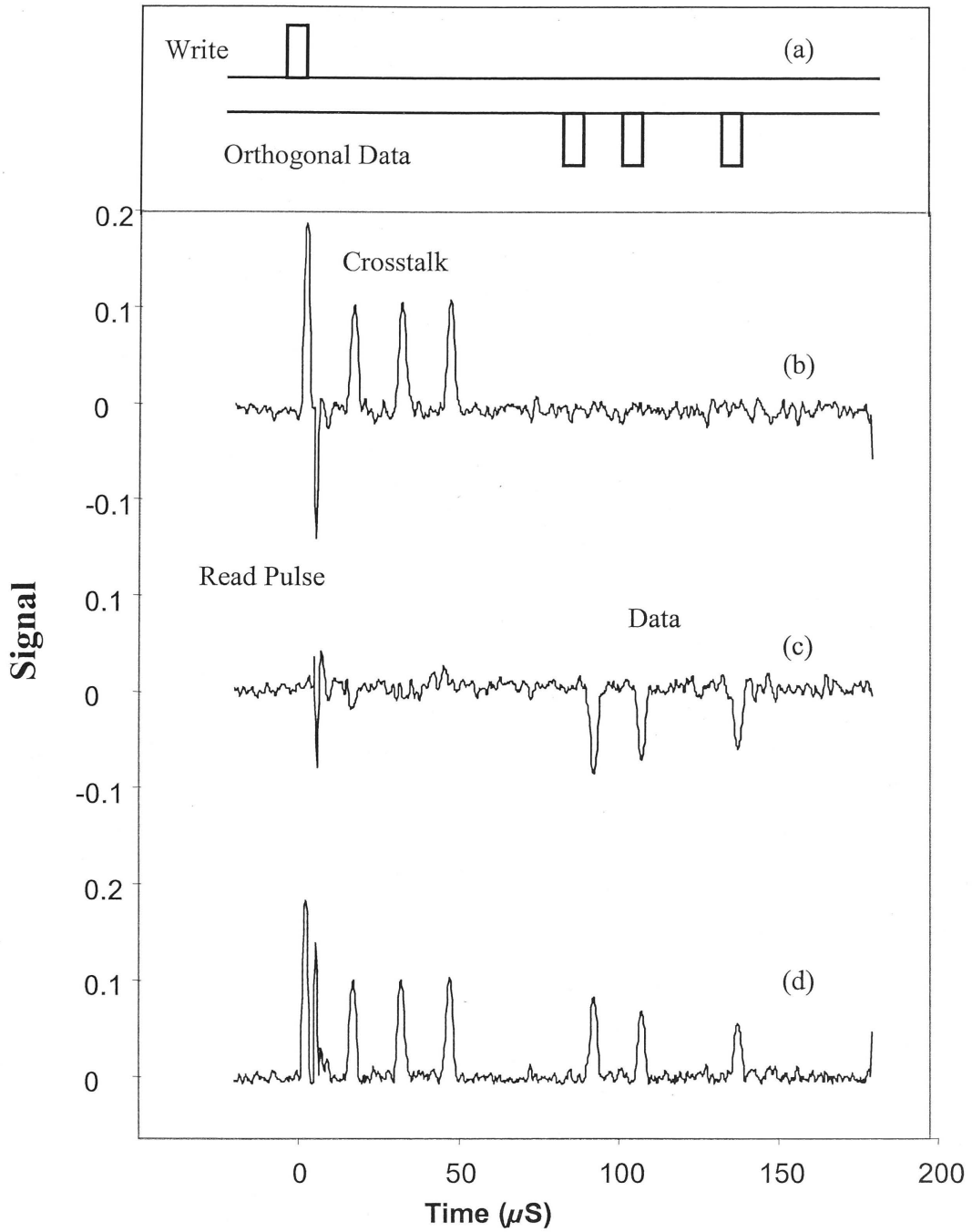

Figure 5.2.1: Separation of crosstalk echoes from data echoes in simple sequence. (a) shows the input pulse sequence used to store 3 data echoes. All pulses were 2 μs long with the pulse area. The pulse timing was chosen to separate data from crosstalk for clarity. The phase of the data pulses was shifted by -90° from the write pulse. (b) shows the component in phase with the read pulse, with only crosstalk echoes visible. (c) shows the in quadrature component, with only data echoes visible. (d) shows the total amplitude component, with both types of echoes observed.

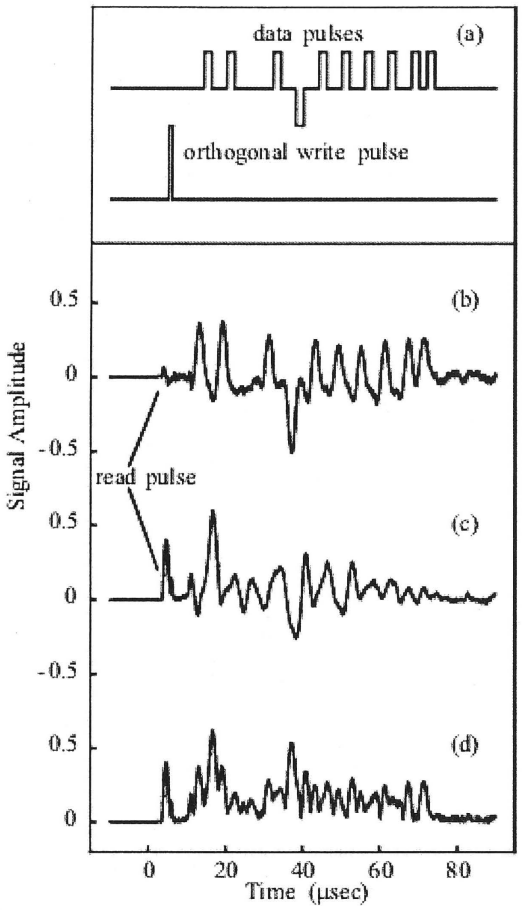

Figure 5.2.2: Separation of crosstalk echoes from data echoes in more complex sequence. (a) input pulse sequence used, 1 μs equal intensity pulses, the 10 data pulses were shifted by 90° from the write pulse, with one shofted a further 180°. The read pulse was applied 10 ms later. (b) displays the observed in quadrature component, containing a good reproduction of the input data. (c) displays the component in phase with the read pulse, and shows a complex pattern of crosstalk. (d) displays the total amplitude, with the data effectively lost in the crosstalk noise.

5.3 Arbitrary Pulse Structures; Storage and Retrieval

Arbitary Data sequence storage

The key aspect of a phase stable system with phase sensitive detection is that signals with both arbitrary amplitude and arbitrary phase variations can be stored and retrieved accurately and completely. A demonstration of this is given in figure 5.3.1, where a complex input signal, with variations in both amplitude and phase has been stored and later retrieved from the memory. Figure 5.3.1 (a) shows a schematic of the in phase input signal and 5.3.1 (b) displays the observed output signal. Figure 5.3.1 (c) and (d) show the corresponding in quadrature phase components.

The total amplitude of the observed signal is not given, however it should be apparent that it would be of little value in determining the structure of the input data. The actual structure of this data involved a 1 μs write reference pulse of intensity 1 mW and approximate area of $\pi/4$. This was followed by a 120 μs delay before the 60 μs long data sequence shown. The peak intensity of the data sequence was 5 μW, with the sequence being divided into 30 segments, each 2 μs long, and each with a distinct amplitude and phase relative to the reference pulse. The data was read out after a 10 ms delay using another 1 μs pulse identical to the write pulse. From the recovered data it can be seen that the input data has been reproduced reliably, both in amplitude and phase, in the stimulated photon echo signal. The smoothing of the signal is due to both the effective bandwidth of the 1 μs reference pulses and the 2 MHz bandwidth of the heterodyne detection system, and consequently could be improved upon if necessary.

One application of this arbitrary input signal capability that does not appear to have been considered is in the area of data networking and transmission. To date the use of optic fibre technology has had a major impact on the speed and volume of network data transmission, however it suffers from the "collision" and subsequent corruption of overlapping transmitted data packets in the same way that electronic methods do.

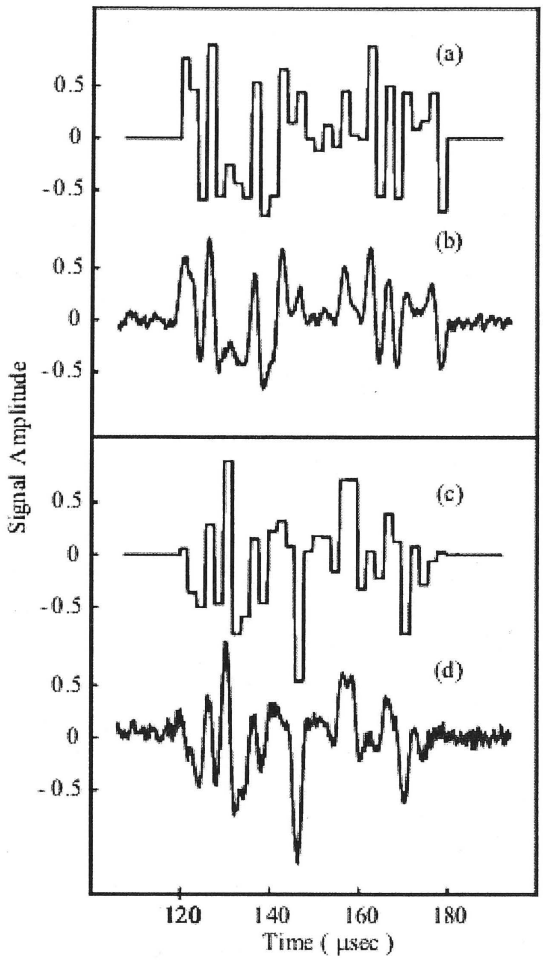

Figure 5.3.1: Recall of data stored with variations in amplitude and phase. Stored with 1μs reference pulse, followed by 120 μs delay then a complex 30 bit pulse, with each segment 2 μs long. The amplitude and phase variations of the in phase and in quadrature components are shown (a), and (c) respectively. (b) and (d) demonstrate the recall of the data. This particular data sequence is a Huffman code.

Computer networks use specific protocols to detect these collisions, after which the data packets must be resent, often multiple times. It is thus necessary to store a copy of each data packet until the receiving system acknowledges that the data has arrived safely. In the case of optic fibre networks, these copies are stored electronically, and are then converted into optical signals each time the data is sent. Using a phase stable stimulated photon echo memory instead of the electronic memory, the data could be optically stored then both retrieved and sent using a single readout pulse, eliminating the need for the repeated conversion of electronic data into optical pulses.

Three State Memory Applications

Another possible application of a TDOM with phase sensitive detection is in the construction of a three state, or trinary memory system. It has been demonstrated repeatedly in this thesis that stored data bits can have both positive and negative values depending on the relative phase between the write and data pulse. For a clear example of this see figure 4.2.2 in chapter 4. In a memory context this means that each data bit can have three values, (+1, 0, -1) rather than the two available from amplitude only detection. Furthermore, chapter 4 also showed the ease with which a data bit can be converted between these values.

While it is simple to use such a system as a standard two state memory, the potential of using an inherently three state memory and possibly a trinary logic system is worth considering. A thorough consideration of this field is beyond the scope of this thesis, however a brief mention of a few possible advantages of such a three state scheme may be worthwhile. The simplest difference between a three state memory and a two state memory is the range of data that could be stored in a given byte. For example a conventional 8 bit byte can take 2^8 (256) different values, whereas an 8 bit byte using a 3 state system could have 3^8 (6561) different values. Alternately a 5 bit byte using a 3 state system, with 243 possible values, would be approximately equivalent to a conventional 8 bit byte. This could increase the available memory capacity by around 30%. The processing speed would also increase; for example the addition of two 8 bit bytes takes 8

distinct operations (one per bit), whereas the addition of two 5 bit bytes takes only 5 distinct operations.

Another potential advantage of a three state memory is in number representation (Dubrova 2002, Hanyu 1995, Radanovic 1996). For example when representing a negative number in a binary memory, an extra bit is typically used to represent whether a number is positive or negative. This results in two different representations for zero, which can complicate subsequent calculations. In a three state system the sign of a number can be determined by the sign of the most significant digit, avoiding this complication.

Potentially the most valuable use of three state memory and logic systems is in the fields of machine learning and artificial intelligence. In these fields one value is often used to indicate a positive response to a question, a second value to a indicate a negative response, and a third to indicate an intermediate response, such as "not enough information available". Such schemes allow the system to be considered "trainable" (Utgoff 2002). The properties of a phase sensitive TDOM system described above would be highly suited to such an application.

Impulse Equivalent Pulses

The final demonstration of this work demonstrates the difficulties that can occur if phase sensitive detection is not used for optical memories. The maximum pulse area suitable for a pulse used to generate a stimulated photon echo is $\pi/2$, higher pulse areas show distortions in the shape of the echoes (Liao 1973, Muramoto 1981, Kunitomo 1982). More specifically $\pi/2$ is the maximum area of a pulse at any given frequency of centre. For a simple pulse the frequency profile of centres affected is given by a smooth Gaussian, with a linewidth determined by the Fourier width of the pulse.

It is possible to use pulse schemes with reference pulses that maximally excite centres over a wider bandwidth than does a single pulse. This allows an increased signal to be

generated without over-exciting any particular centre. One such scheme is "chirping (Shen 1993). In which the frequency of the input laser is ramped during the application of the pulse. Another scheme involves "impulse equivalent pulses". Impulse equivalent pulses include discrete variations of both amplitude and phase during the course of a pulse. This has the effect of producing a frequency excitation profile with a linewidth similar to that of a single short pulse, but with a high proportion of the distribution at or near maximum intensity. The most sophisticated impulse equivalent techniques involve the use of Huffman sequences (Shen96a, Shen96b). An example of a Huffman pulse was used as the input for figure 5.3.1. Another suggested use of Huffman pulse sequences is for the encryption of data stored in time domain optical memory systems, (Shen96a).

The encryption system that was proposed is based on the fact that when an impulse equivalent pulse, such as a Huffman sequence, is used as the reference write pulse then, for accurate data recall, the same pulse is required as the readout reference pulse. If a different pulse is used as the readout pulse then the correlation between the two reference pulses is likely to be a complex function, rather than a single brief pulse. The output data will then be the convolution of this complex function and the stored data sequence. For a write reference pulse that is sufficiently complex, the output data will be unrecognizable. To generate accurate output data it is thus necessary to reconstruct the reference pulse. The suggestion is that encryption based on such a scheme could have a excellent security. For example, in the case of a 128 segment reference sequence there are 3.4×10^{38} different possible Huffman sequences. Based on this it is unlikely that the correct sequence can be readily discovered from trial and error means, even if it is known that a Huffman code was used.

The above discussion is based on the assumption that the data output is being detected as amplitude only, and that phase information, once stored, is not recoverable. When phase information can be reliably recovered, as shown earlier, then the situation, and the security of the encryption, is quite different. With time domain optical memories, what is actually stored is a convolution of the reference pulse and the data sequence. Using phase sensitive detection it is possible to read out this convoluted signal directly, suing a single

short pulse, and breaking the encryption then becomes a matter of deconvolving the reference pulse from the data. The deconvolution process is particularly simple when the data sequence contains a data pulse isolated from the other pulses by more than the length of the encoding reference pulse. In this case the output stimulated photon echo is the Huffman sequence used as the reference write pulse, and the code is immediately broken. With more closely spaced data pulses the situation is more complex, but with sufficient data it should be quite realistic to deduce the correct form of the Huffman reference used.

As a demonstration of this a single data pulse was stored (and encoded) using a Huffman sequence, similar to that shown in figure 5.3.1, with 31 pulse segments, each 2 μs long, and with varying amplitude and phase. An auto-correlation of this sequence with itself is shown in figure 5.3.2 (a), where a single sharp feature, approximating a delta function, is apparent. From this it can be inferred that the sequence is close to being impulse equivalent in character. Experimentally storing the single pulse data with this sequence and then subsequently reading it out using the same sequence likewise gives a single feature, shown in figure 5.3.2 (b). When the code is not known, a single pulse can be applied. Here a single 2 μs pulse was applied, and the echo read with phase sensitive detection. The obtained echo gives the previously unknown reference sequence, and to show that the signal obtained would indeed function as a reliable reference readout pulse, its autocorrelation is shown in figure 5.3.2 (c). The presence of a single prominent peak confirming that the stimulated echo output will adequately replicate the encoding pulse sequence.

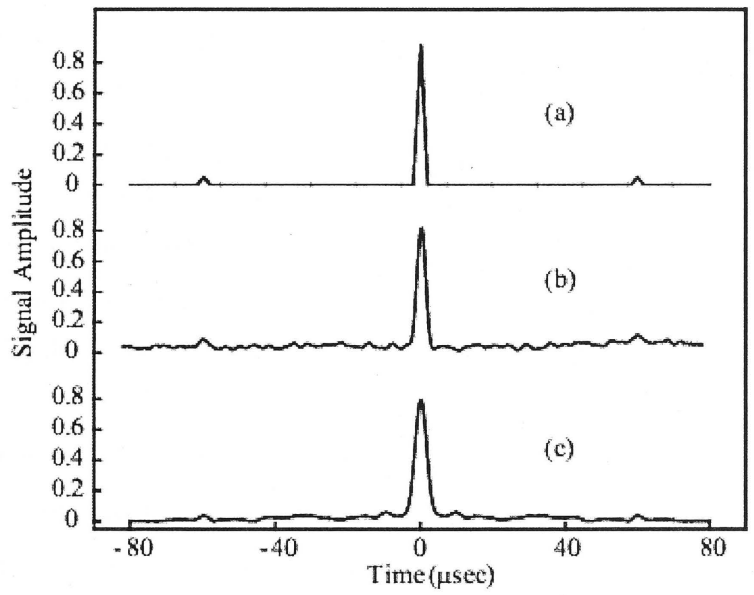

Figure 5.3.2: Cross correlation of a 31 component Huffman pulse sequence. (a) Theoretical cross correlation with itself. (b) A single data pulse is stored using the Huffman pulse sequence as a reference pulse, and the experimental trace shown gives the result of reading this single data bit using an equivalent Huffman reference pulse. (c) The same data is stored using a single sharp reference pulse resulting in a complex stimulated echo. The trace represents the auto correlation of this echo.

Chapter 6: Concluding Remarks

The primary contribution of this thesis is the application of a phase stable laser and a phase sensitive detection system to the development of time domain optical memories.

In chapter 2 the phase stable laser system was described. This system has been under development in the Laser Physics Centre for a number of years and is currently capable of performing with better than 200 Hz resolution over a period of seconds. The phase sensitive detection system was developed during the course of this work by Dr Matt Sellars and myself and with the phase stability of the laser it allows the reliable recall of both phases of the coherent transient signals. The important point to note about this system is that while it has been improved over some years, it does not contain any novel technology. In consequence a system with this level of performance or better could be readily developed as part of a time domain memory elsewhere.

In chapter 3 the $Y_2SiO_5:Eu^{3+}$ holeburning material was investigated. This material had been proposed as a viable storage element for a time domain optical memory system. Measurements of the relevant material parameters showed that this material could be used in a practical system, in which the long spectral hole lifetime of 10 days would be advantageous. Based on these parameters the potential storage density of data in the material was calculated to be 3×10^{11} bits/cm^{-3}, a value that was limited by the effects of instantaneous spectral diffusion. From this approximately 1 cm-3 of the material would be needed to store the equivalent amount of data to a commercially available magnetic hard drive. The memory storage density of $Y_2SiO_5:Eu^{3+}$ is thus comparable with current technologies. To make the implementation of $Y_2SiO_5:Eu^{3+}$ into a memory system worthwhile another advantage, such as access speed or perhaps the all optical nature of the memory would need to be exploited.

Chapter 4 dealt with the benefits of using a phase stable light source as part of a time domain memory system. In the demonstrations presented in this chapter, the phase sensitive detection system served to provide a cleaner picture of the processes, but only

the phase stability was actually essential. Both data reinforcement and data erasure had been demonstrated by other researchers previously, but only on highly restrictive timescales, and there had been no effective demonstrations involving timescales of longer than a few microseconds. The demonstration that application of these techniques need not only be limited by the material properties opens the door for their practical utilization. In particular the demonstration of reliable data erasure is a first step towards using time domain systems for data processing rather than simply storage. Other related techniques that will be practical with this level of phase stability including the frequency chirping of long pulses to produce pulse compression of the emitted echoes, and the use of long timescale impulse equivalent pulses to spread the spectral power more evenly across memory storage centers.

While in chapter 4 the phase sensitive detection was used purely for demonstration purposes, in chapter 5 it was shown to have value in its own right, the demonstration of which represents a significant advance for the field. Prior to this work, all time domain memory systems had used amplitude detection of the signals. Disregarding the phase information in this way amounts to wantonly discarding half of the available signal, and this information is often irretrievable. This was demonstrated through the use of the observed phase information to accurately measure the frequency drift of the laser system over time. Using phase sensitive detection this measurement was both simple and accurate, however it is impossible with amplitude detection without some further information at which point it becomes merely difficult. An example of the degree of unawareness of the phase information value of time domain system was demonstrated by the suggestion that complex reference pulses could be used to allow data encryption. If amplitude only detection is used, then this suggestion may indeed provide a high level of security, but as was demonstrated, acquisition of the phase information allows this encryption to be broken in a single operation.

Another example of the value of retrieving the phase information is given by the use of orthogonal data pulses to eliminate crosstalk noise echoes. Previous aligned beam methods had required either the reduction in the signal to noise by an order of magnitude,

or else the sacrifice of half of the time window used by the memory. With amplitude detection already discarding half of the available information, the storage and retrieval of orthogonal data allows the deliberate selection of what information to discard, in this case the noise due to crosstalk. Perhaps the best illustration of the potential that this thesis has tried to demonstrate is given by the demonstrated capability to both store and recall complex, arbitrary data with any variation of both phase and amplitude over time.

In short the work has been highly successful in demonstrating that with optical phase stability and phase sensitive detection time domain memories have substantially more capability that previously recognized.

A1 Appendix:

In addition to the experiments described in the preceding chapters, some work was also done to characterize the behaviour of photon echoes when pulse areas were increased beyond the small area approximation described in chapter 1. This work did not have a major impact on other aspects of this thesis, and so it is included here as an appendix.

Large area single pulses

The first experiments examined the behaviour of photon echo shapes when the area of one pulse within the sequence was increased, while the others were maintained at low area values. This is a topic that has received considerable attention for two pulse echoes, including experimental optical studies by Liao and Hartman (Liao 1973) and Muramoto et al, experimental NMR studies by Kunitomo et al (Kunitomo xxx) and theoretical studies by Schenzle et al, Jaynes, Mims, and Bloom.

The experiments used a three pulse sequence, using 4 μs long pulses, with delays of 100 and 300 μs between the three pulses. From rotary echo measurements the π pulse length was 13 μs. The length of one of the pulses in the sequence was then increased incrementally up to an area of at least 5 π. The pulse intensity was held constant. This data was also modeled using a numerical simulation of the optical Bloch equations.

The three pulse echo shapes produced followed the shape of the "notched echo" observed by both Liao and Muramoto, although the echo produced when the third pulse was lengthened was time reversed compared with the other stimulated echoes. Comparing the experimental echoes with those produced from simulating the optical Bloch equations gave excellent agreement at the lower pulse areas, but at the higher pulse areas, approximately above 4π, much of the oscillatory detail of the echo shape became "washed out", leaving only the notched shape observed. This loss of detail was not apparent in the published NMR studies, but does agree with the published optical studies.

Further modeling indicated that this difference was likely due to the effect of the variation of laser intensity within the Gaussian beam profile, an issue that does not arise in the NMR studies.

Large cumulative area pulse sequence

Based on the single pulse results it was concluded that the Bloch model based assumption that pulse area should be kept below $\pi/2$ for stimulated echo sequences was appropriate. The question that arose out of this was what the effect of a stimulated echo sequence involving more than 3 pulses would be. To investigate this a five pulse stimulated echo sequence, based on the generic bit by bit data storage sequence shown in figure 4.1.1 was used. The pulses used were all of 3 μs, with pulse spacing of 25, 300, 90 and 500 μs, with the last pulse being the readout pulse and all pulses having the same relative phase. The pulse area was incrementally increased from a small area of 0.14 π to a high value of 0.8 π by increasing the pulse intensity.

The in phase component of the observed signals following the read pulse are shown in figure A1.1. The in quadrature component contained no information and has been omitted for clarity. As well as the two stimulated echoes expected occurring at delays of 25 μs and 90 μs after the read pulse, the higher pulse area traces also show echoes at 65 μs and 115 μs. These two additional echoes have a 180o phase shift from the read pulse, and since they occur at the sum and difference delays of the two stimulated echoes they are here called sideband echoes. A substantial search of the literature was unable to find a previous description of these echoes. Given the phase properties, it is likely that a phase stable system for detection and so the lack of optical observations is reasonable. The lack of NMR regime observations is surprising. An optical Bloch model simulation of the experiment produced results that agreed well with the observations.

The pulse area dependence of the signal amplitude of each echo is given in figure A1.2. From this it is clear that the area dependence of the sidebands is quite different to that of the stimulated echoes, in fact the sideband echoes seem to appear when the stimulated

echo begins to saturate. Based on this it is proposed that the sideband echoes are actually created as a result of the saturating of the stimulated echo.

This is similar to the studies of secondary echoes described by da Silva et al and Silberberg et al (da Silva 1991, Silberberg 1992). The mechanism for both can be best explained using the Fourier transform description of stimulated echo formation described in chapter 1. Considering a three pulse sequence, in the low pulse area limit the frequency grating stored into the population distribution by the first two pulses will be sinusoidal. At higher pulse areas this signal will saturate, leading to a flattening of the sinusoid. From basic Fourier series theory this flattened sinusoid can be decomposed into the original sinusoid and one or more higher order sinusoids, in this case of opposite phase – leading to flattening rather than enhancing. Thus when the read pulse acts to Fourier transform the distribution, a stimulated echo will be emitted due to the primary modulation, and a second echo of opposite phase and twice the delay will be emitted due to the second order modulation. The situation will be the same when two sets of pulses with different delays are used, except that it will be the sum of the two individual sinusoids that will be saturated, and thus the higher order Fourier terms needed will be at the sum and difference frequencies of the two sinusoids. Thus two sideband echoes, at the sum and difference delay timing, will occur in the signal. This description was confirmed using a simple threshold saturation model to show secondary echoes and sidebands in the modeled Fourier transform signal.

It was discussed in chapter 1 that the low area stimulated echo equations are the equivalent of the equations used for four wave mixing. From the observations of the sidebands it is apparent that the analogy with four wave mixing is also valid in the non-linear regime, at least qualitatively.

From the perspective of the remainder of this thesis, pulse areas were used that were sufficiently low to ensure that sidebands would not complicate other studies.

References

Akhmediev, N. N., 1990, Opt. lett., 15, 1035.

Anderson, A. G., R. L. Garwin, E. L. Hahn, J. W. Horton, G. L. Tucker and R. M. Walker, 1955, J. Appl. Phys., 26(11), 1324.

Arend, M., E. Block and S. R. Hartmann, 1993, Opt. Lett., 18, 1789.

Bloch, F., 1946, Phys. Rev., 70, 460

Bloom, A. L., 1955, Phys. Rev., 98(4), 1105.

Broer, M. M. and B. Golding, 1986, J. Opt. Soc. Am. B, 3(4), 523.

Carlson, N. W., W. R. Babbitt and T. W. Mossberg, 1983, Opt. Lett., 8, 623.

Castro, G., D. Haarer, R. M. Macfarlane and H. P. Trommsdorff, 1978, "Frequency selective optical data storage", U.S. Patent 4,101,976.

Cone, R. L., R. W. Equall, Y. Sun, R. M. Macfarlane and R. Hutcheson, 1995, Laser Physics, 5(3), 573.

da Silva, V. L., and Y. Silberberg, 1993, Phys. Rev. Lett., 70(8), 1097.

Drever R. W. P., Hall J. L., Kowalski F. V., Hough J., Ford G. M., Munley A. J., Ward H., 1983, Appl. Phys. B, 31 97

DeVoe, R. G. and R. G. Brewer, 1983, Phys. Rev. Lett., 50(17), 1269.

Dubrova, E., J. Yusuf and J. Mathew, 2002, "Non-Silicon, Non-Binary Computing: Why not?" from "First Workshop on Non-Silicon Computation", Cambridge, MA.

Dyke, T. R., M. J. Sellars, G. J. Pryde, N. B. Manson, U. Elman, U. and S. Kro"ll, 1999, J. Opt. Soc. Am. B 16(5), 805.

Dyke, T. R., N. M. Strickland, J. P. D. Martin and N. B. Manson, 1996, J. Lumin., 66&67, 36.

Elman, U., and S. Kroll, 1996, Laser Phys., 6(4), 721.

Elman, U., B. Luo and S. Kroll, 1996, J. Opt. Soc. Am. B, 13(9), 1905.

Elyutin, S. O., S. M. Zakharov and E. A. Manykin, 1979, Sov. Phys. J.E.P.T., 49, 421.

Equall, R. W., R. L. Cone and R. M. Macfarlane, 1995, Phys. Rev. B, 52(6), 3963.

Equall, R. W., Y. Sun, R. L. Cone and R. M. Macfarlane, 1994, Phys. Rev. Lett., 72(14), 2179.

Equall, R. W., Y. Sun, R. L. Cone and R. M. Macfarlane, 1995, Laser Phys., 5, 573.

Feynman, R. P., Vernon Jr F. L., Hellwarth R.W., 1957, J. Appl. Phys., 28, 49

Hahn, E. L., 1950, Phys. Rev., 80(4), 580.

Hanyu, T and M. Kameyama, 1995, IEEE J. Solid-State Circ., 30(11), 1239.

Hesselink, W. H. and D. A. Wiersma, 1979, Phys. Rev. Lett., 43, 1991.

Hesselink, W. H. and D. A. Wiersma, 1981, J. Chem. Phys., 75, 4192.

Huang, J., J. M. Zhang, A. Lezama and T. W. Mossberg, 1989, Phys. Rev. Lett., 63, 78.

Jaynes, E. T., 1955, Phys. Rev., 98(4), 1099.

Kim, M. K. and R. Kachru, 1987, J. Opt. Soc. Am. B., 4, 305.

Kreyszig, E., "Advanced Engineering Mathematics", 6th Ed., John Wiley & Sons, Inc., 1988, p. 1068.

Kroll, S. and P. Tidlund, 1993, Applied Optics, 32(35), 7233.

Kroll, S. and U. Elman, 1993, Opt. Lett., 18(21), 1834.

Kroll, S. Xu E. Y., Kachru R., 1991, Phys. Rev. B, 44(1), 30

Kunitomo, M., and M. Kaburagi, 1984, Phys. Rev. A., 29(1), 207.

Kunitomo, M., T. Endo, S. Nakanishi and T. Hashi, 1980, Phys. Lett., 80A(1), 84.

Kunitomo, M., T. Endo, S. Nakanishi and T. Hashi, 1982, Phys. Rev. A., 25(4), 2235.

Kurnit, N. A., I. D. Abella and S. R. Hartmann, 1964, Phys. Rev. Lett., 13(19), 567.

Levenson M.D., Kano S.S., Introduction to nonlinear laser spectroscopy", Revised edition, Academic Press, San Diego, 1988

Liao, P. F., and S. R. Hartmann, 1973, Phys. Lett., 44A(5), 361.

Macfarlane, R. M. and R. M. Shelby, "Coherent Transient and Holeburning Spectroscopy of Rare Earth Ions in Solids" in "Spectroscopy of Solids containing Rare Earth Ions", A. A. Kaplananskii and R. M. Macfarlane, eds., Elsevier Science Publishers B. V., 1987.

Macfarlane, R. M., 1995, Laser Physics, 5(1), 567.

Maniloff, E. S., S. B. Altner, S. Bernet, F. R. Graf, A. Renn and U. P. Wild, 1995, 34(20), 4140.

Manson, N. B., and A. J. Silversmith, 1987, J. Phys. C, 20, 1507.

Martin, J. P. D, M. J. Sellars, P. Tuthill, N. B. Manson, G. Pryde and T. Dyke, 1998, J. Lumin., 78, 19.

Mims, W. B., 1966, Phys. Rev., 141(2), 499.

Mitsunaga, M., 1992, Opt. Quant. Elect., 24, 1137.

Mitsunaga, M., R. Yano and N. Uesugi, 1991, Opt. Lett., 16, 1890.

Moerner, W. E., "Persistent Spectral Hole-Burning: Science and Applications", Springer, New York, 1988.

Mossberg, T. W., 1982, Opt. Lett., 7, 77.

Muramoto, T., S. Nakanishi, T. Endo and T. Hashi, 1981, Optics Comm., 36(5), 409.

Pryde, G. J. , 1999, "Ultrahigh resolution spectroscopic studies of optical dephasing in solids", Ph.D. Thesis, The Australian National University.

Radanovic, B. and M. Syrzycki, 1996, "Current-mode CMOS adders using multiple-valued logic" in "Proc. Canadian Conference on Electrical and Computer Engineering", 190.

Schenzle, A., N. C. Wong and R. G. Brewer, 1980, Phys. Rev. A., 21(3), 887.

Sellars, M. J., 1995, "Ultra-High Resolution Laser Spectroscopy of Rare Earth Doped Solids", Ph.D. Thesis, The Australian National University.

Sellars, M. J., T. R. Dyke, G. J. Pryde and N. B. Manson, 1999, Materials Science Forum Vols. 315-317, 59.

Sergeev, N. A., A. V. Sapiga and D. S. Ryabushkin, 1989, Phys. Lett. A, 137(4,5), 210.

Shen, X. A. and R. Kachru, 1993, Opt. Lett., 18(22), 1967.

Shen, X. A. and R. Kachru, 1996, Opt. Lett., 21, 2020.

Shen, X. A., R. Hartman and R. Kachru, 1996, Opt. Lett., 21, 833.

Skoog, D. A and J. J. Leary, 1992, "Principles of Instrumental Analysis", 4th Ed., Saunders College Publishing, p. 338

Solomon, I., 1959, C.R. Hebd Seances Acad. Sci., 248, 92.

Szabo, A., 1975, "Frequency selective optical memory", U.S. Patent 3,896,420.

Utgoff, P. E. and D. J. Stracuzzi, 2002, to appear in Neural Computation.

Yano, R., M. Mitsunaga and N. Uesugi, 1991, Opt. Lett., 16(23), 1884.

Yano, R., M. Mitsunaga and N. Uesugi, 1992, J. Opt. Soc. Am. B, 9(6), 992.

Yariv, A., "Optical Electronics", 3rd Ed., 1985, CBS College Publishing, p. 361.

Boonyarith T., Martin J. P. D., Luo B., Manson N. B., 1992, J. Lumin., 51, 149

Reeves R. J., Macfarlane R. M., 1993, Phys Rev B, 47, 158

Macfarlane R. M., Shelby R. M., Burum D. P., 1981, Opt. Lett., 6, 593

Masui H., Ibuki S., 1967, J. Phys. Soc. Japan, 22 1387

Cockroft N. J., Han T. P. J., Reeves R. J., Jones G. D., Syme R. W. G., 1987, Opt. Lett., 12, 36

Hasan Z., Manson N. B., 1987, J. Lumin., 38, 40

Macfarlane R. M., Burum D. P., Shelby R. M., 1984, Phys. Rev. B, 29, 2390

Burum D. P., Shelby R. M., Macfarlane R. M., 1982, Phys. Rev. B, 25, 3009

Pelletier-Allard N., Pelletier R., 1984, J. Phys. C, 17, 2129

Pelletier-Allard N., Pelletier R., 1985, Phys. Rev. B, 2661

Silversmith A. J., Macfarlane R. M., 1992, Phys. Rev. B, 45, 5811

Thorne A. P., 1988, "Spectrophysics", 2nd Ed., Chapman and Hall, p 290, p335

Graf F. R., Renn A., Zumofen G., Wild U. P., 1998, Phys. Rev. B, 58, 1998

Babbitt W. R., 1987, "The response of Inhomogeneously broadened optical absorbers to temporally complex light pulses.", Ph. D. Thesis, Harvard University.